ISSN 1732-9353
eISSN 2543-7496

Scientific Review

Engineering and Environmental Sciences

Przegląd Naukowy

Inżynieria i Kształtowanie Środowiska

Vol. 29 (1) 2020 Nr 87

Quarterly – Kwartalnik

SCIENTIFIC REVIEW
ENGINEERING AND ENVIRONMENTAL SCIENCES
Kwartalnik / Quarterly

RADA PROGRAMOWA / EDITORIAL BOARD
Kazimierz Adamowski (University of Ottawa, Canada), Monim Hakeem Khalaf Al-Jiboori, Kazimierz Banasik – Chairman (Warsaw University of Life Sciences – SGGW, Poland), Andrzej Ciepielowski (Warsaw University of Life Sciences – SGGW, Poland), Tomáš Dostál (Czech Technical University in Prague, Czech Republic), Valentin Golosov (Moscow State University, Russia), Vidmantas Gurklys (Aleksandras Stulgniskis University, Kaunas, Lituania), Małgorzata Gutry-Korycka (University of Warsaw, Poland), Zbigniew Heidrich (Warsaw University of Technology, Poland), Silvia Kohnová (Slovak University of Technology, Bratislava, Slovak Republic), Andrzej J. Kosicki (Maryland State Highway Administration, Baltimore, USA), Pavel Kovar (Czech University of Life Sciences, Prague, Czech Republic), Hyosang Lee (Chungbuk National University, Korea), Athanasios Loukas (University of Thessaly, Volos, Greece), Jurík L'uboš (Slovak Agriculture University, Nitra, Slovak Republic), Viktor Moshynskyi (National University of Water Management and Nature Resources Use, Rivne, Ukraine), Magdalena Daria Vaverková (Mendel University in Brno, Czech Republic)

ZESPÓŁ REDAKCYJNY / EDITORIAL OFFICE
Mieczysław Połoński (przewodniczący / Chairman), Zbigniew Popek, Katarzyna Pawluk (sekretarz / Editorial Assistant), Weronika Kowalik, Grzegorz Wrzesiński, Grzegorz Wierzbicki

Lista recenzentów jest publikowana w ostatnim numerze danego rocznika i na stronie http://iks_pn.sggw.pl.
The list of reviewers is published in the last issue of the volume and on the http://iks_pn.sggw.pl.

ADRES REDAKCJI / EDITORIAL OFFICE ADDRESS
Wydział Budownictwa i Inżynierii Środowiska SGGW
ul. Nowoursynowska 159, 02-776 Warszawa
tel. (48 22) 59 35 248, 59 35 240
e-mail: iks_pn@sggw.pl
http://iks_pn.sggw.pl

ISSN 1732-9353
e-ISSN 2543-7496

Wydawnictwo drukowane jest pierwotną wersją Przeglądu Naukowego Inżynieria i Kształtowanie Środowiska.

„Przegląd Naukowy Inżynieria i Kształtowanie Środowiska" jest indeksowane w bazach: AGRO(Poznań), Biblioteka Nauki, CrossRef, DOAJ, E-publikacje Nauki Polskiej, Google Scholar, Index Copernicus, INFONA,POL-Index, SCOPUS, SIGŻ(CBR).

Scientific Review

Engineering and Environmental Sciences

Przegląd Naukowy

Inżynieria i Kształtowanie Środowiska

Vol. 29 (1) 2020 Nr 87

Spis treści
Contents

PRACE ORYGINALNE
Original papers

RAJAB J.M., HASSAN A.S., KADHUM J.H., Al-SALIHI A.M., SAN LIM H.: Analysis of tropospheric NO_2 over Iraq using OMI satellite measurements 3

SÓWKA I., PAWNUK M., GRZELKA A., PIELICHOWSKA A.: The use of ordinary kriging and inverse distance weighted interpolation to assess the odour impact of a poultry farming plant 17

WRÓBEL M., RYBAK J., ROGULA-KOZŁOWSKA W.: Przykłady wykorzystania testu OSTRACODTOXKIT F™ do oceny zanieczyszczenia pyłów drogowych metalami w aglomeracji wrocławskiej 27
The application of OSTRACODTOXKIT F™ test to assess metals contamination in road dust in Wrocław agglomeration

HADI F.A., ABDULSADA Al-KNANI B., ABDULWAHAB R.A.: An assessment the wind potential energy as a generator of electrical energy in the coastal area of southern Iraq 37

HO H-CH., PUIKA K.S., KASIH T.P.: Development of IoT-based water reduction system for improving clean water conservation 54

WASIELEWSKI R., GŁÓD K.: Emission results of combustion process of fatty acids distillation residue in an oil boiler – comparison to heavy fuel oil 62

WRZESIŃSKI G.: Permeability coefficient tests in non-cohesive soils 72

FIGIEL E., LECIEJ-PIRCZEWSKA D.: The way to limit emission – energy efficient buildings. The example of the largest facility in Poland in nearly zero-energy building standard 82

SUGIONO S., NURLAELA S., KUSUMA A., WICAKSONO A., LUKODONO R.P.: Impact of elevated outdoor MRT station towards passenger thermal comfort: A case study in Jakarta MRT 93

PRACE NAUKOWO-PRZEGLĄDOWE

Research review papers

CZERWIŃSKA J., WIELGOSIŃSKI G.: Functioning of the flue gas treatment system in Polish municipal waste incineration plants 108

© Copyright by Wydawnictwo SGGW, Warszawa 2020

Opracowanie redakcyjne – Anna Dołomisiewicz, Krystyna Piotrowska

ISSN 1732-9353 eISSN 2543-7496

Druk: ZAPOL sp.j., al. Piastów 42, 71-062 Szczecin

PRACE ORYGINALNE
ORIGINAL PAPERS

Scientific Review – Engineering and Environmental Sciences (2020), 29 (1), 3–16
Sci. Rev. Eng. Env. Sci. (2020), 29 (1)
Przegląd Naukowy – Inżynieria i Kształtowanie Środowiska (2020), 29 (1), 3–16
Prz. Nauk. Inż. Kszt. Środ. (2020), 29 (1)
http://iks.pn.sggw.pl
DOI 10.22630/PNIKS.2020.29.1.1

Jasim M. RAJAB[1], Ahmed S. HASSAN[2], Jasim H. KADHUM[2], Ali M. Al-SALIHI[2], Hwee SAN LIM[3]

[1] Laser and Photonics Research Center, University of Al-Hamdaniya
[2] College of Science, Mustansiriyah University
[3] School of Physics, Universiti Sains Malaysia

Analysis of tropospheric NO_2 over Iraq using OMI satellite measurements

Key words: nitrogen dioxide, air pollution, remote sensing, Baghdad, Iraq

Introduction

There is an agreement, since the onset of the industrial revolution, the continuous emissions of the anthropogenic and pollutions in the atmospheric have increased due to the human activity, industrialization, and deforestation. This increase has redounded significantly to economic dullah, 2012; Rao, Hutyra, Radevelopment and the birth of the anthropogenic reached over 50% (Rajab, Jafri, Lim & Abciti & Templer, 2014; Al-Salihi, 2018). Also, it is a massive source of many air pollutants because of growing anthropogenic emissions related with growth rates of megacities, large urban agglomerations and rapid traffic growth (Molina & Molina, 2004). The significant external variables controlling the climate contains aerosols, solar irradiance and greenhouse gases (GHGs), e.g.: carbon dioxide (CO_2), water vapour (H_2O_{vapor}), methane (CH_4), nitric acid (N_2O) and ozone (O_3). As a result of human vitalities since 1750, the global atmospheric densities of CO_2, CH_4 and N_2O have increased perceptibly and beat pre-industrial measurements specified by ice cores for many thousands years (Rajab, MatJafri & Lim, 2014; Al-Salihi, Rajab & Salih, 2019).

Nitrogen dioxide is one of the most important air pollutants trace gases in the atmosphere with important impact on tropospheric and stratospheric chemical processes and human health. It plays a major role for production of ground level O_3. Moreover, NO_2 contributes to the formation of secondary aerosols and

acid rain (Zyrichidou et al., 2013; Yang, Carn, Ge, Wang & Dickerson, 2014; Chan et al., 2015; Al-Salihi, 2017). There are still several disputes about the exact amount of the diverse influx and sources for NO_x. The NO_2 creating by both natural and anthropogenic activities: biofuel combustion and fossil fuel, thermal power plants, transportation, industries, biomass burning, residential use, aircrafts and microbiological processes in soil. Natural sources of NO_2 are lightning and microbial activity in soil by the oxidation of ammonium nitrate (Constantin, Voiculescu & Georgescu, 2013).

In many researches, the spatiotemporal differences of the troposphere vertical column densities (VCDs) NO_2 during 2005–2016 was investigated with level of urban development across many large countries such as China. And the relationship between urban development and NO_2 pollution analysed by using the night-time light (NTL) data. The NTL data and NO_2 column data are both measured by satellite observations (Cui et al., 2019). In addition, the regional variations emissions of CO_2 from airports were increased due to the civil aviation sector activities. These emissions evaluated by using geographically weighted regression (GWR) models and ordinary least square (OLS), separately, to investigate spatial heterogeneity, and whether urbanization drives airport CO_2 emissions at the city level (Zhang et al., 2019).

The profusion of atmospheric parameters was been measured four decades ago using airplanes, weather balloons, and distributed ground stations. These measurements are cost so much money and staff and incapable to get continuous long term recordings for global climate variability. Therefore, there is a shortage in data for upper and lower troposphere. The satellite remote sensing has useful global and regional coverage's, which raised our capability to analyse the influence of human activity on the climate change and the atmosphere chemical composition. Also, equip continuous data with high temporal and spatial resolution (Lin et al., 2014; Salih, Al-Salihi & Rajab, 2018). Satellite measurements provide necessary information of distributions for the atmospheric trace gases column densities. The satellite tropospheric NO_2 data have found prevalent utility. Observational analyses have explained the strong weekly cycles in the observed NO_2 (Beirle, Platt, Wenig & Wagner, 2003; Chan et al., 2015), the continental scale outflow and the influence of biomass burning (Ladstaetter-Weissenmayer, Burrows & Perner, 1998; Burrows et al., 1999).

From environmental scenery, Iraq encountering severe problems of fast motorization, deforestation and energy trouble cases a strong rise of NO_2 emissions with additional pressure on the local and regional environment. Therefore, a comprehensive spatio-temporal study of tropospheric NO_2 over Iraq is an important issue. In order to develop the efficient strategies to minimize its emissions, which from fossil fuel combustion and biomass burning reduce local air quality and affect global tropospheric chemistry. The purposes of this research to analyses the yearly hotspots emissions, tropospheric NO_2 monthly distribution, and assess its long termtrends above Iraq employing Ozone Monitoring Instrument (OMI) data dur-

ing 2005–2014. A trend and air mass trajectory data were analysed over Baghdad city. The results help to analysis and identify the hotspots for territorial NO_2 emissions above study area. The annual and monthly mean NO_2 maps were generated using GIS software.

Material and methods

Iraq is a country lies in the western part of Asia, located in southwestern Asia, and take possession of usually the Mesopotamian Plain, situated, between 39° and 49° E longitudes and 29° and 38° N latitudes (a small regions lie west of 39°). An area (Fig. 1) involves of 437,072 km^2. The most north areas of the country are made up of mountains; the highest point being at 3,611 m. Tigris and Euphrates rivers, run from the middle of Iraq, taking place from northwest towards southeast where fecund alluvial plains. Iraq has a narrow coastal strip north of the Arabian Gulf with a length of 58 km. Most of Iraq has a hot and arid climate with subtropical influence. The

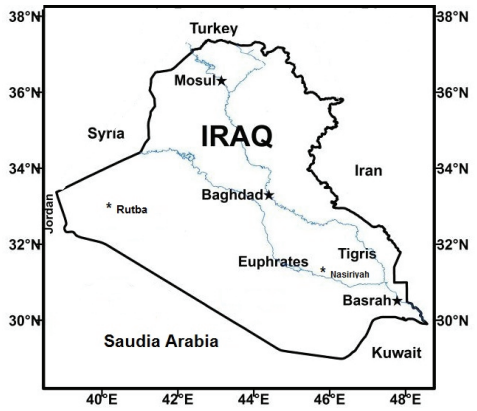

FIGURE 1. The geographical feature of the study area

northern mountainous regions have cold winters with occasional heavy snows. Summer temperatures rate above 40°C in most parts of the country and frequently exceed 48°C. Winter temperatures infrequently exceed 21°C with maximums roughly 15–19°C and nighttime lows to 2–5°C. Typically, precipitation is low; except for the northern regions, the rainfall is extremely rare during the summer. The maximum rainfall occurs during the winter months, and most places receive less than 250 mm annually (Metz, 1993; Abed, Al-Salihi & Rajab, 2018).

Ozone Monitoring Instrument is one of the several, flying on-board NASA's Aura satellite put to space on 15 July 2004, with orbital period of around 100 min and has a Sun synchronous polar orbit passes the equator at around 13:30 local time (Zyrichidou et al., 2013). It observes the atmosphere in 60 cross-track ground pixels measuring 13–26 km along track and 24–128 km across track has a 114° field of scenery, which matched to about 2,600 km vast swath on the Earth's surface, providing daily global NO_2 maps. Due to the vast swath of the 14–15 orbits per day, OMI realizes global covering nearly in a day (exclude for tropics). It is nadir visibility imaging spectrograph quantify backscattered and direct sunlight in the ultraviolet-visible (UV/VIS) range from 270 to 500 nm with a spectral resolution of about 0.5 nm and its performance and design explained in detail in (Levelt et al., 2006).

Tropospheric NO_2 columns are restored by utilizing differential optical absorption spectroscopy (DOAS) analysis in the 405–465 nm spectral range, and has an unreliability of $0.1 \cdot 10^{15}$ molecules per 1 cm^2 and it is undervalued by

15–30%. The recapture of NO_2 used to record the pure and 0–30% cloudy situations in the air mass element acquired for the simulated NO_2 profiles. The seasonal differences of NO_2 reclamation from OMI agree with the NASA GSFC's global modelling initiative (GMI) chemical transport model (Levelt et al., 2006).

In this study, ten-year information from January 2005 to December 2014 were utilized to assess and analyse the NO_2 distributions above research area. The Baghdad city been selected and fitted with a linear function. Results from the analysis of NO_2 concentrations was acquired by OMI satellite ascending Level-3 data. In general, 120 L3 ascending monthly granules loaded to gain the required output. Using OMI website file data, comprising the identical time and location along the satellite course, in a HDF (hierarchical data format) format for monthly basis, were took out from the satellite and organized in schedule utilizing MS Excel. To analysis the annual long-term allocation of tropospheric NO_2 above Iraq, the monthly data averaged for the period (2005–2014) of OMI measurements. While for monthly analysis, the data of tropospheric NO_2 averaged for the each month along the study period. The GIS software used for plotting the averaged for the each month and annual for the study period.

Results and discussion

Annual analysis long-term NO_2 data over Iraq

Figure 2 illustrated the annual distribution of tropospheric NO_2 over Iraq by the OMI opportunity to monitor urban emissions from space for the study pe-

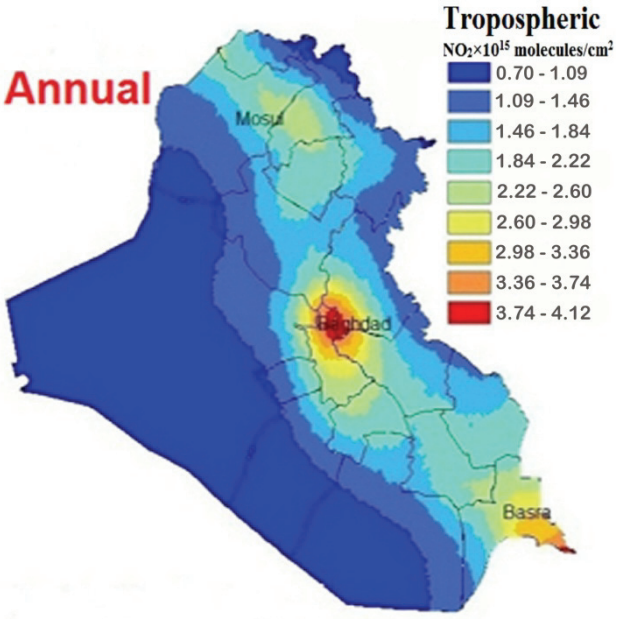

FIGURE 2. Annual mean distributions of tropospheric NO_2 over Iraq, produced by the global data of Aura OMI monthly mean tropospheric NO_2 during 2005–2014

riod. There is a reduction in the concentration of tropospheric NO_2 over western and south western parts of Iraq, less than ($1{\cdot}10^{15}$ molecules per 1 cm^2) due to arid desert areas where sand and lack of urban activity. Also the same reduction in the eastern region where the mountainous areas and high-rise mountain peaks, because of less population, urban and industrial activity. There is an increase on troposphere NO_2 values at the belt extended from the northern to the southern of Iraq, ranged from $1.46{\cdot}10^{15}$ to $2.22{\cdot}10^{15}$ molecules per 1 cm^2. The highest value was at central of Iraq, Baghdad and its sounding regions, more than $2.6{\cdot}10^{15}$ molecules per 1 cm^2. The hot spot of pollutions was over Baghdad city (up $3.74{\cdot}10^{15}$ molecules per 1 cm^2) due to high population, congestion, wide urban and industrial areas.

Monthly analysis long-term NO_2 data over Iraq

Figure 3 illustrated the average monthly NO_2 for winter and spring seasons (December–May) and for summer and autumn seasons (June–November), respectively, over study area for the period 2005–2014. The significant spatial variations of NO_2 observed over the most parts of Iraq. The NO_2 expertise diverse seasonal variations depend on the weather situations and topography. The seasonal fluctuation in the NO_2 varied highly noted among four seasons. A specific checking shows subtle changes in the NO_2 spatial types for each season, with higher values for NO_2 in the winter and summer than in the spring and autumn seasons. Also, increases in NO_2 values observed along the year above the manufacturing and crowded urban regions, i.e. Baghdad and Basra. A less NO_2 values happen at the clean desert environment over western and southwest areas, i.e. Anbar and Samawa.

Figure 3a illustrated the highest value of NO_2 occurred during the winter (January), especially at central region of Iraq over capital Baghdad and its surrounding areas. Because of the high precipitation rates, which reach to (240 mm), increased the microbial activity that contribute to more soil emissions due to the agricultural fields activities, and the reduction of removing NO_2 by photolysis process because of less solar radiation at existence of clouds. In January NO_2 increased to its highest value throughout the year at Baghdad was $5.13{\cdot}10^{15}$ molecules per 1 cm^2 (red pixels), though it lightly decrease to moderate in March, compare to past months, and low in May. The lowest value was over authentic desert environment over western areas on April $0.92{\cdot}10^{15}$ molecule per 1 cm^2 (blue pixels). This variations in the NO_2 concentrations during this period (December–May) caused by the human activity, geographic species of the regions and weather fluctuations.

As shown in Figure 3b for the summer and autumn seasons (June–November), a decrease in the NO_2 values during September and October, whereas lightly elevate to moderate concentrations of NO_2 in August and November, and high in June and July. There was a rising of NO_2 concentrations on the southeastern area compared to its measurements on the rest of the areas during June to September. These are because of the emissions by the oil extraction and residues burning in the paddy fields. The highest value placed in this period was over Baghdad

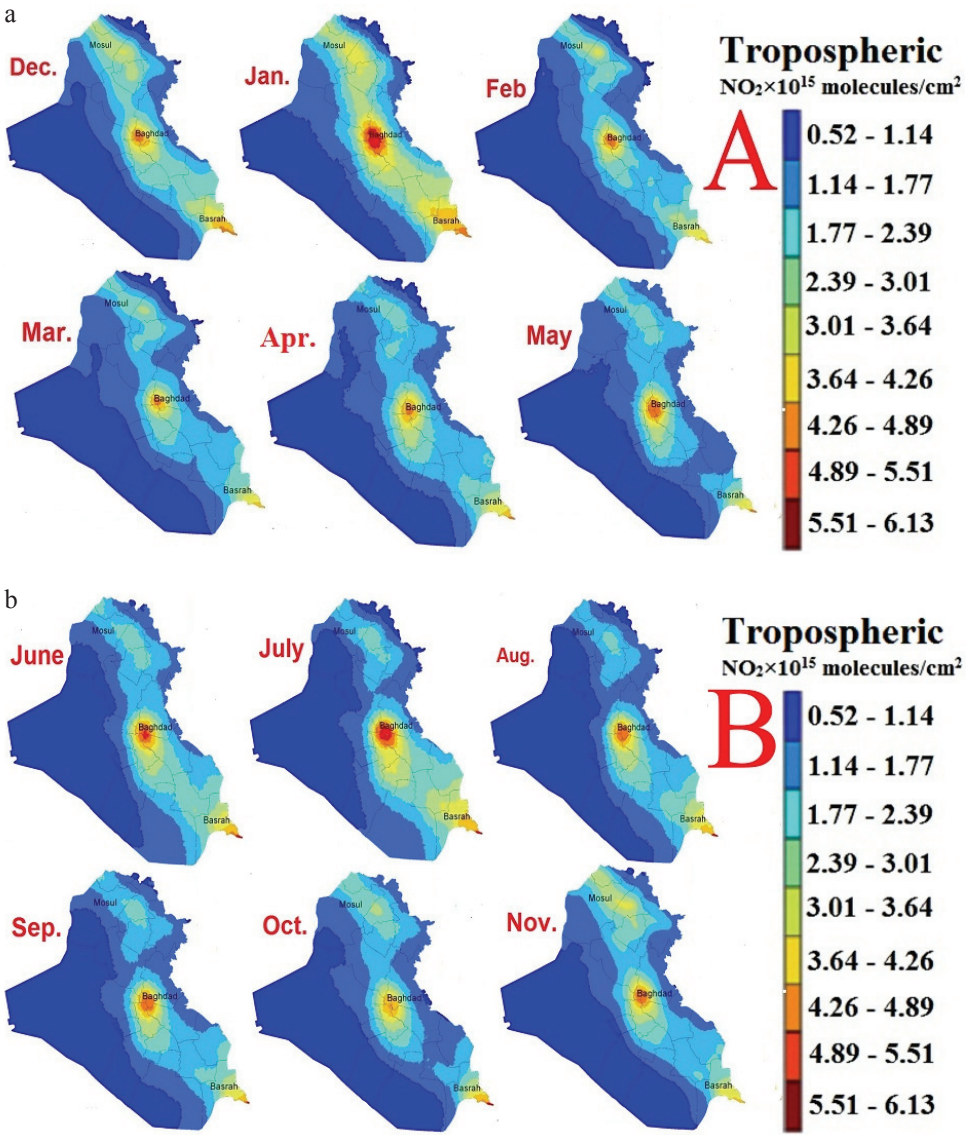

FIGURE 3. The OMI monthly coverage retrieved NO_2 in Iraq for the period of 2005–2014: a – for winter and spring seasons (December–May); b – for summer and autumn seasons (June–November)

during July $4.61 \cdot 10^{15}$ molecules per 1 cm^2 (red pixels), and the minimal value was in October $0.83 \cdot 10^{15}$ molecules per 1 cm^2 (blue pixels) at the western region. The high levels of NO_2 appeared in summer months due to the long hour's use of civil and commercial generators because of electrical power shortage with average ranges from 12 to 18 h through the summer days. It is one of the main reasons for increasing the levels of NO_2 during this period.

Trend analysis long-term NO_2 data over Baghdad city

The high density of population (1,637 persons per 1 km^2), and high population growth from 4.5 million in 2003 to 7.6 million peoples in 2013 (The Ministry of Planning internal report 2014); Baghdad is the economic and administrative centre in Iraq. Moreover, the frequent presence of electric generators in residential due to the lack of electric power, commercial, and industrial neighbourhoods increase the pollution. In addition, the considerable increasing of vehicles from 450,000 in 2003 to 1,350,000 in the year 2014, making it the largest city in Iraq and the second largest city in the Arab world after Cairo. A significant NO_2 emission hotspot observed during the study period.

Figure 4 shows the average monthly NO_2 for capital Baghdad from January 2005 to December 2014, the formal peak of OMI sensitivity and the vastness of the seasonal changes in troposphere NO_2. The seasonal oscillations depend on weather's situations and topography. The seasonal fluctuation in the troposphere NO_2 varied appreciably observed between winter and spring seasons. A more appointed checking shows subtle alteration in the NO_2 spatial influence for each season, with maximum values for NO_2 in the winter. Seasonal fluctuations are visible, but none is as declared or regular through the study period. The highest value existed in this period was on during January ($6.13 \cdot 10^{15}$ molecules per 1 cm^2) and the lowest value was during April ($4.2 \cdot 10^{15}$ molecules per 1 cm^2). There was evaluation in NO_2 values during July, August and October. Such exemplary seasonal cycle is because of the longer lifetime of NO_x through the cooling period, elevated local NO_x emissions from the domestic heating system (with odd behaviour in July) and repeated events of calm and

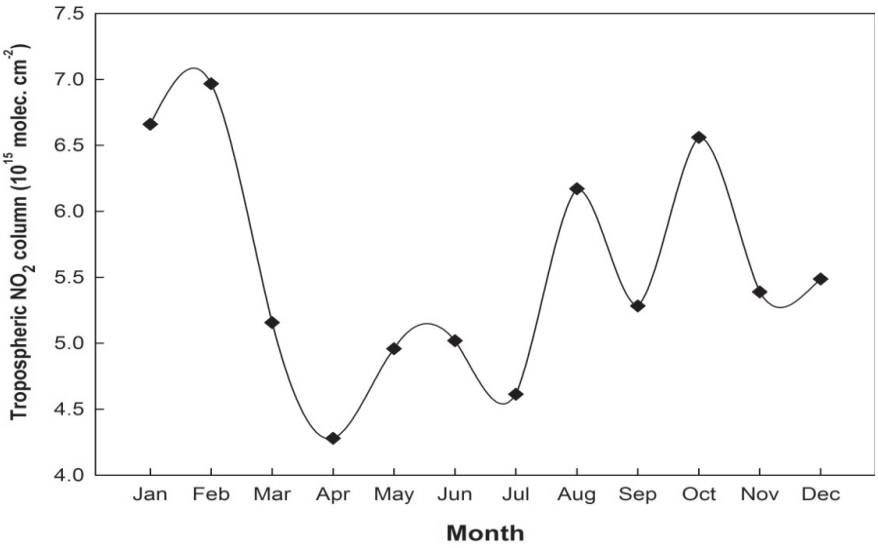

FIGURE 4. Monthly average tropospheric NO_2 variations over Baghdad in the period of 2005–2014

temperature inversion, facilitating the cumulating of pollutants during winter time surface air.

The resulting trend estimate for monthly average tropospheric NO_2 column over Baghdad provides a linear growth rate 9.8% per year (growth is the percentage calculated with respect to the mean NO_2 column, $5.71 \cdot 10^{15}$ molecules per 1 cm^2, as shown in the Figure 5. There is a progressive increase in the NO_2 values with distinct growth rate variations observed during the study period. An increasing, long-term trend in NO_2 attributed to the human activity; combustion of fossil fuels and a significant net flux of NO_2 to the atmosphere because of land use changes, such as agricultural activities in the paddy fields. Year-to-year variations in NO_2 emissions relatively increased because of different sources, comprising agricultural, motor vehicles and other manufacturer sources.

The mean, minimum and maximum annual NO_2 are presented in Figure 6, which present a graph of a month-long series of the NO_2 from the mean (solid line and square mark), minimum (solid line and circular mark), and maximum (dotted line) for hotspot over Baghdad city in the period from January 2005 till December 2014. Observed a stagnation feature as obvious during 2005 until 2009, and then increased significantly the rest of the study period. This due to increase of anthropogenic emissions and large economic activities in Baghdad, leading to rapid increase of tropospheric NO_2. To reach the highest levels 1.8, 2.3, 2.8 times for minimum, annual mean and maximum values compare to 2005 values.

Finally, the influences of air mass transportation on controlling of tropospheric NO_2 concentration investigated. Baghdad city selected as hotspot point, 24-hour backward and forward trajectory analysis employing NOAA HYSPLIT (hybrid signal-particle Lagrangian integrated trajectory) model at 500 m and 3,000 m above ground level. The trajectories observed for 8 November 2013

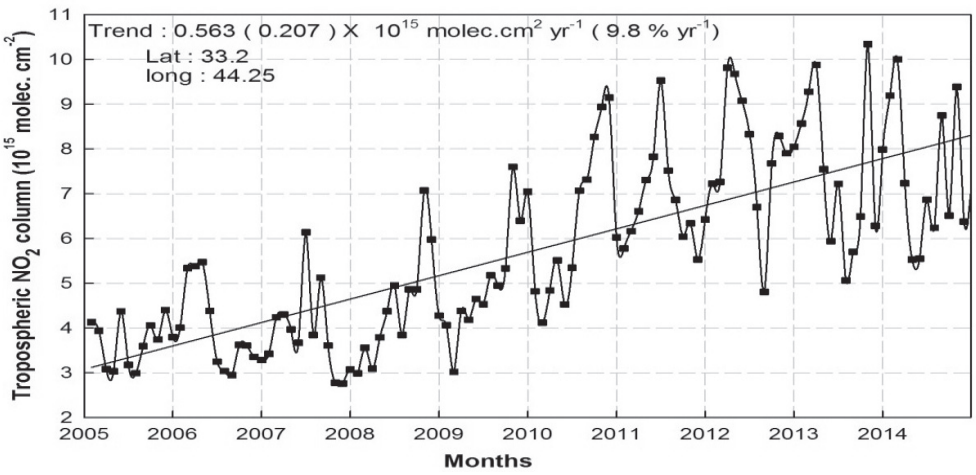

FIGURE 5. Time series of monthly mean tropospheric NO_2 over Baghdad for the period from January 2005 to December 2014

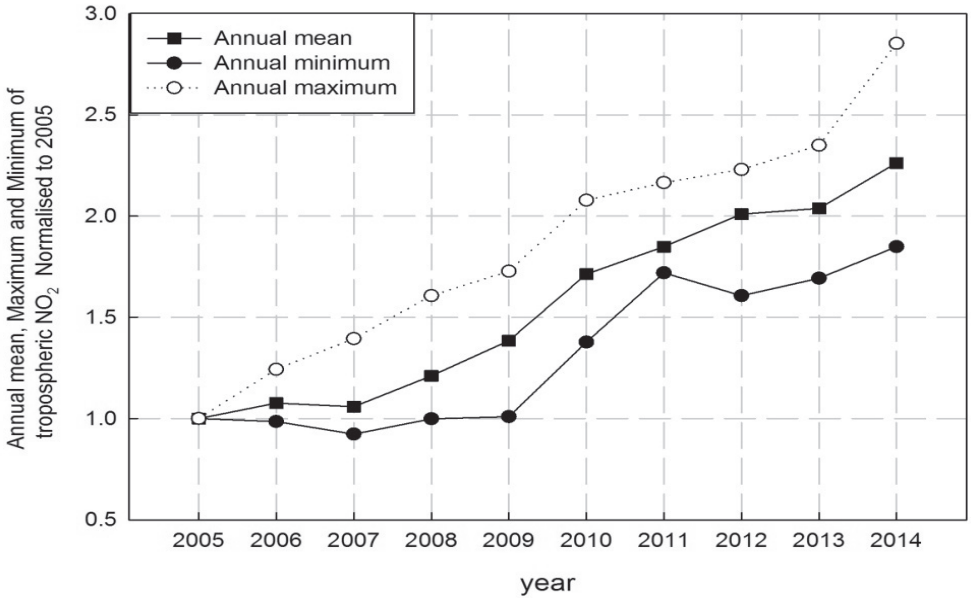

FIGURE 6. Observed the mean (solid line and square mark), minimum (solid line and circular mark), and maximum (dotted line) temporal evolutions of tropospheric NO_2 in the period of 2005–2014 for Baghdad

shown in Figure 7 at 500 m the ground level. Over Baghdad shown significant increasing trend of 9.8% per year and high values observed in winter and summer.

Trajectory analysis (Fig. 7) illustrate the seasonal changes in the troposphere NO_2 vibrate highly between winter and summer seasons. In winter, the evaluations due to anthropogenic emission of thermal heating used excessively during cold season. In addition, the subsequent plumes contributed from Europe bring by northwesterly wind driven by the passage of a strong synoptically forced cold front. Whereas during summer, the high NO_2 because of hot weather, the local emissions affect from the oil extraction at central and southern regions. In addition, the emissions from large paddy fields and the substantial contribution of anthropogenic from Turkey and Europe carried by eastward wind. The lowest NO_2 values detected during the monsoon interval mostly related to the rains.

Conclusions and summary

Nitrogen dioxide recognized as one of the main pollutants that degrade air quality. The objective of this study was to analysis the NO_2 distributions over Iraq. We have start to examine the fortune information contained in the more than ten-year (2005–2014) satellite data. The NO_2 concentrations strongly correlated with weather situations. From annual NO_2 distributions, there is a reduction in tropospheric NO_2 over western and south western parts of Iraq, less than $1{\cdot}10^{15}$ molecules per 1 cm^2, and the same

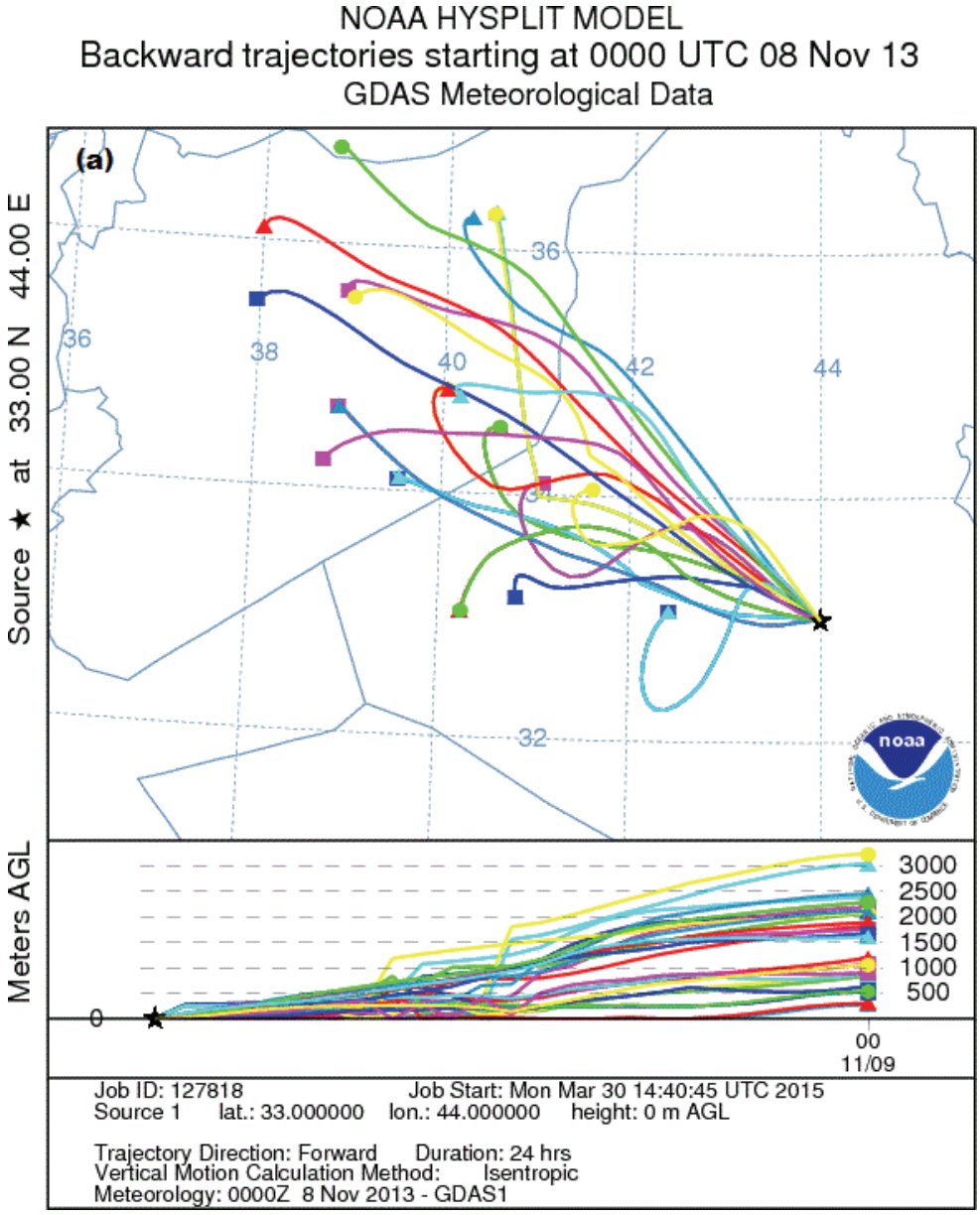
NOAA HYSPLIT MODEL
Backward trajectories starting at 0000 UTC 08 Nov 13
GDAS Meteorological Data
(a)
Source ★ at 33.00 N 44.00 E
Meters AGL
36
38
40
42
44
34
32
3000
2500
2000
1500
1000
500
0
00
11/09
noaa
Job ID: 127818 Job Start: Mon Mar 30 14:40:45 UTC 2015
Source 1 lat.: 33.000000 lon.: 44.000000 height: 0 m AGL
Trajectory Direction: Forward Duration: 24 hrs
Vertical Motion Calculation Method: Isentropic
Meteorology: 0000Z 8 Nov 2013 - GDAS1

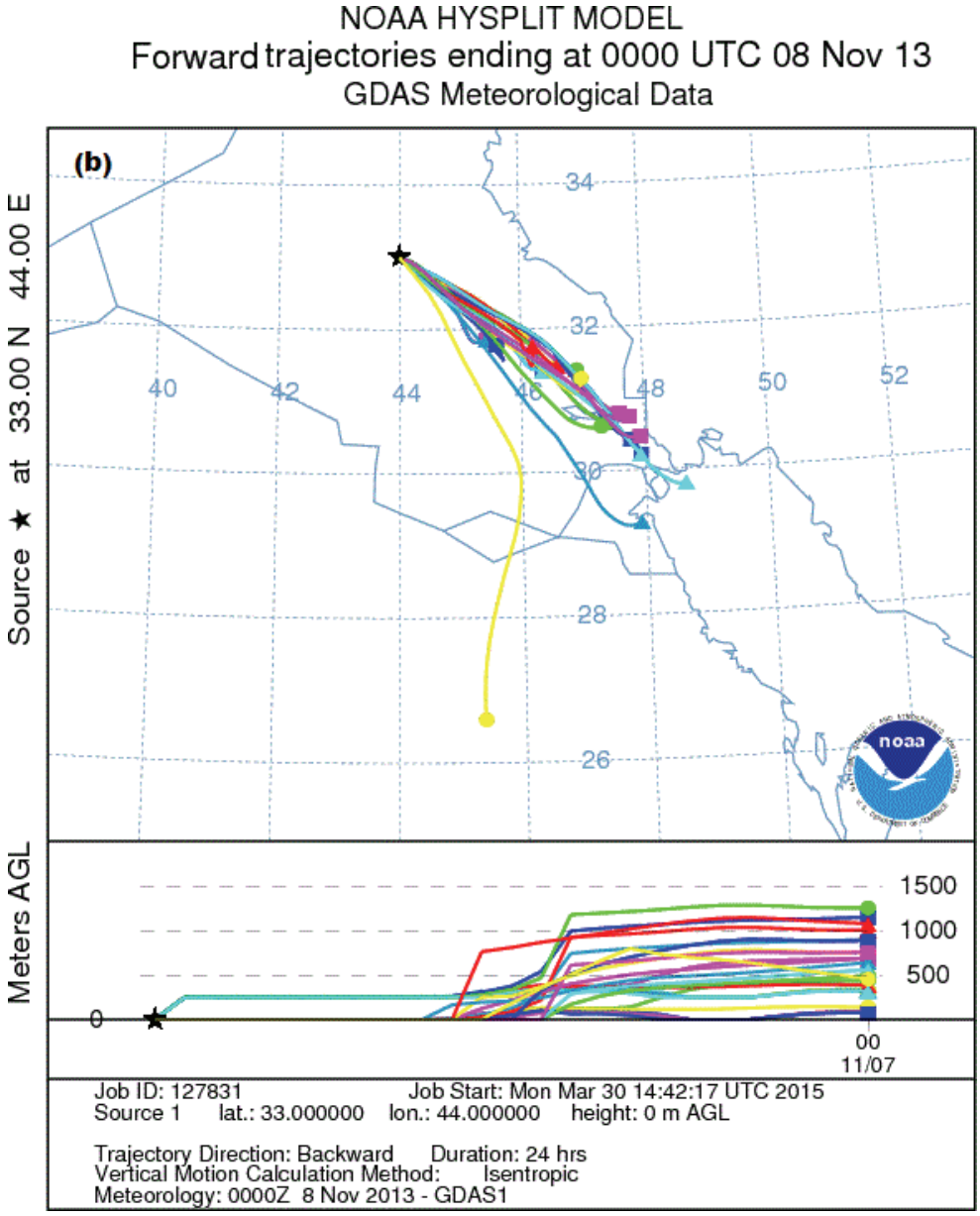

FIGURE 7. Twenty four-hour backward and forward air mass trajectories hotspots for Baghdad on 8 November 2013 at 00:00 UTC above 500 m, calculated using NOAA's hybrid single particle Lagrangian integrated trajectory – HYSPLIT model – GDAS (the hot spot marked with stars): a – backward trajectories; b – forward trajectories

reduction in the eastern region where the mountainous areas and high-rise mountain peaks. There is an increase on troposphere NO_2 values at the belt extended from the northern to the southern of Iraq, ranged from $1.46 \cdot 10^{15}$ to $2.22 \cdot 10^{15}$ molecules per 1 cm^2. The highest value was more than $2.6 \cdot 10^{15}$ molecules per 1 cm^2 at central of Iraq. The hot spot of pollutions was over Baghdad city (up $3.74 \cdot 10^{15}$ molecules per 1 cm^2).

The monthly distributions shows significant spatial variations of NO_2 detected over the most parts of Iraq and a different of seasonal variations depend on the weather situations and topography. The higher concentrations for NO_2 in the winter and summer than in the spring and autumn seasons, and the elevation in NO_2 values noted during the year over the manufacturing and crowded urban regions. The variation in the NO_2 values on December–May period due to the human activity, geographic nature of the areas and weather variations. While during June–November period, the highest value was on July at Baghdad $4.61 \cdot 10^{15}$ molecules per 1 cm^2, and the less value in October $0.83 \cdot 10^{15}$ molecules per 1 cm^2, at the western region. The resulting trend estimate over Baghdad for monthly average tropospheric NO_2 column provides a linear growth rate 9.8% annually. Long-term trend in NO_2 attributed to the human activity; combustion of fossil fuels and a significant net flux of NO_2 to the atmosphere. Trajectory analysis illustrate the seasonal variation in the troposphere NO_2 varied appreciably observed between winter and spring seasons. The lowest NO_2 values was during the monsoon period mostly related to the rains. The OMI data and the satellite measurements are can measure the elevations of the troposphere NO_2 concentrations above different areas.

Acknowledgements

The authors gratefully acknowledge the National Aeronautics and Space Administration (NASA) Goddard Earth Sciences Data Information and Services Centre (DISC) for the provision of the Ozone Monitoring Instrument (OMI) data utilized in this paper.

References

Abed, F.G., Al-Salihi, A.M., Rajab, J.M. (2018). Spatiotemporal monitoring of methane over Iraq during 2003-2015: retrieved from Atmospheric Infrared Sounder (AIRS). *ARPN Journal of Engineering and Applied Sciences*, *13*(22), 8650-8663.

Al-Salihi, A.M. (2017). Impact of precipitation on aerosols index over selected stations in Iraq using remote sensing technique. *Modelling Earth Systems and Environment*, *3*(3), 861-871.

Al-Salihi, A.M. (2018). Characterization of aerosol type based on aerosol optical properties over Baghdad, Iraq. *Arabian Journal of Geosciences*, *11*(20), 633. https://www.doi.org/10.1007/s12517-018-3944-1

Al-Salihi, A.M., Rajab, J.M. & Salih, Z.Q. (2019). Satellite monitoring for Outgoing Longwave Radiation and Water Vapor during 2003--2016 in Iraq. *Journal of Physics: Conference Series*, *1234*(1), 012009. https://doi.org/10.1088/1742-6596/1234/1/012009

Beirle, S., Platt, U., Wenig, M. & Wagner, T. (2003). Weekly cycle of NO_2 by GOME measurements: A signature of anthropogenic sources. *Atmospheric Chemistry and Physics, 3*(6), 2225-2232.

Burrows, J.P., Weber, M., Buchwitz, M., Rozanov, V., Ladstätter-Weißenmayer, A., Richter, A., DeBeek, R., Hoogen, R., Bramstedt, K., Eichmann, K.U., Eisinger, M. & Perner, D. (1999). The global ozone monitoring experiment (GOME): Mission concept and first

scientific results. *Journal of the Atmospheric Sciences*, *56*(2), 151-175.

Chan, K., Hartl, A., Lam, Y., Xie, P., Liu, W., Cheung, H.M., Lampel, J., Pöhler, D., Li, A., Xu, J., Zhou, H.J., Ning, Z. & Wenig, M.O. (2015). Observations of tropospheric NO_2 using ground based MAX-DOAS and OMI measurements during the Shanghai World Expo 2010. *Atmospheric Environment*, *119*, 45-58.

Constantin, D.E., Voiculescu, M. & Georgescu, L. (2013). Satellite observations of NO_2 trend over Romania. *The Scientific World Journal*, *2013*, 261634. https://doi.org/10.1155/2013/261634

Cui, Y., Zhang, W., Bao, H., Wang, C., Cai, W., Yu, J. & Streets, D.G. (2019). Spatiotemporal dynamics of nitrogen dioxide pollution and urban development: Satellite observations over China, 2005–2016. *Resources, Conservation and Recycling*, *142*, 59-68.

Ladstaetter-Weissenmayer, A., Burrows, J.P. & Perner, D. (1998). Biomass burning over Indonesia as observed by GOME. *Earth Observation Quarterly*, *58*, 28.

Levelt, P.F., Oord, G.H. van den, Dobber, M.R., Malkki, A., Visser, H., Vries, J. de, Stammes, P., Lundell, J.O.V. & Saari, H. (2006). The ozone monitoring instrument. *IEEE Transactions on Geoscience and Remote Sensing*, *44*(5), 1093-1101.

Lin, J.T., Martin, R.V., Boersma, K.F., Sneep, M., Stammes, P., Spurr, R., Wang, P., Van Roozendael, M., Clémer, K., Irie, H. (2014). Retrieving tropospheric nitrogen dioxide from the Ozone Monitoring Instrument: effects of aerosols, surface reflectance anisotropy, and vertical profile of nitrogen dioxide. *Atmospheric Chemistry and Physics*, *14*(3), 1441-1461.

Metz, H.C. (1993). *Area Handbook Series: Persian Gulf States Country Studies*. Washington: Library of Congress Washington DC Federal Research Division.

Molina, M.J. & Molina, L.T. (2004). Megacities and atmospheric pollution. *Journal of the Air & Waste Management Association*, *54*(6), 644-680.

Rajab, J.M., Jafri, M.Z.M., Lim, H.S. & Abdullah, K. (2012). Regression analysis in modeling of air surface temperature and factors affecting its value in Peninsular Malaysia. *Optical Engineering*, *51*(10), 101702. https://doi.org/10.1088/1742-6596/1234/1/012009

Rajab, J.M., MatJafri, M. & Lim, H. (2014). Air surface temperature correlation with greenhouse gases by using airs data over peninsular malaysia. *Pure and Applied Geophysics*, *171*(8), 1993-2011.

Rao, P., Hutyra, L.R., Raciti, S.M. & Templer, P.H. (2014). Atmospheric nitrogen inputs and losses along an urbanization gradient from Boston to Harvard Forest, MA. *Biogeochemistry*, *121*(1), 229-245.

Salih, Z.Q., Al-Salihi, A.M. & Rajab, J.M. (2018). Assessment of Troposphere Carbon Monoxide Variability and Trend in Iraq Using Atmospheric Infrared Sounder During 2003--2016. *Journal of Environmental Science and Technology*, *11*, 39-48.

Yang, K., Carn, S.A., Ge, C., Wang, J. & Dickerson, R.R. (2014). Advancing measurements of tropospheric NO_2 from space: New algorithm and first global results from OMPS. *Geophysical Research Letters*, *41*(13), 4777--4786.

Zhang, W., Jiang, L., Cui, Y., Xu, Y., Wang, C., Yu, J., Streets, D.G. & Lin, B. (2019). Effects of urbanization on airport CO_2 emissions: A geographically weighted approach using nighttime light data in China. *Resources, Conservation and Recycling*, *150*, 104454. https://doi.org/10.1016/j.resconrec.2019.104454

Zyrichidou, I., Koukouli, M., Balis, D., Kioutsioukis, I., Poupkou, A., Katragkou, E., Melas, D., Boersma, K.F. & Van Roozendael, M. (2013). Evaluation of high resolution simulated and OMI retrieved tropospheric NO_2 column densities over Southeastern Europe. *Atmospheric Research*, *122*, 55-66.

Summary

Analysis of tropospheric NO_2 over Iraq using OMI satellite measurements. Tropospheric nitrogen dioxide (NO_2) is a trace gas with important impact on atmospheric chemistry, human health and a key pollutant in particular cities, measured from space since the mid-1990s by the GOME,

SCIAMACHY, OMI, and GOME-2 instruments. This study present ten years (monthly and yearly averaged) dataset from Ozone Monitoring Instrument (OMI) used to investigate tropospheric NO_2 characteristics and variations over Iraq during 2005–2014. Annual NO_2 shows an elevation from the northern to the southern and highest values was at central parts of Iraq. Monthly distributions revels higher values NO_2 in winter and summer than spring and autumn seasons, and rising NO_2 throughout study period over industrial and crowded urban zones. The trend analysis over Baghdad shows a linear growth rate 9.8% per year with an annual average ($5.6 \cdot 10^{15}$ molecules per 1 cm^2). The air mass trajectory analysis as hotspot regions shows seasonal fluctuations between winter and summer seasons depend on weather conditions and topography. The increased NO_2 values in winter are due to anthropogenic emissions and subsequent plumes from Europe. In addition, in summer because of hot weather and large paddy fields emissions. The lowest NO_2 value was at monsoon period mostly linked to the rains. The OMI data and satellite information are able to observe the troposphere NO_2 elevation at different regions.

Authors' address:
Ahmed S. Hassan
(https://orcid.org/0000-0002-0901-472X)
Mustansiriyah University
College of Science
Department of Atmospheric Sciences
Palestine Street, 46131 Baghdad, Iraq
e-mail: ahmed.s.atmsc@uomustansiriyah.edu.iq

Scientific Review – Engineering and Environmental Sciences (2020), 29 (1), 17–26
Sci. Rev. Eng. Env. Sci. (2020), 29 (1)
Przegląd Naukowy – Inżynieria i Kształtowanie Środowiska (2020), 29 (1), 17–26
Prz. Nauk. Inż. Kszt. Środ. (2020), 29 (1)
http://iks.pn.sggw.pl
DOI 10.22630/PNIKS.2020.29.1.2

Izabela SÓWKA, Marcin PAWNUK, Agnieszka GRZELKA, Anna PIELICHOWSKA

Faculty of Environmental Engineering, Wrocław University of Science and Technology

The use of ordinary kriging and inverse distance weighted interpolation to assess the odour impact of a poultry farming plant

Key words: odour nuisance, field olfactometry, GIS, kriging, IDW

Introduction

Rearing and breeding of livestock is often a source of a negative odour impact and can be a cause of odour nuisance (Grzelka, Sówka & Miller, 2018), with poultry farming being the most common cause of people's complaints about odorous air quality (Kośmider, Mazur-Chrzanowska & Wyszyński, 2012). Therefore, for many years in Poland work on the regulation of the legal issues related to the excessive odour emission associated with the operation of, among others, animal husbandry is underway. As a result of the taken actions, in 2019 the Ministry of the Environment has developed a project proposal called Anti-odour Act – A draft act on the minimum distance for planned projects of the agricultural sector, the functioning of which may be associated with the risk of odour nuisance (Ministerstwo Środowiska, 2019). The document defines the minimum distance of locating emerging agricultural sector projects from residential buildings or public facilities depending on the breeding stocking size. However, it does not indicate emission standards for odours or odorants characteristic for this type of activity and does not refer to existing facilities. For the EU Member States, best available techniques conclusions (Commission Implementing Decision (EU) 2017/302), created as a result of the reference document on best available techniques for intensive poultry and pigs breeding, are an important legislative tool. Best available techniques conclusions are a set of legally binding recommendations created for the needs of breeders. They refer to large farms

with > 40,000 poultry stands. They indicate the need to create, implement and regularly review the odour management plan. For facilities that may cause a risk of odour nuisance, they recommend the use of countermeasures, i.e. end-of-pipe methods or special recommendations regarding animal nutrition and maintenance, and for newly emerging facilities they suggest maintaining appropriate distances from sensitive facilities, e.g. residential buildings (Commission Implementing Decision (EU) 2017/302).

Many methods are used to assess the odour nuisance of agricultural facilities (in particular those dealing with animal husbandry). One of the most commonly used are sensory methods, including dynamic olfactometry and field olfactometry (Korczyński et al., 2011; Gębicki, Byliński & Namieśnik, 2016; Sówka, Pachurka, Bezyk, Grzelka & Miller, 2017b). In the latter case, the test results obtained at the measuring points can be used in the analysis of spatial distributions, which allow, among others assessment of variability of pollution concentrations and assessment of air quality (Wong, Yuan & Perlin, 2004; Sówka, Grzelka, Bezyk & Miller, 2017a; Núñez-Alonso, Pérez-Arribas, Manzoor & Cáceres, 2019).

GIS-based model tools are used, among others, in the study of odour dispersion based on measurement data obtained by dynamic olfactometry and measurement data from the so-called field inspections (Sówka et al., 2017a, 2017b). However, there have been no attempts to perform geostatistical analyses based on the results of odour concentration measurements by field olfactometry. The aim of the study is to assess the suitability of the use of ordinary kriging and the inverse distance weighted method as potential ways of spatial data interpolation in analyses of the odour impact of objects from the poultry (turkeys and chickens) farming, slaughter and cutting industries, using data obtained from measurements conducted with the sensory method, i.e. field olfactometry.

Methodology and research area

The area covered by the study lies within the administrative boundaries of a small town in western Poland, in the Lubuskie Voivodeship. The measurement area is adjacent to the plant involved in the breeding, slaughtering and cutting of poultry – turkeys and chickens. The plant covers an area of about 3 ha, on its territory there are production buildings, warehouse buildings, intended for among others feed storage, wastewater treatment plant and administrative and production building. Biologically degradable wastewater from office buildings and social rooms as well as from the slaughterhouse plant is discharged to the wastewater treatment plant. On the south-west, west and north-west sides, single and multi-family residential buildings are located within 20–300 m from the plant's borders. The plant is adjacent to the forest from the north, east and south, and then, at a distance of about 100 m, there are farmlands. Figure 1 shows the research area.

In order to estimate the odour concentration in the areas adjacent to the plant, field olfactometry measurements were carried out using a Nasal Ranger® portable field olfactometer. As part of the

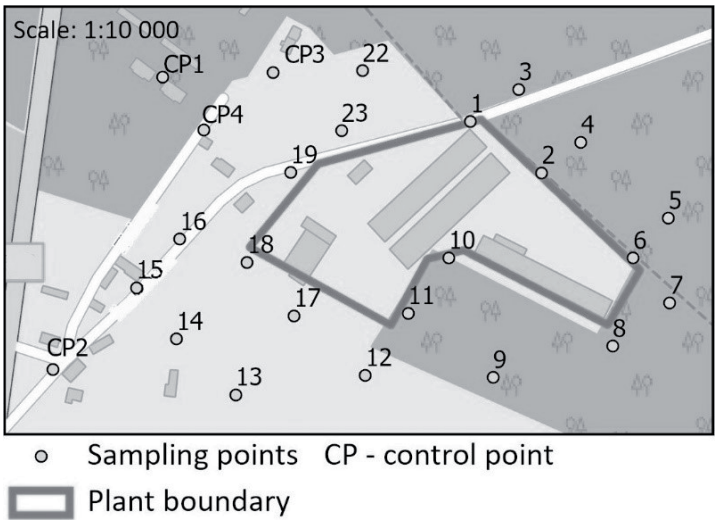

FIGURE 1. Map of the examined area with the location of the measuring points (OpenStreetMap, 2019)

study, measurements were carried out in two series: the first in the autumn–winter season (November 2018) and the second in the spring–summer season (May 2019). Table 1 summarizes the meteorological conditions recorded before the measurements were made for each series.

Taking into account the accessibility of the terrain and topographic conditions, a measuring grid with a 100 m step was created, consisting of 25 measuring points, of which four were control points coinciding with the places designated for earlier questionnaire surveys. The measurements were carried out by a team previously trained in the use of equipment and tested for olfactory sensitivity in accordance with the standard PN-EN 13725:2007. Each individual measurement was started with the intake and exhalation of air in the BLANK position for a period of 1 min, and then, starting from the D/T 60 value (dilution-to-threshold level), it was tested whether the odour was perceptible in the air. Between successive, decreasing dilutions, BLANK trials were presented. The measurement was completed when the odour was noted. The D/T values at which the odour was perceptible were used in further calculations of the odour concentration for

TABLE 1. Meteorological data

Parameter	Unit	Series 1 (November 2018)	Series 2 (May 2019)
Temperature	°C	–2.5	22.6
Relative humidity	%	54.5	47.3
Wind speed	$m \cdot s^{-1}$	2.5	1.9
Wind direction	–	NE	N

a given measuring point. The measurement results were entered into the protocol, in which the character of the identified odour was also noted. The obtained results of odour concentrations using field olfactometry were used for spatial analyses. Point measurement data has been transformed into a continuous surface using data interpolation methods. Two methods were used: the inverse distance weighted (IDW) and the ordinary kriging (OK).

The IDW method is an example of the commonly used deterministic method of interpolation of spatial data (Huisman & de By, 2009). With this method, values at unknown measurement points are calculated as a weighted average of known measurement points. Its main assumption is that each point has a certain impact on its surroundings (Sówka et al., 2017a). This impact decreases with distance. The IDW method is based on Tobler's law, which says that points that are closer together in time or space are more correlated with each other than those that are away from each other (Zhu, 2016). Thus, the closer the estimated points are to the known points, the higher the weight is assigned to them, the further away it is in space, the weight is lower. The spatial correlation described by Tobler's law is expressed by the following equations (Xie et al., 2017):

$$u(x,y) = \frac{\sum_{n=1}^{N} \frac{u_n(x_n, y_n)}{d_n}}{\sum_{n=1}^{N} \frac{1}{d_n}}$$

$$d_n = \sqrt{\left\{\left[(x - x_n)\right]^2 + (y - y_n)^2\right\}^i}$$

where:
$u(x, y)$ – value in an unknown location,
d_n – distance between points,
N – number of unknown locations,
i – exponential function, usually equal 2.

Kriging techniques belonging to geostatistical methods, similarly to the deterministic IDW method, predict values at unknown points based on weighted averages obtained from known measurement points, with the difference that they depend on the spatial variability of the studied data (Zhu, 2016). Spatial data variability is described by the phenomenon of autocorrelation, which allows determining statistical relationships between the analysed points (ESRI, 2016). Autocorrelation is based directly on Tobler's law mentioned earlier. Kriging methods are considered as best linear unbiased estimators. The OK method is considered as the standard kriging method, which assumes that the mean of data set is unknown (Zhu, 2016; Borkowski & Kwiatkowska-Malina, 2017). Using this method, values at unknown locations are calculated using the following equation (ESRI, 2016):

$$\hat{Z}(s_0) = \sum_{i=1}^{N} \lambda_i Z(s_i)$$

where:
$\hat{Z}(s_0)$ – estimated value,
s_0 – estimated point,
λ_i – weight for the point at i-th location,
$Z(s_i)$ – measured value at the i-th location.

The weights are calculated based on linear equations that assume the minimization of the expected data variability. To determine data variability, this meth-

od, like all techniques in this family, uses variogram analysis.

Cross-validation was performed to verify the correctness of the mentioned interpolation methods. This validation allows comparing and determining the quality of interpolations performed. It involves removing known measurement points from the data set and their estimation using a selected interpolation model. The differences between the measured and estimated values at these points are used to calculate useful statistics that allow the analysis of performed interpolations (Ding et al., 2018). The mean error and the root mean square error were the basic parameters used in validation of obtained interpolation results. The ME index was used for analysing interpolation errors, while the RMSE was used to compare interpolation quality.

Results and discussion

Table 2 summarizes the results of measurements carried out in two measuring series from all measuring points and the characteristic types of odours noted during field tests. The odour character was described in accordance with the odour descriptors contained in the Nasal Ranger® manual. The conducted measurements show that during the research performed in the autumn/winter season, the smell of poultry manure and smoky was characteristic, there were also woody and grain silage odours identified. However, during the spring/summer season, only the smell of poultry manure was noticeable in the field. The range of measured odour concentrations for the poultry manure odour, which is characteristic of the plant's production profile, was in the range of 4–78 ou·m^{-3} during the first measurement series and was recorded at seven measurement points, while in the second measurement series the range of the recorded concentration of odour for poultry manure was 2–78 ou·m^{-3} and was recorded at 11 measuring points. The maximum odour concentration in the first series for the character of the poultry manure odour was reported at measuring point 1 (78 ou·m^{-3}), and in series 2 at measuring points 1 and 3.

The odour concentration values obtained at the measuring points where the poultry manure odour was noted were used as input for the calculation of statistical surfaces representing the distribution of odour concentrations in the examined variants using the ordinary kriging (OK) method and the inverse distance weighted (IDW) method.

Figures 2–5 show the results of interpolation of measurement data obtained during the sampling campaigns with the use of dynamic olfactometry. Figures 2 and 3 show the results of the inverse distance weighted method for measurement series 1 and 2 respectively. Figures 4 and 5 show the results of surface modelling with the use of the ordinary kriging method for measuring series 1 and 2 respectively.

Interpolations carried out for selected scenarios allowed to obtain a spatial representation of given odour concentrations. Visualization of odour concentrations on the obtained distributions was presented using eight classes representing a given concentration level (from $\leq$ 10 to $\leq$ 80 ou$_E$·m^{-3}). The obtained distributions allow for spatial analysis of odour concentrations and allow for

TABLE 2. A summary of odour concentrations measured by field olfactometry at measuring points in the autumn–winter and spring–summer seasons

Measuring point	Latitude	Longitude	Odour concentration [ou·m^{-3}]	Odour descriptor	Odour concentration [ou·m^{-3}]	Odour descriptor
			series 1 (November 2018)		series 2 (May 2019)	
1	51.4473	15.1131	78	poultry manure	78	poultry manure
2	51.4469	15.1139	4	poultry manure	22	poultry manure
3	51.4475	15.1136	22	poultry manure	78	poultry manure
4	51.4471	15.1144	43	poultry manure	43	poultry manure
5	51.4466	15.1154	7	poultry manure	43	poultry manure
6	51.4463	15.1150	7	poultry manure	11	poultry manure
7	51.4459	15.1154	2	woody	43	poultry manure
8	51.4456	15.1147	BL*	–	43	poultry manure
9	51.4454	15.1133	4	burnt wood	7	poultry manure
10	51.4463	15.1128	BL	–	2	poultry manure
11	51.4459	15.1123	4	burnt wood	4	poultry manure
12	51.4454	15.1118	BL	–	BL	–
13	51.4453	15.1103	2	smoky	BL	–
14	51.4457	15.1096	BL	–	BL	–
15	51.4461	15.1092	2	smoky	BL	–
16	51.4464	15.1097	2	smoky	BL	–
17	51.4459	15.1110	2	smoky	BL	–
18	51.4462	15.1105	2	grain silage	BL	–
19	51.4469	15.1110	BL	–	BL	–
20 = CP4	51.4472	15.1100	BL	–	BL	–
21 = CP3	51.4476	15.1108	BL	–	BL	–
22	51.4476	15.1118	1,73	smoky	BL	–
23	51.4472	15.1116	1,73	smoky	BL	–
CP1	51.4476	15.1095	BL	–	BL	–
CP2	51.4455	15.1082	BL	–	BL	–

*BL – below the limit of quantification.

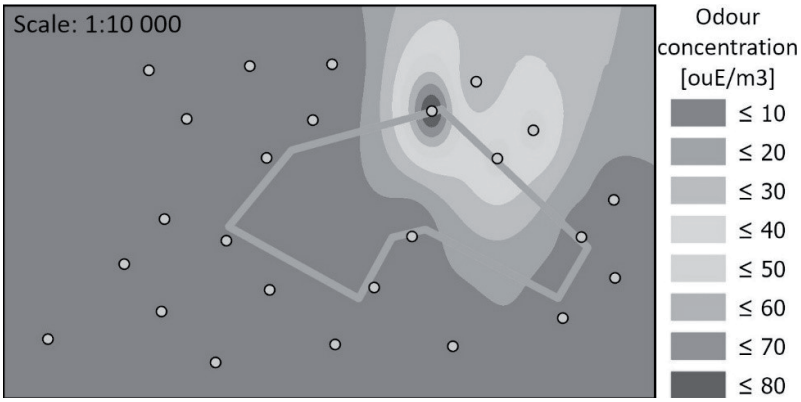

FIGURE 2. Spatial representation of odour concentrations using the IDW method for measurement series 1

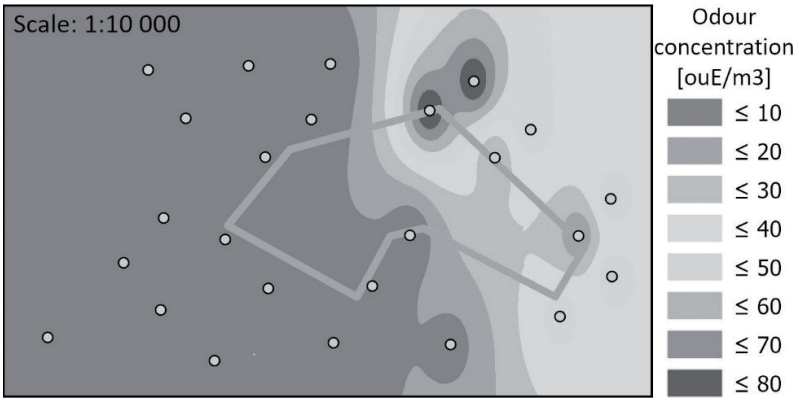

FIGURE 3. Spatial representation of odour concentrations using the IDW method for measurement series 2

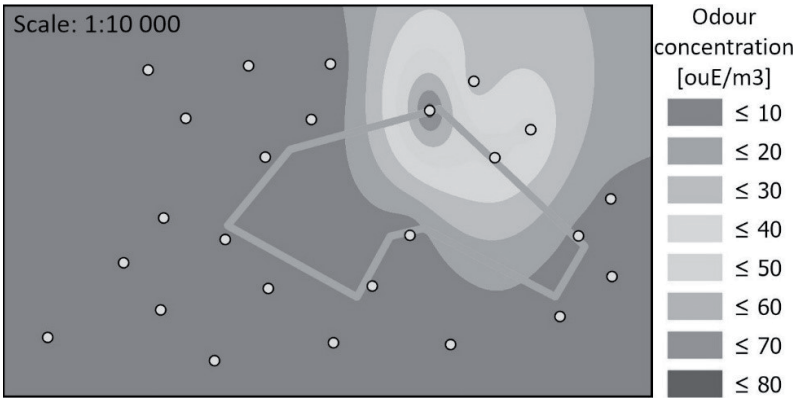

FIGURE 4. Spatial representation of odour concentrations using the OK method for measurement series 1

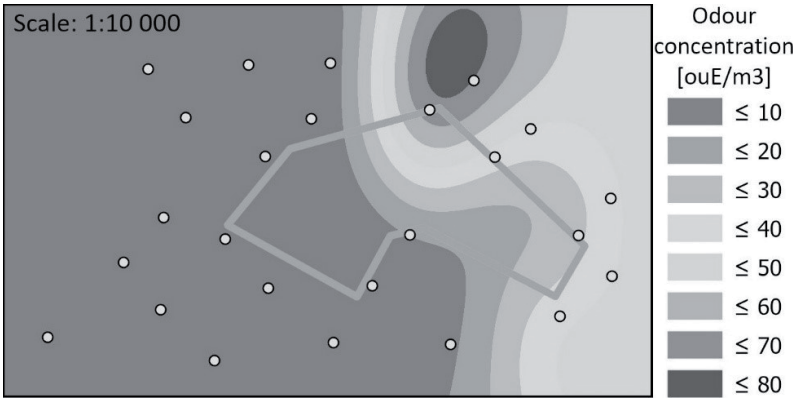

FIGURE 5. Spatial representation of odour concentrations using the OK method for measurement series 2

obtaining information on concentrations in places not covered by measurements during sampling campaigns. The visualization of IDW (Fig. 2) and OK (Fig. 4) method for series 1 are similar in terms of spatial distribution. The biggest visual difference can be found between IDW (Fig. 3) and OK (Fig. 5) during the second measurement series.

In order to validate the continuous surface modelling carried out, cross-validation was performed for all four variants. The validation results are summarized in Table 3.

Results gathered from the preformed cross-validation shows that the ME index, which allows the assessment of the average interpolation error, obtained the lowest values in the case of the first series of measurements for both methods (IDW: 0.17; OK: 0.21). The highest values were obtained in the second measurement series (IDW: –0.53; OK: –0.58). This indicator is largely dependent on the data analysed, therefore the differences in the cases taken into account are observed due to the differences in data variability between the two measurement series. Due to the fact that this indicator to compare data interpolation methods should be used when the RMSE parameters are equal (Ding et al. 2018), which did not take place in the analysed situations, the RMSE parameter was used as the main comparative indicator. The RMSE indicator was used to compare the models used in terms of interpolation quality and correct model matching. Lower values indicate higher quality of obtained interpolations (Ding et al., 2018). The lowest values of this indicator were obtained in the case of OK method, 14.47 and 14.20 for series 1 and 2. The IDW method is character-

TABLE 3. The cross-validation results for used interpolation methods (series 1 and 2)

Measure	IDW, series 1	IDW, series 2	OK, series 1	OK, series 2
ME	0.17	–0.53	0.21	–0.58
RMSE	14.82	16.33	14.47	14.20

ized by slightly higher values, in series 1 this indicator reaches the value of 14.82 while 16.33 in series 2 and it is the highest of all analysed cases. The order of the best match is: OK series 1 > OK series 2 > IDW series 1 > IDW series 2. Despite the fact that RMSE indicator was lower in case of kriging technique, in both cases values of RMSE were relatively high. The reason of that is the high spatial variability of input data, odour concentration used in interpolation techniques vary from 2 to 78 $ou_E \cdot m^{-3}$, which can cause increased prediction errors. To prevent that it is recommended to increase amount of sampling points during field olfactometry. When analysing obtained continuous surfaces (Figs. 2–5) it is clear that ordinary kriging gives better spatial visualization of odour concentration in the cases under consideration. Obtained visualization and values from cross-validation indicate possible application of ordinary kriging in spatial presentation of odour pollutants obtained from field olfactometry.

Conclusions

The obtained visualizations and the results of the cross-validation carried out for the method of weighted inverse distances and ordinary kriging indicate a potential better use of the ordinary kriging method in spatial modelling of continuous surfaces using measurement data obtained using field olfactometry. Due to high concentration variability, both methods were burdened with measurement errors obtained during cross-validation.

Acknowledgements

The research was co-financed with 0401/0058/18 statutory funds.

References

Borkowski, A.Sz. & Kwiatkowska-Malina, J. (2017). Geostatistical modelling as an assessment tool of soil pollution based on deposition from atmospheric air. *Geoscience Journal*, *21*(4), 645-653. https://www.doi.org/10.1007/s12303-017-0005-9

Commission Implementing Decision (EU) 2017/302 of 15 February 2017 establishing best available techniques (BAT) conclusions, under Directive 2010/75/EU of the European Parliament and of the Council, for the intensive rearing of poultry or pigs (notified under document C(2017) 688). OJ L 43/231 of 21.02.2017.

Ding, Q., Wang, Y. & Zhuang, D. (2018). Comparison of the commo spatial interpolation methods used to analyze potentially toxic elements surrounding mining regions. *Journal of Environmental Management*, *212*, 23-31. https://www.doi.org/10.1016/j.jenvman.2018.01.074

Environmental Systems Research Institute [ESRI] (2016). *How Kriging Works*. Retriev from: https://desktop.arcgis.com/en/arcmap/10.3/tools/3d-analyst-toolbox/how-kriging-works.htm [accessed: 08.03.2019].

Gębicki, J., Byliński, H. & Namieśnik, J. (2016). Measurement techniques for assessing the olfactory impact of municipal sewage treatment plants. *Environmental Monitoring and Assessment*, *188*(1), 32, 1-15. https://www.doi.org/10.1007/s10661-015-5024-2

Grzelka, A., Sówka, I. & Miller, U. (2018). Metody oceny emisji odorów z obiektów gospodarki hodowlanej. *Inżynieria Ekologiczna*, *19*(2), 56-64. https://www.doi.org/10.12912/23920629/86054

Huisman, O. & By, R.A. de (2009). *Principles of geographic information system, an introductory textbook*. 4th edn. Enschede: The

International Institute for Geo-Information Science and Earth Observation.
Korczyński, M., Opaliński, S., Sówka, I., Szołtysik, M., Cwynar, P. & Kołacz, R. (2011). Odour nuisance at pig farm. In Animal hygiene and sustainable livestock production. In *Proceedings of the 15th International Congress of the International Society for Animal Hygiene*, Vienna, 3-7.07.2011 (pp. 1139-1141). Brno: Tribun EU.
Kośmider, J., Mazur-Chrzanowska, B. & Wyszyński, B. (2012). *Odory* [*Odours*]. Warszawa: Wydawnictwo Naukowe PWN.
Ministerstwo Środowiska (2019). Projekt z dnia 28 marca 2019 r. Ustawa o minimalnej odległości dla planowanego przedsięwzięcia sektora rolnictwa, którego funkcjonowanie może wiązać się z ryzykiem powstawania uciążliwości zapachowej [A draft act on the minimum distance for planned projects of the agricultural sector, the functioning of which may be associated with the risk of odour nuisance]. Retrieved from: https://legislacja.rcl.gov.pl/docs//2/12321413/12579301/12579302/dokument387162.pdf [accessed: 21.08.2019].
Núñez-Alonso, D., Pérez-Arribas, L.V., Manzoor, S. & Cáceres, J.O. (2019). Statistical tools for air pollution assessment: multivariate and spatial analysis studies in the Madrid region. *Journal of Analytical Methods in Chemistry*, *9*, 1-9. https://www.doi.org/10.1155/2019/9753927
PN-EN 13725:2007. Jakość powietrza. Oznaczanie stężenia zapachowego metodą olfaktometrii dynamicznej [Air quality. Determination of odour concentration by dynamic olfactometry].
Sówka, I., Grzelka, A., Bezyk, Y. & Miller, U. (2017a). GIS-based modeling of odour emitted from the waste processing plant: case study. *E3S Web of Conferencess*, *17*, 1-8. https://www.doi.org/10.1051/e3sconf/20171700085
Sówka, I., Pachurka, Ł., Bezyk, Y., Grzelka, A. & Miller, U. (2017b). Application of field studies and geostatistical methods in assessment of odour nuisance based on selected examples from municipal, industrial and agricultural environments. *Ochrona Środowiska i Zasobów Naturalnyc*h, *28*(2), 16-21.
Wong, D.W., Yuan, L. & Perlin, S.A. (2004) Comparison of spatial interpolation method for the estimation of air quality data. *Journal of Exposure Analysis and Environmental Epidemiology*, *14*(5), 404-415.
Xie, X., Semanjski, I., Gautama, S., Tsiligianni, E., Deligiannis, N., Rajan, R.T., Pasveer, F. & Philips, W. (2017). A review of urban air pollution monitoring and Exposure Assessment Methods. *International Journal of Geo-Information*, *6*(12), 389. https://www.doi.org/10.3390/ijgi6120389
Zhu, X. (2016). *GIS for Environmental Applications: A practical approach*. London: Routledge.

Summary

The use of ordinary kriging and inverse distance weighted interpolation to assess the odour impact of a poultry farming plant. The aim of the study was to determine the usefulness of spatial data interpolation methods in analyses of the odour impact of animal husbandry facilities. The interpolation methods of data obtained from measurements using the field olfactometry technique were the ordinary kriging method (OK) and the inverse distance weighted method (IDW). The quality of the analyses that have been obtained indicates the potentially better use of the OK method in the presentation of spatial odour concentration distributions.

Authors' address:
Izabela Sówka
(https://orcid.org/0000-0001-9810-4673)
Politechnika Wrocławska
Wydział Inżynierii Środowiska
Zespół Inżynierii i Ochrony Atmosfery
pl. Grunwaldzki 9, 50-377 Wrocław
Poland
e-mail: izabela.sowka@pwr.edu.pl

Scientific Review – Engineering and Environmental Sciences (2020), 29 (1), 27–36
Sci. Rev. Eng. Env. Sci. (2020), 29 (1)
Przegląd Naukowy – Inżynieria i Kształtowanie Środowiska (2020), 29 (1), 27–36
Prz. Nauk. Inż. Kszt. Środ. (2020), 29 (1)
http://iks.pn.sggw.pl
DOI 10.22630/PNIKS.2020.29.1.3

Magdalena WRÓBEL[1], Justyna RYBAK[1], Wioletta ROGULA-KOZŁOWSKA[2]

[1]Wydział Inżynierii Środowiska, Politechnika Wrocławska
Faculty of Environmental Engineering, University of Science and Technology
[2]Instytut Inżynierii Bezpieczeństwa Pożarowego, Szkoła Główna Służby Pożarniczej w Warszawie
Institute of Fire Safety Engineering, The Main School of Fire Service

Przykłady wykorzystania testu OSTRACODTOXKIT F™ do oceny zanieczyszczenia pyłów drogowych metalami w aglomeracji wrocławskiej
The application of OSTRACODTOXKIT F™ test to assess metals contamination in road dust in Wrocław agglomeration

Słowa kluczowe: pył drogowy, metale ciężkie, toksyczność, ruch drogowy, małżoraczki, Wrocław
Key words: road dust, heavy metals, toxicity, traffic, ostracods, Wrocław

Wprowadzenie

Komponenty pyłu drogowego są ściśle zależne od składu gleby, emisji przemysłowych, depozycji składników spalin samochodowych, startej nawierzchni dróg i startych elementów samochodu takich jak opony samochodowe (Rogula-Kozłowska, Rogula-Kopiec & Majewski, 2014). Jako że pył drogowy składa się z tak wielu różnych składników (w dodatku występujących w różnych formach: stałej, ciekłej i gazowej), może być szczególnie niebezpieczny dla zdrowia i życia organizmów żywych, a także wpływać na stan środowiska naturalnego. Ważne jest też, że może on bardzo łatwo przedostawać się do jednolitych części wód za sprawą spływów powierzchniowych. Zanieczyszczony metalami ciężkimi i węglowodorami aromatycznymi pył drogowy przedostając się do wód, skaża osady denne, co ma negatywne konsekwencje dla biocenozy wodnej. Często prowadzi się więc badania dotyczące zawartości zanieczyszczeń

w pyłach drogowych oraz osadach dennych, ale zwykle polegają one jedynie na analizach chemicznych (Hwang, Fiala, Park & Wade, 2016). Doskonałym ich uzupełnieniem jest zastosowanie metod biologicznych (Soldner i in., 2004). Jedną z takich metod jest test toksyczności chronicznej OSTRACODTOXKIT F™, który użyto w prezentowanych badaniach. Polega on na badaniach rozwoju skorupiaków – małżoraczków *Heterocypris incogruens* (Ostracoda), które naturalnie zamieszkują osady denne (Shuhaimi-Othman, Yakub, Ramle & Abas, 2011). Toksyczność osadów dennych dla organizmów wodnych była często przedmiotem badań z wykorzystaniem tego testu, ale toksyczność pyłów drogowych, a konkretnie wymywanie pyłów do fazy wodnej i ich toksyczność wobec organizmów dennych, rzadko była badana (Watanabe, Nakajima, Kasuga & Furumai, 2013). Co więcej większość badaczy skupiła się na ocenie wpływu rozpuszczalnego ekstraktu organicznego, który może zawyżać wskaźniki biodostępności związków organicznych i wykluczać związki nieorganiczne jako substancje toksyczne (Watanabe, Nakajima, Kasuga & Furumai, 2011). Jak wiadomo, drobna frakcja pyłu z drogi jest uważana za główne źródło substancji toksycznych w wodzie (Watanabe i in., 2011). W Polsce nie badano wpływu wymytych pyłów drogowych na biocenozę wodną. Jednocześnie czystość i jakość wód są bardzo ważnymi aspektami oceny stanu środowiska (Wolf & Siedlecka, 2018), a testowanie toksyczności jest niezbędnym narzędziem do oceny wpływu i losu substancji toksycznych w ekosystemie wodnym i jest powszechnie wykorzystywane na całym świecie.

Podsumowując, celem prezentowanej pracy było wykazanie przydatności testów toksyczności z zastosowaniem organizmów dennych do oceny toksyczności pyłów drogowych, które są spłukiwane wraz z deszczem do wód, a w konsekwencji deponowane na wiele lat w osadach dennych, zagrażając biocenozie wodnej, a pośrednio też wpływając na jakość środowiska przyrodniczego i zdrowie ludzi.

Materiały i metody

Badania przeprowadzono w aglomeracji wrocławskiej, zarówno w centrum miasta, jak i na przedmieściach (rys. 1). Stanowiska, gdzie pobierano pył drogowy, różniły się intensywnością ruchu samochodów. Szczegółowy opis przedstawiono w tabeli 1.

Próbki były zbierane na przełomie kwietnia i maja 2018 roku. Uzyskane pyły przesiano przez sita w celu usunięcia większych zanieczyszczeń (do badań wykorzystano frakcję pyłu o średnicy mniejszej niż 63 μm). Aby otrzymać roztwory wodne, wysuszone próbki pyłu zmieszano z wodą w stosunku 1 : 2, następnie próbki trzymano w ciemności i odwirowano według procedury podanej przez Watanabe i innych (2013). Końcowym etapem przygotowania próbek było ich wytrząsanie przez 12 h.

RYSUNEK 1. Plan rozmieszczenia miejsc poboru próbek (źródło: Geoportal)
FIGURE 1. Map of sampling sites (source: Geoportal)

Test OSTRACODTOXKIT F™

Test ekspozycji małżoraczków na pyły drogowe przeprowadzono w formie sześciu powtórzeń. Zbadano ekstrakty wodne pyłów drogowych oraz próbki kontrolne, które stanowił osad referencyjny przygotowany zgodnie z procedurami operacyjnymi zestawu testowego MicroBiotest Inc., Belgia (OSTRACODTOXKIT F™). Początkowym etapem testu było przeprowadzenie wyklucia z jaj organizmów testowych (małżoraczków). W tym celu użyto inkubatora, gdzie utrzymywano stałą temperaturę 25°C oraz stałe oświetlenie. Inkubacja trwała 52 h. Po upływie 48 h przeprowadzono wstępne karmienie larw proszkiem zawierającym spirulinę. Testy przeprowadzono w sześciu powtórzeniach z użyciem płytek wielodołkowych zawierających mieszaninę 1 ml badanej próbki, 2 ml pożywki i 2 ml zawiesiny glonów. Następnie próbki inkubowano w ciemności w temperaturze 25°C przez

TABELA 1. Charakterystka stanowisk badawczych
TABLE 1. Basic characteristics of sampling sites

Miejsce pobierania próbek Sampling site	Współrzędne Coordinates	Opis Description	Natężenie ruchu pojazdów [średnia liczba pojazdów·$\cdot h^{-1}$] Traffic density [vehicles number averaged·h^{-1}]
Most Grunwaldzki	51°06'33.9"N 17°03'07.6"E	Most w centrum miasta przy drodze krajowej 94 w kierunku Warszawy. Okolica o bardzo intensywnym ruchu samochodowym	800
Legnicka	51°07'14.4"N 16°59'41.6"E	Ulica znajduje się w zachodniej części miasta i prowadzi w kierunku autostradowej obwodnicy Wrocławia (AOW). W pobliżu jedno z największych centrów handlowych w mieście. Okolica o bardzo intensywnym ruchu samochodowym	800
Oławska	51°06'28.1"N 17°02'24.9"E	Ulica zlokalizowana w centrum miasta, blisko rynku. Okolica o wzmożonym ruchu samochodowym	400
Obornicka	51°08'44.9"N 17°01'20.7"E	Ulica na północy miasta. Jest to trasa wylotowa w kierunku Poznania. Okolica o wzmożonym ruchu samochodowym	300
Gliniana	51°05'39.6"N 17°01'57.1"E	Ulica znajduję się na południu miasta przy drodze krajowej 98 w kierunku Bielan Wrocławskich i dalej na południe Polski. Okolica o wzmożonym ruchu samochodowym	300
Bielany Wrocławskie	51°02'55.5"N 16°57'01.6"E	Przedmieścia Wrocławia (na południowy wschód od miasta). Znajduje się tam wiele fabryk (przemysł rolno-spożywczy) i centrów handlowych. Okolica o bardzo intensywnym ruchu samochodowym	700
Maślice	51°09'03.1"N 16°57'00.2"E	Jedno z nowych osiedli Wrocławia położone na północnym zachodzie, nieopodal autostradowej obwodnicy Wrocławia i stadionu miejskiego. Okolica o niewielkim ruchu samochodowym	250
Radwanice	51°02'46.5"N 17°07'09.5"E	Przedmieścia Wrocławia na południowy wschód od miasta, przy drodze krajowej 94 w kierunku Opola i niedaleko wschodniej obwodnicy Wrocławia. Okolica o niewielkim ruchu samochodowym	200
Mirków	51°09'56.2"N 17°09'37.1"E	Przedmieścia położone na północny wschód od miasta, w odległości około 12 km, położona wzdłuż drogi krajowej 98 w kierunku południowym. Okolica o niewielkim ruchu samochodowym	100

6 dni. Po upływie tego czasu zliczono wszystkie żywe osobniki i zmierzono ich długość, używając szkiełka mikrometrycznego i mikroskopu stereoskopowego. Test toksyczności uznano za prawidłowo wykonany, gdyż spełnione zostały następujące kryteria w próbkach kontrolnych: procentowa śmiertelność małżoraczków nie przekroczyła 20%, a średnia długość organizmów wzrosła o współczynnik 1,5 w porównaniu do początkowej średniej długości (Niyommaneerat, Nakajima, Tobino & Yamamoto, 2017).

Analizy chemiczne

Oznaczono zawartość 12 pierwiastków: Mn, Ni, Cu, Zn, As, Rb, Sr, Ba, Cr, Mo, Mg, Al. W celu ich oznaczenia w pyle drogowym próbki suszono przez 48 h w temperaturze 50°C, następnie sortowano w celu usunięcia większych zanieczyszczeń, a potem zważono (0,3–0,7 g). Kolejnym etapem było trawienie próbek w mieszaninie 3 cm^3 HNO_3 (65%) i 1 cm^3 HF (40%) przez 6 min. Po tym czasie próby przeniesiono do kolb miarowych o pojemności 10 ml i zmierzono stężenia metali za pomocą płomieniowej spektrometrii atomowej z absorpcją z użyciem SpectrAA 880 (Varian) z lampami UltrAA. Stężenie metali w próbkach obliczono za pomocą wcześniej przygotowanych standardów Merck. Stężenie metali wyrażono w 1 ng metalu na 1 g suchej masy.

Wyniki i dyskusja

Próbki pyłów drogowych pobrane w centrum miasta oraz na terenach przemysłowych (przemysł rolno-spożywczy), tj. przy ul. Oławskiej i na Bielanach Wrocławskich, wskazują na silną toksyczność pyłów drogowych. Pył z Bielan Wrocławskich cechuje 100-procentowa śmiertelność małżoraczków,

TABELA 2. Wyniki testu OSTRACODTOXKIT F™
TABLE 2. Results of OSTRACODTOXKIT F™ test

Miejsce poboru próby Sampling site	Średnia długość organizmu, dzień 0 The average length of the body, day 0	Średnia długość organizmu, dzień 6 The average length of the body, day 6	Śmiertelność Mortality	Zahamowanie wzrostu Growth inhibition
	mm		%	
Kontrola	182	510	–	–
Most Grunwaldzki	191	300	0	76
ul. Legnicka	185	380	0	46
ul. Oławska	186	360	60	45
ul. Obornicka	196	370	0	44
ul. Gliniana	190	300	0	65
Bielany Wrocławskie	147	0	100	–
Maślice	154	470	0	15
Radwanice	199	470	0	18
Mirków	153	490	0	12

a z ul. Oławskiej 60-procentowa śmiertelność organizmów testowych. Śmiertelność na innych stanowiskach nie była obserwowana, chociaż odnotowano zahamowanie wzrostu małżoraczków, które wynosiło od 12 do 76% (tab. 2). Pył z ulic Legnickiej, Obornickiej i Glinianej cechuje stosunkowo duży procent zahamowania wzrostu małżoraczków (44–65%), co ma związek z dużym natężeniem ruchu w tych miejscach, gdyż są to drogi wylotowe miasta. Badania wykazały słabe zahamowanie wzrostu małżoraczków jedynie na przedmieściach Wrocławia (Radwanice, Maślice, Mirków). Ma to prawdopodobnie związek z mniejszym natężeniem ruchu na tych terenach, co zostało potwierdzone w obserwacjach. Badania prowadzone przez Watanabe i innych (2011) wykazały, że substancje toksyczne pochodzą głównie z ruchu drogowego. Z przeprowadzonych wcześniej testów toksyczności (Khanal, Furumai & Nakajima, 2014; Niyommaneerat i in., 2017) wynika, że czasami zróżnicowanie śmiertelności małżoraczków może być też spowodowane różnym czasem przechowywania bądź niejednorodnością próbek osadów, ponieważ drobne cząstki mogą akumulować wyższe stężenia substancji toksycznych niż cząsteczki piasku lub pyły gruboziarniste. Jednakże w omawianym przypadku czas przechowywania nie miał wpływu na poziom toksyczności, gdyż próbki były przechowywane tylko kilka dni przed rozpoczęciem badań. Jeśli chodzi niejednorodność próbek, to badaniom poddano jedynie frakcję pyłu o średnicy mniejszej niż 63 µm, dlatego też można wykluczyć, że różnice śmiertelności mogły być spowodowane wymienionymi czynnikami.

TABELA 3. Stężenie metali w pyle drogowym na stanowiskach badawczych [ng·g^{-1}]
TABLE 3. Metal concentrations in road dust at sampling sites [ng·g^{-1}]

Miejsce poboru próby Sampling site	Mn	Ni	Cu	Zn	As	Rb	Sr	Ba	Cr	Mo	Mg	Al
Most Grunwaldzki	47,68	9,45	27,84	5,32	3,42	7,70	541,83	81,47	12,49	20,24	5643,5	5,68
ul. Legnicka	0,68	5,25	26,78	11,07	1,46	3,86	166,45	40,21	2,54	24,97	2839	3,81
ul. Oławska	153,28	6,27	15,23	1,43	2,09	10,52	180,40	52,45	1,83	19,23	3710	7,29
ul. Obornicka	34,50	4,12	4,25	1,64	0,77	3,09	136,92	43,32	2,86	19,61	4396	0,67
ul. Gliniana	1,53	12,29	56,89	11,34	4,02	19,82	350,94	34,48	5,17	19,76	3003	4,24
Bielany Wrocławskie	21,56	4,99	22,02	6,66	2,35	1,65	100,88	26,16	1,80	12,21	3073,5	3,83
Maślice	193,21	7,00	14,16	5,45	2,67	6,40	293,26	45,77	3,82	15,32	4440	2,73
Radwanice	7,76	8,61	15,33	1,95	3,97	2,60	103,28	22,99	4,25	17,48	3511,5	3,21
Mirków	51,25	7,96	23,88	9,00	3,67	6,54	1061,54	63,05	14,32	12,28	4538,5	5,70

Zawartość metali w ekstrakcie wodnym badanych pyłów drogowych przedstawiono w tabeli 3. Pył drogowy pobrany z mostu Grunwaldzkiego cechował się wysokimi stężeniami badanych pierwiastków w stosunku do innych stanowisk, stężenie manganu wynosiło 47,68 $ng \cdot g^{-1}$, miedzi 27,84 $ng \cdot g^{-1}$, strontu 541,83 $ng \cdot g^{-1}$, baru 81,47 $ng \cdot g^{-1}$ (w tym punkcie poboru odnotowano najwyższe stężenie tego pierwiastka), a stężenie magnezu wynosiło aż 5643,5 $ng \cdot g^{-1}$, co sugeruje, że ten pierwiastek może pochodzić głównie z pyłu nawiewanego (Zechmeister i in., 2006). Duża zawartość wymienionych pierwiastków w pyle drogowym pobranym w okolicy mostu Grunwaldzkiego znajduje potwierdzenie w szczególnie dużym natężeniu ruchu w tym miejscu, co znalazło bezpośrednie odzwierciedlenie w wynikach testu toksyczności na małżoraczkach. Zaobserwowano tam zahamowanie wzrostu badanej populacji skorupiaków na poziomie 76%. Pyły pobrane przy ul. Legnickiej cechuje z kolei duża zawartość miedzi, cynku, molibdenu i magnezu. Stężenie molibdenu osiągnęło tam wartość maksymalną (24,97 $ng \cdot g^{-1}$) w porównaniu z innymi stanowiskami. Molibden jest pierwiastkiem występującym w stopach, elektrodach i katalizatorach wykorzystywanych w procesie rafinacji ropy naftowej. Jak wynika z obserwacji odnośnie zahamowania wzrostu badanych organizmów, wpływ wymienionych pierwiastków nie był aż tak toksyczny, ponieważ odnotowano 46-procentowe zahamowanie wzrostu małżoraczków. Z kolei pył drogowy pochodzący z ul. Oławskiej okazał się bardziej toksyczny od tego zebranego przy ul. Legnickiej, ponieważ odnotowano tam 60-procentową śmiertelność skorupiaków przy jednoczesnym porównywalnym poziomie zahamowania ich wzrostu (pył z ul. Legnickiej powodował zahamowanie wzrostu na poziomie 46%, a z ul. Oławskiej na poziomie 45%). Jest to prawdopodobnie rezultat odnotowanych niższych stężeń metali ciężkich takich jak miedź, cynk czy molibden na tym stanowisku. Stwierdzono tam jednakże najwyższe spośród badanych stanowisk stężenie glinu (7,29 $ng \cdot g^{-1}$), co może wpływać na śmiertelność skorupiaków i świadczyć o toksycznym oddziaływaniu glinu na organizmy żywe. Glin w pyle drogowym może pochodzić m.in. z karoserii samochodowej. Na ul. Glinianej odnotowano z kolei maksymalne stężenie niklu (12,29 $ng \cdot g^{-1}$) oraz miedzi (56,89 $ng \cdot g^{-1}$). Stopy miedzi używane są do poprawy odporności na korozję i wytrzymałości części samochodowych, a nikiel może pochodzić ze spalania węgla, ropy, gazu lub z emisji przemysłowych (Chen, Lu, Li, Gao & Chang, 2014). Na tym stanowisku odnotowano również największą zawartość cynku spośród badanych pyłów, który może pochodzić ze zużycia opon samochodowych i z korozji ocynkowanych części samochodowych (Naderizadeh, Khademi & Ayoubi, 2016). Stwierdzone wysokie stężania tych metali znalazły także odzwierciedlenie w zahamowaniu wzrostu skrorupiaków, zaobserwowano stosunkowo duży procent zahamowania ich wzrostu (65%). Próbki pyłów drogowych pochodzące z przedmieść Wrocławia (Radwanice, Maślice, Mirków) zawierają stosunkowo niskie stężenia metali ciężkich w porównianiu z pyłami zebranymi w centrum miasta (most Grunwaldzki, ul. Oławska) oraz rejonach

o dużym natężeniu ruchu (ul. Legnicka, ul. Obornicka, ul. Gliniana, Bielany Wrocławskie). Znalazło to odzwierciedlenie w obserwacji wzrostu małżoraczków. Stwierdzono bowiem, że znajdujące się w próbkach pochodzących z przedmieść oraz obszarów o małym natężeniu ruchu drogowego skorupiaki nie dość, że wszystkie przeżyły eksperyment (śmiertelność na tych stanowiskach wynosiła 0%), to w małym stopniu miały zahamowany wzrost.

Wnioski

Stwierdzono, że pył drogowy może mieć istotny wpływ na zahamowanie wzrostu oraz żywotność małżoraczków. Badania wykazały, że na obszarach o dużym natężeniu ruchu (ul. Oławska i Bielany Wrocławskie) śmiertelność skorupiaków była znacząca. Pył drogowy charakteryzował się wysokimi stężeniami badanych pierwiastków na skrzyżowaniach i w obrębie głównych dróg (ul. Oławska, most Grunwaldzki, ul. Legnicka, ul. Obornicka), co bezpośrednio wpłynęło na rozwój skorupiaków. Pył drogowy zebrany na przedmieściach Wrocławia (Maślice, Radwanice, Mirków) nie powodował śmiertelności małżoraczków i tylko nieznacznie wpłynął na ich rozwój (zaobserwowano niewielkie zahamowanie wzrostu). Po przeprowadzeniu badań stwierdzono, że test toksyczności chronicznej na skorupiakach jest przydatny do oceny toksyczności pyłu drogowego, który jest spłukiwany z nawierzchni i wpływa na ekosystem wodny. Należy mieć na uwadze, że z tego typu pyłu mobilne formy metali i metaloidów migrują w dalszej kolejności do wód podziemnych i powierzchniowych. Szybka i prosta wskaźnikowa ocena toksyczności wymywanego pyłu jest więc narzędziem niezwykle przydatnym do oceny stopnia zanieczyszczenia wód na danym obszarze właśnie związkami metali pochodzącymi ze spływów powierzchniowych.

Literatura

Chen, H., Lu, X., Li, L.Y., Gao, T. & Chang, Y. (2014). Metal contamination in campus dust of Xi'an, China: A study based on multivariate statistics and spatial distribution. *Science of the Total Environment*, *484*, 27-35. https://doi.org/10.1016/j.scitotenv.2014.03.026

Hwang, H.M., Fiala, M.J., Park, D. & Wade, T.L. (2016). Review of pollutants in urban road dust and stormwater runoff: part 1. Heavy metals released from vehicles. *International Journal of Urban Sciences*, *20*(3), *334-360*. https://doi.org/10.1080/12265934.2016.1193041

Khanal, R., Furumai, H. & Nakajima, F. (2014). Toxicity assessment of size-fractionated urban road dust using ostracod *Heterocypris incongruens* direct contact test. *Journal of Hazardous Materials*, *264*, 53-64. https://doi.org/10.1016/j.jhazmat.2013.10.058

Naderizadeh, Z., Khademi, H. & Ayoubi, S. (2016). Biomonitoring of atmospheric heavy metals pollution using dust deposited on date palm leaves in southwestern Iran. *Atmosfera*, *29*(2), 141-155. https://doi.org/10.20937/ATM.2016.29.02.04

Niyommaneerat, W., Nakajima, F., Tobino, T. & Yamamoto, K. (2017). Development of a chronic sediment toxicity test using the benthic ostracod *Heterocypris incongruens* and their application to toxicity assessments of urban road dust. *Ecotoxicology and Environmental Safety*, *143*, 266-274. https://doi.org/10.1016/j.ecoenv.2017.05.011

Rogula-Kozłowska, W., Rogula-Kopiec, P. & Majewski, G. (2014). Udokumentowane skutki oddziaływania aerozolu atmosferycznego na środowisko. *Przegląd Naukowy – Inżynieria i Kształtowanie Środowiska*, *23*(3), 290-303.

Shuhaimi-Othman, M., Yakub, N., Ramle, N.A. & Abas, A. (2011). Toxicity of metals to a freshwater ostracod: *Stenocypris major*. *Journal of Toxicology*, *2011*, 136104. https://doi.org/10.1155/2011/136104

Soldner, M., Stephen, I., Ramos, L., Angus, R., Wells, N.C., Grosso, A., Crane, M. (2004). Relationship between macroinvertebrate fauna and environmental variables in small streams of Dominican Republic. *Water Research*, *38*(4), 863-874.

Watanabe, H., Nakajima, F., Kasuga, I. & Furumai, H. (2013). Application of whole sediment toxicity identification evaluation procedures to road dust using a benthic ostracod *Heterocypris incongruens*. *Ecotoxicology and Environmental Safety*, *89*, 245-251. https://doi.org/10.1016/j.ecoenv.2012.12.003

Watanabe,H.,Nakajima,F.,Kasuga,I.&Furumai,H. (2011). Toxicity evaluation of road dust in the runoff process using a benthic ostracod *Heterocypris incongruens*. *Science of the Total Environment*, *409*(12), 2366-2372. https://doi.org/10.1016/j.scitotenv.2011.03.001

Wolf, M. & Siedlecka, A. (2018). Variability of bacterial biofilms under environmental stress conditions in water supply networks – a review. *Transylvanian Review*, *36*(31), 1-15.

Zechmeister, H.G., Dullinger, S., Hohenwallner, D., Riss, A., Hanus-Illnar, A. & Scharf, S., 2006. Pilot study on road traffic emissions (PAHs, heavy metals) measured by using mosses in a tunnel experiment in Vienna, Austria. *Environmental Science and Pollution Research*, *13*(6), 398-405. https://doi.org/10.1065/espr2006.01.292

Streszczenie

Przykłady wykorzystania testu OSTRACODTOXKIT F™ do oceny zanieczyszczenia pyłów drogowych metalami w aglomeracji wrocławskiej. Zanieczyszczenia obecne w pyle drogowym, pochodzące z ruchu ulicznego takie jak WWA i inne związki organiczne czy metale ciężkie, są wymywane wraz z deszczem i dostają się do wód, ostatecznie kumulując się w osadzie dennym na wiele lat, tym samym zagrażając organizmom wodnym oraz istotnie wpływając na jakość wód. Aby zbadać wpływ tych związków na zdrowie organizmów żywych, nie wystarczą tylko rutynowe badania chemizmu wód i badania osadów dennych, ponieważ do tego celu bardziej nadają się organizmy żywe. Z tego powodu chcąc poznać reakcję na tego typu zanieczyszczenia organizmów żywych, do badania toksyczności pyłów drogowych spłukiwanych z dróg po raz pierwszy w Polsce zastosowano test toksyczności chronicznej OSTRACODTOXKIT F™, który polega na obserwacji rozwoju *Heterocypris incongruens* naturalnie występującego w osadach dennych. Małżoraczki *H. incongruens* wykorzystane w badaniach są bardzo wrażliwe na zanieczyszczenie metalami ciężkimi, stanowią zatem odpowiednie narzędzie do badania toksyczności pyłu drogowego wymywanego do fazy wodnej. Badania prowadzono w aglomeracji wrocławskiej (w centrum miasta i na przedmieściach), na stanowiskach różniących się intensywnością ruchu drogowego. Stwierdzono, że pył drogowy ma istotny wpływ na zahamowanie wzrostu oraz żywotność małżoraczków, ponieważ na obszarach o dużym natężeniu ruchu drogowego ich śmiertelność była bardzo duża, co korespondowało z podwyższonymi poziomami stężenia badanych pierwiastków na tych stanowiskach badawczych. Z kolei pył drogowy zebrany na przedmieściach Wrocławia nie powodował śmiertelności małżoraczków i tylko nieznacznie wpłynął na ich rozwój. Podsumowując, stwierdzono, że test toksyczności chronicznej OSTRACODTOXKIT F™ jest odpowiednim narzędziem do badania wpływu pyłów drogowych na ekosystem wodny.

Summary

The application of OSTRACODTOXKIT F™ test to assess metals contamination in road dust in Wrocław agglomeration. Pollutants present in road dust deriving from traffic, such as PAHs and other organic compounds or heavy metals, are

washed out with rain and get into the water bodies accumulating in sediments for many years and simultaneously posing a threat to aquatic life and significantly affecting water quality. To study the impact of these toxic compounds on the health of living organisms, routine tests of water and sediments chemistry are insufficient as studies based on living organisms are much more reliable. And therefore, in order to know the response of living organisms to road dust pollutants which enter the water bodies the chronic toxicity test OSTRACODTOXKIT F™ was used. This test is based on the observation of development of *Heterocypris incongruens* that normally lives in sediments. Ostracod, *H. incongruens* is very sensitive to heavy metal contamination, thus it is a very good tool to study toxicity of road dust washed out with rain into the water bodies. The research was conducted in the Wrocław agglomeration (in the city centre and suburbs) at sites differing in the intensity of car traffic. We observed that road dust had a significant effect on growth inhibition and death of ostracods, as highest growth inhibition and mortality in the busy areas occurred which also corresponded with highest concentrations of studied elements at these sites. On the other hand, road dust collected in the suburbs of Wrocław did not cause death of *H. incongruens* and only slightly affected their development. In conclusion, we can state that the chronic toxicity test OSTRACODTOXKIT F™ is a suitable tool to study the impact of road dust on the aquatic ecosystem.

Authors' address:
Magdalena Wróbel
Justyna Rybak
(https://orcid.org/0000-0002-3606-4220)
Politechnika Wrocławska
Wydział Inżynierii Środowiska
ul. Wybrzeże Wyspiańskiego 27, 50-370
Wrocław
Poland

Wioletta Rogula-Kozłowska
(https://orcid.org/0000-0002-4339-0657)
Szkoła Główna Służby Pożarniczej w Warszawie
Instytut Inżynierii Bezpieczeństwa Pożarowego
ul. Słowackiego 52/54, 01-629 Warszawa
Poland
e-mail: wrogula@sgsp.edu.pl

Scientific Review – Engineering and Environmental Sciences (2020), 29 (1), 37–53
Sci. Rev. Eng. Env. Sci. (2020), 29 (1)
Przegląd Naukowy – Inżynieria i Kształtowanie Środowiska (2020), 29 (1), 37–53
Prz. Nauk. Inż. Kszt. Środ. (2020), 29 (1)
http://iks.pn.sggw.pl
DOI 10.22630/PNIKS.2020.29.1.4

Firas A. HADI[1], Basim ABDULSADA Al-KNANI[2], Rawnak Adel ABDULWAHAB[3]

[1] College of Energy and Environmental Sciences, Al-Karkh University of Science
[2] Collage of Science, Almustansiriyah University
[3] Ministry of Science and Technology, Remote Sensing Center

An assessment the wind potential energy as a generator of electrical energy in the coastal area of southern Iraq

Key words: wind energy, Basrah, wind speed analysis, wind potential

Introduction

Energy is the basis of the economic, social growth of countries, and is a measure of human development for all countries, including Iraq. The need for the energy sector, especially electric power, is constantly increasing, which in turn increases the demand for energy to meet these requirements (Keyhani, Ghasemi-Varnamkhasti, Khanali & Abbaszadeh, 2010). On the other hand, fossil fuels are considered to be depleted and non-renewable. It is therefore necessary to find new alternative and non-exhaustible energy such as wind energy. By the end of 2018 the overall output energy harvest from all wind turbines installed worldwide reached 600 GW, depending on the statistics published by WWEA (2009). Such that, about 54 GW were added in the year 2018, little more than year 2017 where about 53 MW were installed. The preceding amount of electricity generation represents a third largest number installed since the years 2015 and 2014. However, the recorded annual growth rate shows that the year 2017 has the most growing number with almost 11%. While 2018 represents the lowest growth in wind energy since the renewable industrial was begun at the end of 20th century (WWEA, 2009; Elmokadem, Megahed & Noaman, 2016). In Iraq there are many natural resources available in different geographical sources, most of these resources are distributed over large geographical area, which allows for a degree of flexibility in choosing locations (Kazem & Chaichan, 2012).

In recent years, many studies dedicated to study wind energy in Iraq. In 2007, Amani (2007) presented a study that included the possibility of using wind in power generation, the study included (18) stations distributed in different areas in Iraq. Firas (2014) presented a study that includes building a statistical-mathematical model for wind energy in Iraq using different Weibull distributions functions of wind data over five locations in Iraq. Ali (2014) presented a study to guess the best sites for erecting wind farms in southern Iraq using WAsP model. Abaas (2015) presented a comparative study of five numerical methods to estimate Weibull coefficients for wind applications in Iraq, and use three hourly wind speed data over 22 regions. Firas, Oudah and Al-Baldawi (2018) presented a feasibility study of wind power at Al-Shehabi site was conducted using measured wind data at different altitudes. Also, Kamal, Ali and Amani (2018) studied the possibility of erecting 2 MW wind turbine in the south of Iraq (Barjisiah site) utilizing WAsP model. Taghreed, Monim and Amani (2019) presented a wind speed and direction analysis by employing the fast Fourier transform (FFT) spectrum in Ali Al-Gharbi location in Iraq at three different heights. It is known, the abundance of wind in the coastal areas due to the lack of obstacles and roughness almost close to zero. Therefore, the aim of this study is to know the usefulness extent of use wind energy in Iraq coastal region.

Area of study

The study area is located in the southern part of Iraq, specifically in the province of Basra and bordered on the east by Iran and from the south side waters of the Gulf Coast and the south-west of Kuwait. The site was chosen as a coastal area overlooking the Arabian Gulf, so it is expected that its production of electricity generated from wind turbines is high due to the small surface roughness of the site. Figure 1 shows the area of study and can be described by geographical coordinates 268796.78m E, 3305314.19m N. Wind data are taken from the NASA Agency website for the period 1979–2016 with a time interval 10 min and taken at height of 50 m above the surface of the Earth (Earthdata, 2020).

FIGURE 1. Area of study (Google Earth, 2020)

Distribution of wind speed in Iraq

According to International Renewable Energy Agency (IRENA) wind atlas map it is possible to divided Iraq into three areas. The first area covered 85% from the total area and it possesses wind speeds that vary between 6–7 $m \cdot s^{-1}$. The second territory covered about 10% of total Iraq area and it possesses wind speeds that vary between 4–5 $m \cdot s^{-1}$. The third one covered about 5% of total Iraq area and possesses low wind speeds less than 4 $m \cdot s^{-1}$ (Fig. 2). The approximate wind power densities for all preceding areas at height of 100 m are as follows: 150–800, 75–150 $W \cdot m^{-2}$ and less (Fig. 3; Kazem & Chaichan, 2012; IRENA, 2015).

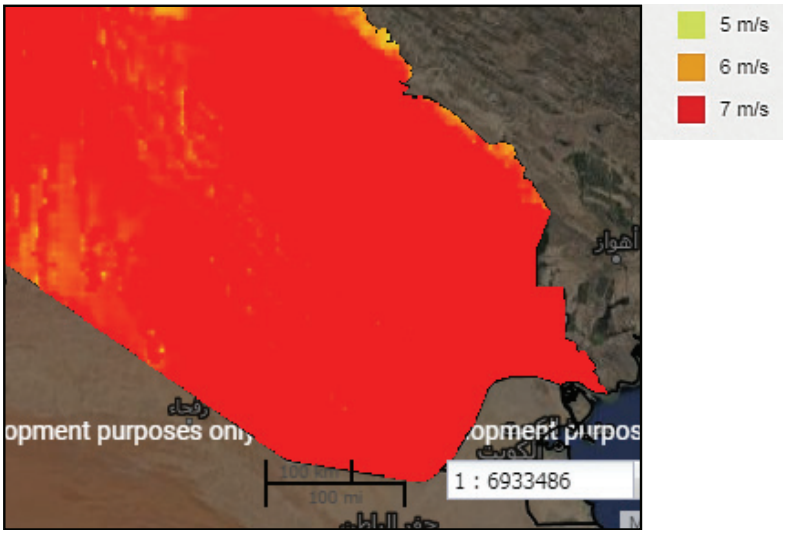

FIGURE 2. Wind speed classes in Iraq (IRENA, 2015)

The factors affecting the wind energy conversion systems (WECS) production at any given location over a certain period of time can be summarized as follows: (1) the power and energy produced by the turbine is determined by the different wind velocities; (2) the potential energy of wind regime and (3) the wind speed distribution and behaviour within the regime.

The total power produced by a wind turbine can be calculated over a specified period of time by adding the power corresponding to all wind velocities available in the regime where systems operate. Also, from probability density function belongs to different wind speed and wind turbine characteristics it is possible to make energy calculations. It is easy to determine the appropriate turbine type for that location by determining cut-in velocity, rated velocity, and the cut-out velocity. Thus, it is necessary to know the characteristics of the winds for a site in order to reach a conclusion on the possibility of investing wind energy for a particular site (Keyhani et al, 2010; Firas, 2014).

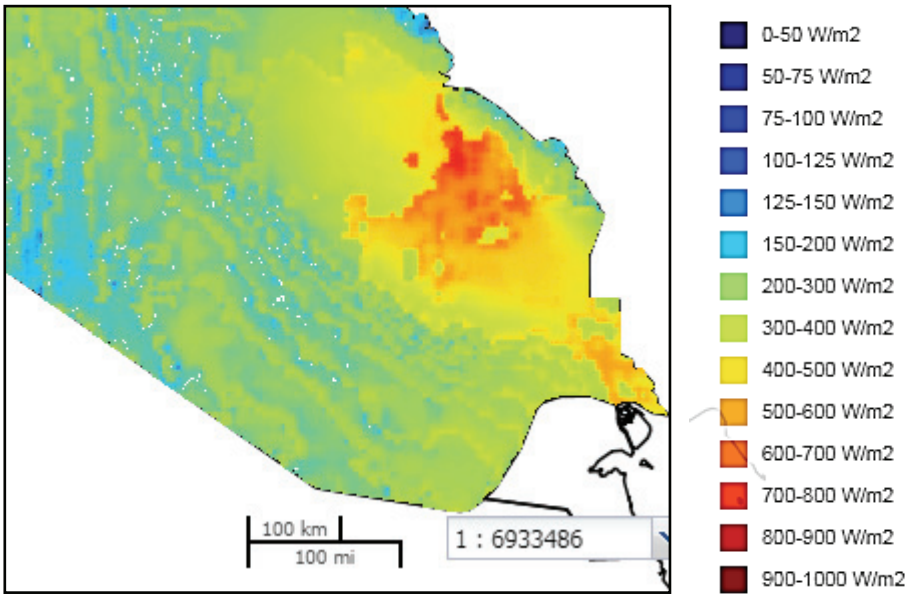

FIGURE 3. Wind power density in Iraq (IRENA, 2015)

Equivalent energy method (EEM)

This method uses a function optimization procedure based on the distribution energy content in order to obtain Weibull parameters which fit wind speed distribution. The wind speed probability which greater than a specific value (v), is defined by (Firas, 2014):

$$P_r(v) = e^{-\left(\frac{v}{c}\right)^k} \quad (1)$$

The probability of wind speeds ($P(v)$) greater than or equal to $v - 1$ and lower than v

$$P(v) = P_r(v-1) - P_r(v) \quad (2)$$

$$P(v) = e^{-\left(\frac{v-1}{c}\right)^k} - e^{-\left(\frac{v}{c}\right)^k} \quad (3)$$

Statistically, P_v represented a stochastic variable which can be defined as:

$$P_v = P(v) + \varepsilon = \left(e^{-\left(\frac{v-1}{c}\right)^k} - e^{-\left(\frac{v}{c}\right)^k} \right) + \varepsilon \quad (4)$$

Where ε corresponds to the stochastic term. The Weibull scale factor (c) can be written as:

$$c = \left(v_m^3 / \Gamma\left(1 + \frac{3}{k}\right) \right)^{1/3} \quad (5)$$

By substituting Eq. (5) in Eq. (4) it yields:

$$P_v = e^{-\left(\frac{(v_i-1)\left(\Gamma\left(1+\frac{3}{k}\right)\right)^{\frac{1}{3}}}{v_m}\right)^k} - e^{-\left(\frac{v_i\left(\Gamma\left(1+\frac{3}{k}\right)\right)^{\frac{1}{3}}}{v_m}\right)^k} + \varepsilon \tag{6}$$

Now, in order to find the Weibull shape factor (k), the least squares technique to the following expression can be estimated

$$\sum_{i=1}^{n}\left[P_{vi} - e^{\left(\frac{-(v_i-1)\left(\Gamma\left(1+\frac{3}{k}\right)\right)^{\frac{1}{3}}}{v_m}\right)^k} + e^{\left(\frac{-v_i\left(\Gamma\left(1+\frac{3}{k}\right)\right)^{\frac{1}{3}}}{v_m}\right)^k}\right]^2 = \sum_{i=1}^{n}(\varepsilon_i)^2 \tag{7}$$

where:
P_{vi} – probability of having wind speeds for i^{th} bin;
n – number of bins of the wind speed histogram;
v_i – the highest wind speed value of the for i^{th} bin;
v_m^3 – mean cube (observed).

After k is compute, the scale factor is calculated from Eq. (5).

Results and discussions

Wind speed analysis at height of 50 m

In contrast to solar energy, electrical energy production from wind is difficult to estimate. Wind energy depends on site characteristics and topography. Wind speeds can be significantly affected on the advantages of local topography. The description and classification of any area to high potential and extensive effort to classify the site of the study to low or high winds, where the speed and direction of the wind in severe shifts in most locations and require a detailed study of the spatial and temporal changes of wind speed values. Before locating the wind farm, monthly and daily wind speed distributions, wind speed distributions and wind power density should be analysed carefully (Amani, 2007).

Monthly wind speed

The monthly mean wind speed values at Basrah coast are presented in Figure 4 for duration time 37 years (from 1 January 1979 to 3 January 2016). By analysed mean wind speed data of 444 months, it can be inferred that the average wind speed distribution varies markedly from month to month. This figure also shows that the most monthly frequent mean wind speed values are between two values 5 and 6 $m \cdot s^{-1}$, but

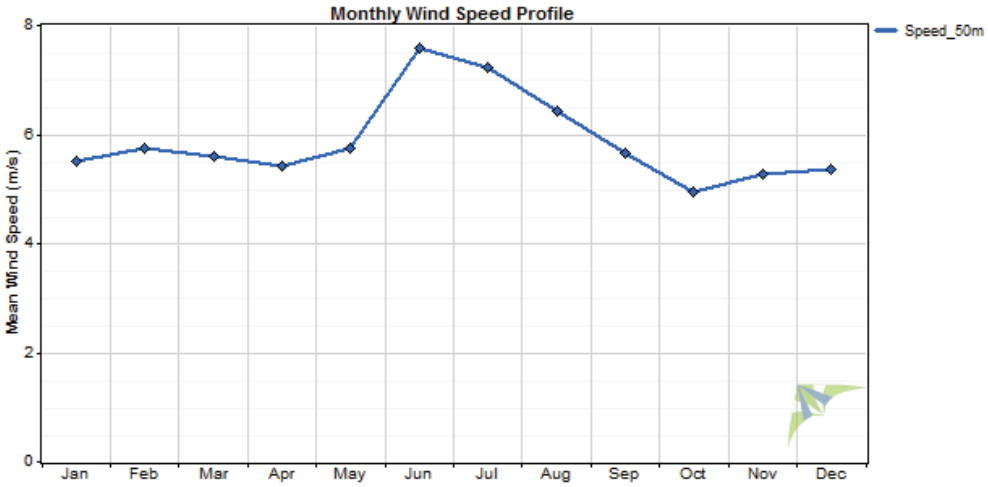

FIGURE 4. Monthly mean wind speeds

there are also mean wind speeds over than 6 $m \cdot s^{-1}$ by rate 25%, From other side, only a few mean wind speeds are over 7 and under 5 $m \cdot s^{-1}$ by rate 16 and 8% respectively. The highest mean wind speed value in June with 7.5 $m \cdot s^{-1}$, while the minimum mean wind speed value is observed in October with 4.9 $m \cdot s^{-1}$. In such a case, wind energy can be used to boost electricity.

Diurnal wind speed

Another important property of site characteristics which should be studied when preparing to any wind power project is the profile of daily wind regime at area of study. Figure 5 shows the change in daytime of mean wind speeds at height of 50 m above ground level (a.g.l.). From this figure, we can also find that the hourly mean wind speeds start in increasing gradually from 12 pm up to the highest value at 8 pm. Mean wind speeds then become decreasing, while from 4 am to 11 am wind speed will remain calm. This mean that at night time is almost windy through whole the year, while the daytime is quiet through whole the year.

Wind direction frequency

Wind direction calculations is important for conducting wind energy researches and wind farms geometry. Also, it displays the impact of geographical features on the wind. There are many ways used for wind direction charts representations one of these is shown in the polar chart (concentric circles) and the method of measurement is in degrees and the direction of rotation is clockwise. This diagram consist of 360° concentric cycles divided into 16 sections, each one of them included arc with 22.5°. In Figure 6, the wind direction and its frequency data are combined in the polar diagram for Basrah coast (the area of study) are presented for the period 1979–2016. It is clear that the prevailing trend of wind throughout this period is the northwest and within section 15 between 292.5° and 337.5°.

Also, it is convenient to study the average monthly occurrences of wind

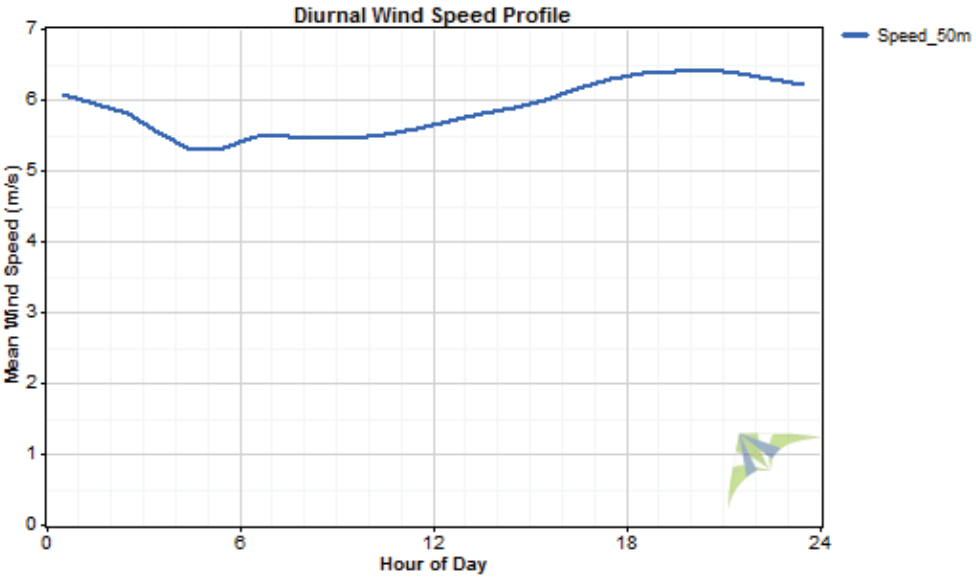

FIGURE 5. Daily mean wind speeds

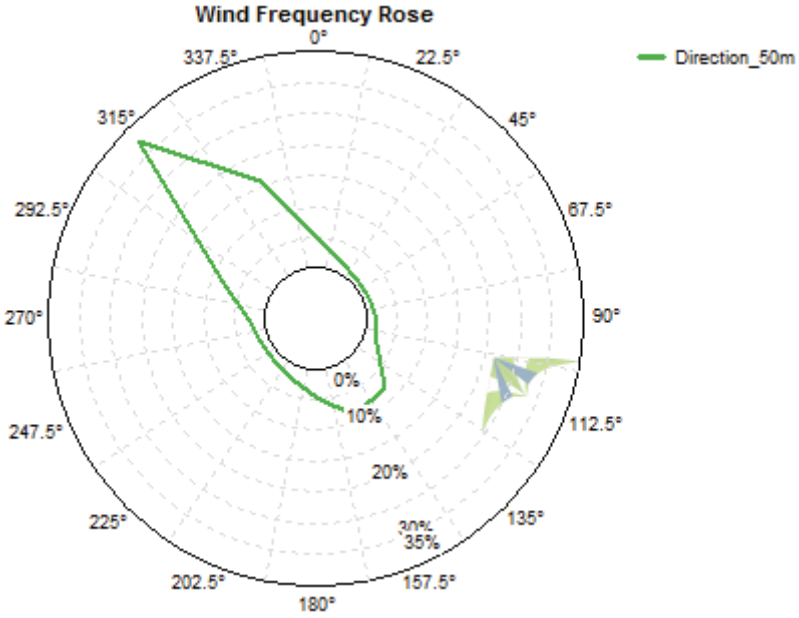

FIGURE 6. Polar diagram – wind direction at height of 50 m

speed blowing direction, this will give an idea of how the wind changes for different seasons. Figure 7 shows a comparison between different polar diagrams for the monthly average wind speed frequency and its relation with the direction

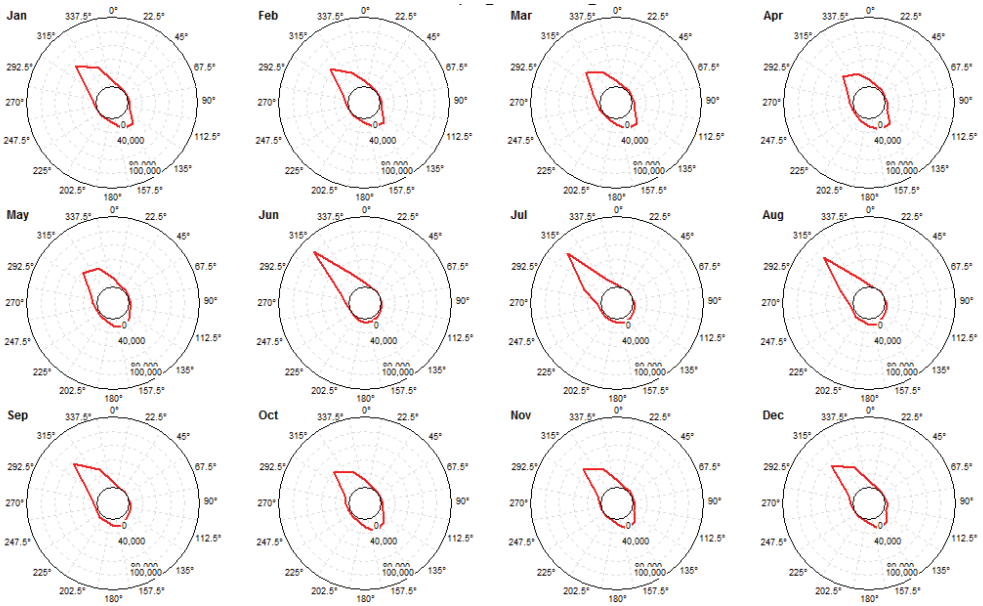

FIGURE 7. Occurrences of speed at height of 50 m versus wind direction

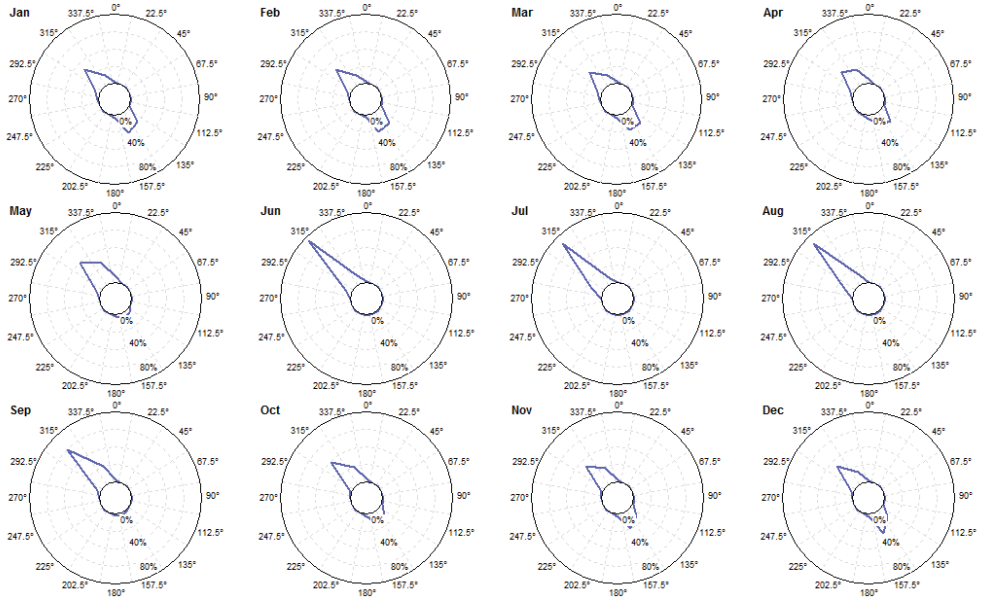

FIGURE 8. Proportion of total wind energy in speed at height of 50 m versus wind direction

from 1979 to 2016. The most probable wind direction for that period is at 315°, i.e. northwesterly winds. In the monthly polar diagrams, specifically in the most prevailing wind direction (northwest), wind frequency seems to be good. On the other hand, it should be noted that the prevailing wind frequency overall years ranges from 40–80%. The more stillness percentage is occurred at three months (June, July and August) which reach about 80%, while the less percentage is shown in April.

Also, it is convenient to study the relation between wind potential energy and wind direction. The average wind energy for each month from 1979 to 2016 as a relation with the direction of wind blow can be given in Figure 8. This figure have the same behaviour of Figure 7 and shows the wind energy percentage for each month. Jun has the most amount of energy, in other side, the dominant direction whole the year is northwest with little amount of energy for southeast direction except for June, July, August and September.

Wind speed analysis at different heights

The wind speed at height of 50 m is taken as a reference height, then it was adjusted and is estimated at different heights: 30, 70 and 100 m a.g.l. Wind speed is calculated using the power law (Firas, 2014):

$$v_2(z_2) = v_1(z_1)\left(\frac{z_2}{z_1}\right)^{\alpha} \tag{8}$$

v_2, v_1 – synthesized and reference wind speeds at elevations z_2 and z_1, respectively;
α – Hellmann exponent (friction or wind shear).

The Internatioximum values in June (about 8.3 $m \cdot s^{-1}$) at height of 100 m a.g.l., while at height of 30 m the wind speed will reach about 7 $m \cdot s^{-1}$ from other side, the wind speed reach the minimum value

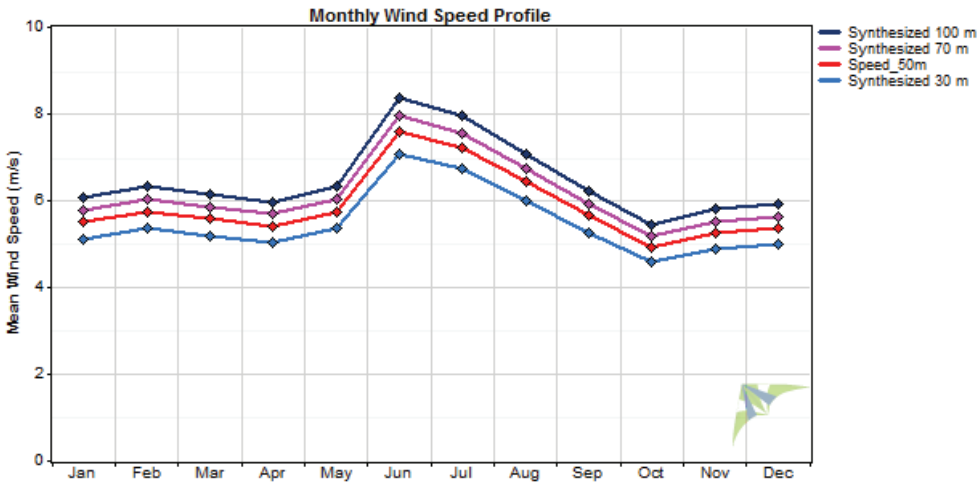

FIGURE 9. Monthly mean wind speed variation in Basrah in 1979–2016

in October, about 5.5 $m \cdot s^{-1}$ at height of 100 m a.g.l., while at height of 30 m the wind speed will reach about 4.5 $m \cdot s^{-1}$ (Fig. 9).

Diurnal wind speed profile

The mean daily wind speed behaviour for the year of study is very important in wind energy projects, its represents one of the facts that determine wind turbines. As in the previous section where the data taken from the source and at a height of 50 m were converted to different heights of 30, 70 and 100 m a.g.l., for our area of study (Basrah), daily wind speed variations are illustrated in Figure 10. From this figure it is possible to say that, at 10 am the wind speed at height of 50 m a.g.l. will increase gradually reaching to its maximum value 6.5 $m \cdot s^{-1}$ at around 8 pm, then wind speed will gradually decrease to its minimum value 5.3 $m \cdot s^{-1}$. The winds in this area are calm during the day time but it starts to increase in the evening, which gives an opportunity to invest solar energy during the day and wind energy at night.

Mean wind power density diurnal profile

Another important characteristic of the site is the diurnal variations for hourly average data (reference and estimated wind speed) along the study time at the Basra coast site is shown in Figure 1. Mathematically, the mean wind power density in terms of wind speed is calculated as (Firas, 2014):

$$PD_v = \frac{1}{2}\rho \sum_{i=1}^{n} \frac{v_i^3}{n} \tag{9}$$

where n is the total sample data for a period of time.

The comparison showed the daily patterns of the average wind speed in

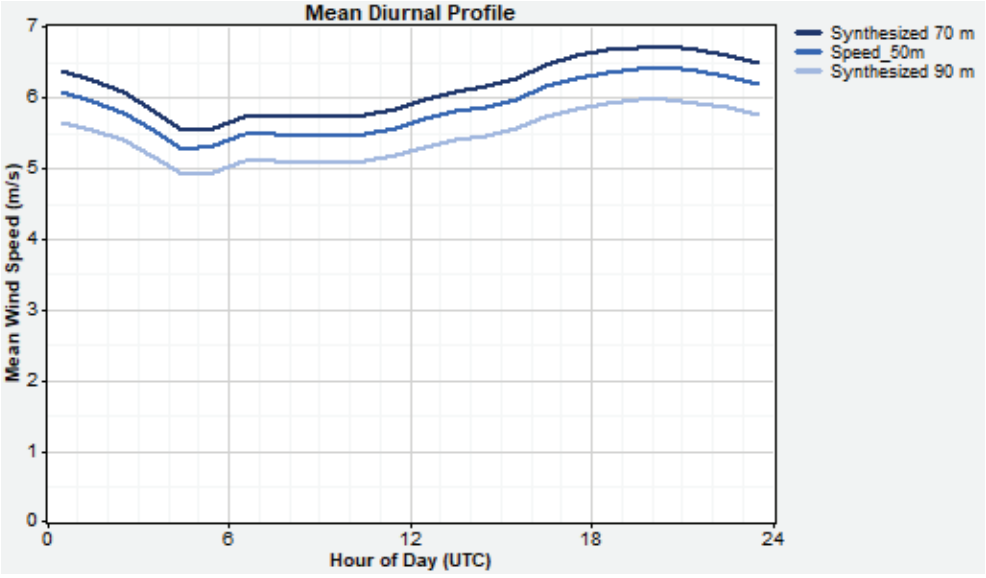

FIGURE 10. Diurnal mean wind speed

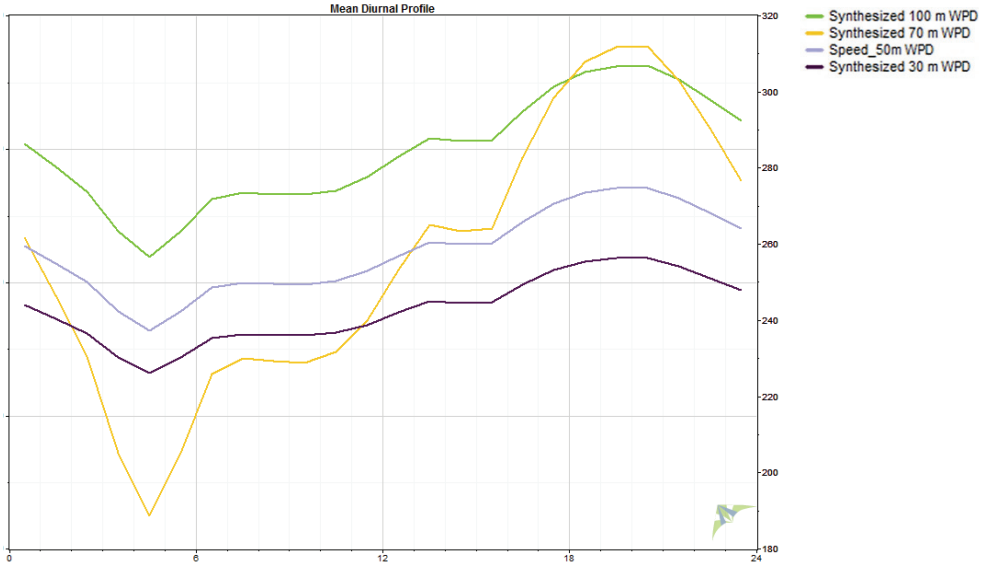

FIGURE 11. Mean wind power density profile

order to obtain and determine the maximum and minimum speed used in the production and generation of electricity from the located turbine. It is possible to observe the average maximum and minimum wind power density during the years of study of the wind at various heights, where the maximum power density at about 8 pm and the minimum power density at 5 am. The maximum value of wind power density for reference high at 50 m is almost 275 $W \cdot m^{-2}$ and near 240 $W \cdot m^{-2}$ for minimum value (Fig. 11).

Probability distribution function

The probability distribution function (PDF) is used to demonstrate how the site is suitable for wind energy systems and also used for wind data analysis. Figure 12 shows the distribution of wind frequency for 12 months at height of 50 m. The bin size of the distribution showing 0.5 $m \cdot s^{-1}$. The curve plotted against the frequency distribution of measured wind speed is called Weibull distribution function, and this curve represent the best fit to the measured wind speed data. The two-parameter Weibull distribution given by (Firas, 2014):

$$f(v) = \frac{k}{c}\left(\frac{v}{c}\right)^{k-1} \exp\left(-\left(\frac{v}{c}\right)^{k}\right) \qquad (10)$$

where:
k – shape parameter;
c – scale parameter [$m \cdot s^{-1}$].

Fitting depends on two parameters called shape and scale parameters, best fit is obtained using the equivalent energy method (EEM) which is explained bellow. Weibull shape parameter for fitting curve is equal to 2.10, while Weibull scale parameter is 6.62 $m \cdot s^{-1}$. The wind speed is not uniform and take different

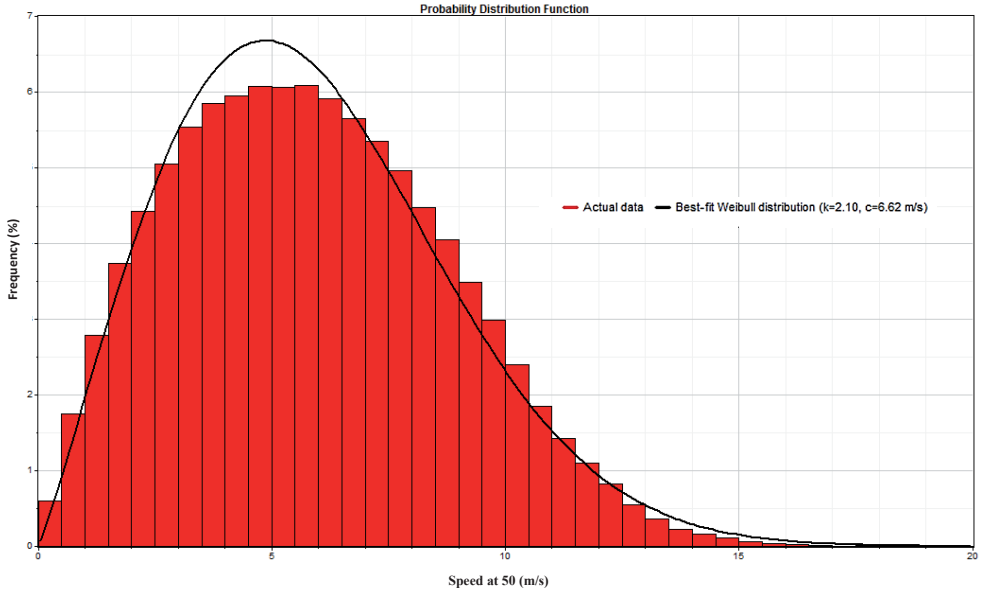

FIGURE 12. Weibull destitution function

values tend to produce different sets of ranges. The value of scale parameter shows the average wind speed at the wind farm, while the low values of shape parameter mean that the wind speed is not uniform.

Monthly frequency by bin

The monthly Weibull probability density of the measured data for the whole year of the location is shown in Figure 13. It is noticeable from this figure that the cold months (December, January, February, March) that the wind tends to quiet speed due to high pressure of cold air masses. We also notice an increase in wind speed in hot months, in contrast to the previous, due to the increasing in convection current of low air masse pressure. It is also possible to observe the increasing in wind speed frequencies in October and May as months in which seasons changes occur.

Wind speed statistical analysis

The Weibull PDF gives a better fit for measured probability density distributions than other statistical functions. This it could be depends on the Weibull PDF in order to find wind statistics. The most important statistics is given in Table 1. It show the characteristics of wind speed for whole years of study at 50 m a.g.l. with following observations:

1. The mean wind speed calculated for this site point out to the suitability of this location for micro and small wind energy systems.
2. The mean and the median are almost equal, then distribution appears to be near symmetric.
3. The maximum frequency is 0.13 at wind speed 4.8 $m \cdot s^{-1}$, which is also called most probable wind speed.
4. The positive sign of 3rd raw moment inferring to skewness of the distribution toward right.

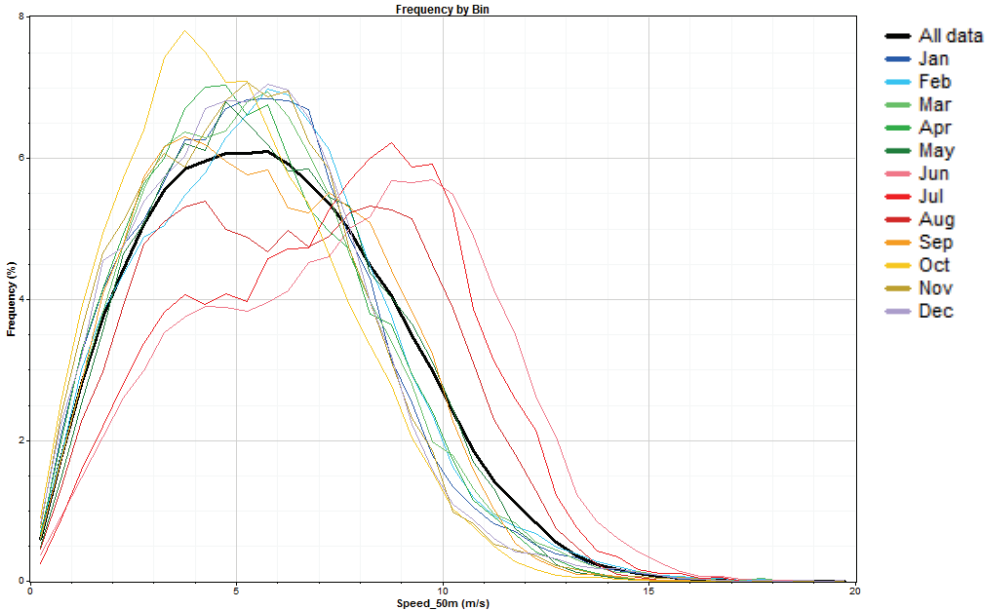

FIGURE 13. Monthly Weibull destitution function

TABLE 1. Some Weibull statistics

Specification	Value
c [m·s^{-1}]	6.62
k	2.1
Mean speed [m·s^{-1}], conventional method	5.8
Median speed [m·s^{-1}]	5.5
Modal speed [m·s^{-1}]	4.8
Maximum frequency	0.13
1st raw moment (mean speed, Weibull-based) [m·s^{-1}]	5.8
2nd raw moment [m·s^{-1}] 2 – measure of spread	42.9
3rd raw moment [m·s^{-1}] 3 – measure of skewness	367
4th raw moment [m·s^{-1}] 4 – measure of peakedness	3 524

The wind power density calculated from Weibull parameters (Fig. 14) is 224 W·m^{-2}. In addition, the wind speed that carrying maximum energy (maximum power density) is 9.1 m·s^{-1}.

Wind statistics at different heights

Since mean wind speed has a logarithmic variation with heights, thus wind statistics will have variation with height. Numerous mathematical equations were

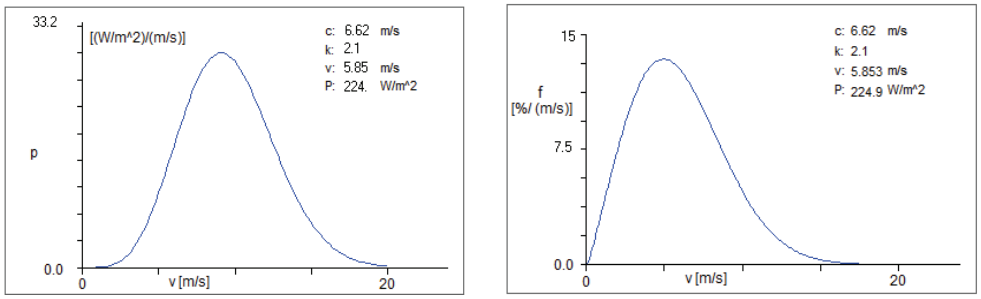

FIGURE 14. Power density versus wind speed at height of 50 m

used for the purpose of deriving wind statistics at different heights from certain source height. The extrapolation equation to get Weibull parameters at different heights can be given in bellow.

If c_1 and k_1 are Weibull functions at some anemometer height h_1 the values of Weibull parameters at different c_2 and k_2 for any desired height h_2 (e.g. the turbine hub height) can be assessed by (Firas, 2014):

$$c_2 = c_1 \left(\frac{h_2}{h_1} \right)^n \tag{11}$$

$$k_2 = k_1 \frac{1 - 0.0881 \ln \left(\frac{h_1}{h_2} \right)}{1 - 0.0881 \ln \left(\frac{h_2}{h_1} \right)} \tag{12}$$

Here h_r is reference height of 10 m, n was found to be:

$$n = \frac{0.37 - 0.0881 \ln(c_1)}{1 - 0.0881 \ln \left(\frac{h_1}{h_2} \right)} \tag{13}$$

The expected monthly or annual wind power density per unit area of a site based on a Weibull probability density function can be expressed as follows (Firas, 2014):

$$PD_w = \frac{1}{2} \rho c^3 \Gamma(1 + 3/k) \tag{14}$$

The total energy generated is given by multiplication between annual wind speed distributions h with turbine power curve at wind speed v_i:

$$E = \sum_{i=1}^{n} h(v_i) p(v_i) \tag{15}$$

In order to yield the best estimation of wind statistics for whole the years, Windographer software uses power law to compute synthesized wind statistics (Firas et al., 2018). Table 2 shows the reference statistics at 50 m a.g.l. and the estimated of the synthesized wind statistics at 30, 70 and 100 m a.g.l.

From Table 2 it is obvious that the wind speed is increased with increasing in height, reaching maximum value 6.4 m·s^{-1} at 100 m a.g.l. The semi-equal values of mean and median wind speed indicates that wind speed distribution at that location tend to be almost regular. Since scale factor (c) is closely related to the mean wind speed thus this value is increased with height. In contrast to scale factor value of shape factor is a fixed

TABLE 2. Synthesized wind statistics

Variable	Synthesized at 100 m	Synthesized at 70 m	Speed at 50 m	Synthesized at 30 m
Measurement height [m]	100	70	50	30
Mean wind speed [m·s^{-1}]	6.4	6.1	5.8	5.4
Median wind speed [m·s^{-1}]	6.2	5.9	5.6	5.2
Weibull c [m·s^{-1}]	7.29	6.94	6.62	6.16
Weibull k	2.09	2.09	2.09	2.09
Mean power density [W·m^{-2}]	298	256	223	180
Mean annual energy content [kWh·m^{-2}]	2 609	2 246	1 950	1 573

value and does not change with height, this is because shape factor (k) is a measurement of the width of the distribution and it does not change with height. Furthermore, it is shown that mean wind power density at height of 50 m was 223 W·m^{-2}, and also keep the same class at height of 100 m.

Wind power class

The wind energy class refers to energy content anywhere. Table 3 shows seven classes and each one has a specific range of wind power density at 50 m a.g.l. By comparison between wind power density and Table 3 it is clear that the study site is assigned to the second class with marginal description. It is clear that the wind farm project is not suitable for electric power generation at height of 50 m, even for heights of 70 and 100 m. It is worth mentioning that our studied area has less power density compared with Figure 3 due to different data sources. Figures 2 and 3 were built by IRENA using atmospheric simulation conditions with SKIRON model and 5 km resolution. Such spatial resolution is small for area representing the study site, while the data studied in this research taken from NASA depends mainly on recording stations with data extrapolation can be done for full coverage area.

TABLE 3. Wind power class (Firas et al., 2018)

Class	Description	Power density at 50 m [W·m^{-2}]
1	poor	100–200
2	marginal	200–300
3	fair	300–400
4	good	400–500
5	excellent	500–600
6	outstanding	600–800
7	superb	800–2 000

Conclusions

In the present study, wind speed data of the Basra coast in Iraq were statistically analysed. Also, the daily and monthly mean wind speed behaviours beside probability density distributions were derived and the distribution parameters were identified, then Weibull parameters were used to study wind potential energy. The most important outcomes of the study can be summarized as follows:

– It was concluded that the study site is not suitable for the installation of large wind turbines, but this wealth

can be used to build small wind generators.
- NASA space data often give less a guess than IRENA wind atlas map.
- May, June, July and August months that the average wind speeds are the highest all around the year.
- The mean wind speed at height of 50 m for the period 1979–2016 was found about 6 $m \cdot s^{-1}$.
- The mean wind power density value at height of 50 m for the period 1979–2016 was found about 224 $W \cdot m^{-2}$.
- The most probable wind direction is 315°, i.e. northwest 315°.
- In case of diurnal wind speed variation evaluation, it was found that wind speed values are higher during the daytime.

Acknowledgements

We would like to express our sincere gratitude to Al-Karkh University of Science, Mustansiriah University, and Ministry of Science and Technology for their assistance with the collection of our data and supporting this work.

References

Abaas, S.A. (2015). *Comparison of five numerical methods for estimating Weibull parameters of wind energy applications in Iraq* (doctoral thesis). Baghdad: Almustansiriyah University.

Ali, K.R. (2014). *Predicting best wind farms site in southern region of Iraq using WAsP Model* (MSc thesis). Baghdad: University of Baghdad.

Amani, I.A. (2007). *Estimating wind energy in Iraq* (doctoral thesis). Baghdad: Almustansiriyah University.

Elmokadem, A.A., Megahed, N.A. & Noaman, D.S. (2016). Systematic framework for the efficient integration of wind technologies into buildings. *Frontiers of Architectural Research*, *5*(1), 1-14.

Firas, A.H. (2014). *Construction of mathematical-statistical model of wind energy in Iraq using different Weibull distribution functions* (doctoral thesis). Baghdad: Al-Nahrain University.

Firas, A.H., Oudah, S.S. & Al-Baldawi, R.A. (2018). Pre-feasibility study of hypothetical wind energy project using simulated and measured data. In *2018 2nd International Conference for Engineering, Technology* and Sciences of *Al-Kitab (ICETS)*: *Karkuk 4–6 December 2018* (pp. 60-65). Karkuk: IEEE. https://www.doi.org/10.1109/ICETS.2018.8724618

International Renewable Energy Agency [IRENA] (2015). *Global atlas for Renewable Energy Agency. Renewable Energy Target Setting, Abu Dhabi, UAE*. IRENA.

Kamal, H.L., Ali, K.R. & Amani, I.A. (2018). Evaluation efficiency of wind turbines for Barjisiah (South of Iraq) wind plant. *Iraqi Journal of Science*, *59*(2A), 813-818.

Kazem, H.A. & Chaichan, M.T. (2012). Status and future prospects of renewable energy in Iraq. *Renewable and Sustainable Energy Reviews*, *16*(8), 6007-6012.

Keyhani, A., Ghasemi-Varnamkhasti, M., Khanali, M. & Abbaszadeh, R. (2010). An assessment of wind energy potential as a power generation source in the capital of Iran, Tehran. *Energy*, *35*(1), 188-201.

Risø DTU National Laboratory for Sustainable Energy (2014). *Wind turbines – design requirements*. Roskilde: Risø National Laboratory.

Taghreed, A.A., Monim, H.K. & Amani, I.A. (2019). Spectral and statistical analysis of wind spectrum for Ali Al-Gharbi area in Iraq. *Iraqi Journal of Science*, *60*(7), 1649-1657.

World Wind Energy Association [WWEA] (2010). *World Wind Energy Report 2009*. Bonn: WWEA.

Summary

An assessment the wind potential energy as a generator of electrical energy in the coastal area of southern Iraq. Renew-

able energies have the potential to provide relatively clean energy, mostly for domestic energy. Wind power generation is expected to rise in the near future and has grown exponentially over the past decade in many countries. The most important parameter that must be taken into consideration when designing and studying wind power conversion systems is the wind speed. Probability density functions (PDF) such as Weibull is often used in wind speed and wind power analyses. This research presents an assessment of wind power based on the Weibull distribution statistics in the coastal of southern Iraq at Basrah province. Wind speed data for the study site were obtained from NASA at a height of 50 m for the period 1979–2016 with a time interval of 10 min. The data at a height of 50 m were extrapolated using the power law in order to estimate the wind speed at new heights: 30, 70 and 100 m. The different parameters of the Weibull function as well as the daily and monthly wind speeds, mean, variance and potential energy at four altitudes were estimated and analysed using Windographer software. Results indicate that the maximum wind speed at 100 m is 6.4 $m \cdot s^{-1}$, giving an average power density of 298 $W \cdot m^{-2}$, which indicates that the location of the study has marginal and useless potential for installing large wind turbines.

Authors' address:
Firas A. Hadi
(https://orcid.org/0000-0002-4392-2545)
Al-Karkh University of Science
College of Energy and Environmental Sciences
Baghdad-Amryah, 632,35,21 Iraq
e-mail: Firas.A.Hadi@kus.edu.iq

Basim Abdulsada AL-knani
(https://orcid.org/0000-0001-9214-624X)
Mustansiriyah University
College of Sciences
Department of Atmospheric Sciences
Palestine Street, Baghdad, Iraq
e-mail: Basim.a.s@uomustansiriah.edu.iq

Scientific Review – Engineering and Environmental Sciences (2020), 29 (1), 54–61
Sci. Rev. Eng. Env. Sci. (2020), 29 (1)
Przegląd Naukowy – Inżynieria i Kształtowanie Środowiska (2020), 29 (1), 54–61
Prz. Nauk. Inż. Kszt. Środ. (2020), 29 (1)
http://iks.pn.sggw.pl
DOI 10.22630/PNIKS.2020.29.1.5

Hwi-Chie HO, Kevin Steven PUIKA, Tota Pirdo KASIH

Faculty of Engineering, Bina Nusantara University

Development of IoT-based water reduction system for improving clean water conservation

Key words: water reduction system, water management, Internet of things, water flow sensor, mobile application

Introduction

Nowadays, the condition in which the demand of domestic water cannot be fulfilled has been perceived by many parts of the world that caused by the rapid growth of population (Liu et al., 2017). One way to prevent water scarcity is by managing the usage of water with the intention of reducing the amount of water used. Developing innovative methodologies, tools and techniques that aim to combat water quantity losses becomes a priority action that must be done (Kanakoudis et al., 2017), in order to provide effective information to the people or community for their contribution to water conservation, thus create more sustainable and desirable future. Currently, there are many tools that can help people to use less water or to limit water consumption, such as flow restrictors, low flow showerheads, water efficient white appliances, water efficient toilets, and urinal sensors (Queensland Government, 2009). Another device that provides real time feedback about water consumption with more accurate to the user is smart water meter. The main advantage of using smart water meter is that the user can monitor directly and receives more accurate information regarding to the user's water consumption compared to conventional water meter, via the Internet of things (IoT) technology and Android smart phone (Sønderlund, Smith, Hulton & Kapelan, 2014).

Household appliances that generally use the largest amount of water in daily life are washing machine, shower, and toilet. The general usage of sanitary water consumption in residential indoor could reach up to 111 l daily, in which: 31.4 is used for shower, 23.3 for toilet, 23.0 for kitchen sink and 12.4 for wash-

ing machine. The use of shower, toilet, kitchen sink, and washing machine make up about 81% of the total apartment water use (Jordán-Cuebas et al., 2018). Depends on the tank reservoir volume, toilet water use could vary considerably. The general water usage for ordinary toilets could be 7.5, 9, or 13 l per flush (Gormley, Aspray, Kelly & Rodriguez--Gil, 2017). However, for the sake of water usage reduction, it is also possible to flush the toilet with 6 l of water (USDoE, 2013).

The Internet of things has been utilized to monitor and evaluate the system of energy consumption in almost every aspect of daily life, including in the field of water management system. In the present paper, clean water reduction strategy is designed by the help of IoT devices such as water flow sensor to measure the volume of water consumption on washing machine, shower, and toilet. The amount of water consumption will be monitored in real time through an Android application in smart phone that connected to those IoT devices. By the help of user consideration, the application of this system on such a small house or apartment may has a great potential in reducing the amount of clean water used.

Methodology

The designed framework of water reduction strategy using IoT-based system is illustrated in Figure 1. The system starts by reading the water consumption that used by three household appliances that were considered using a lot of water, which are: washing machine, shower, and toilet. The water volume usage will be measured by water flow sensors that installed to the washing machine, show-

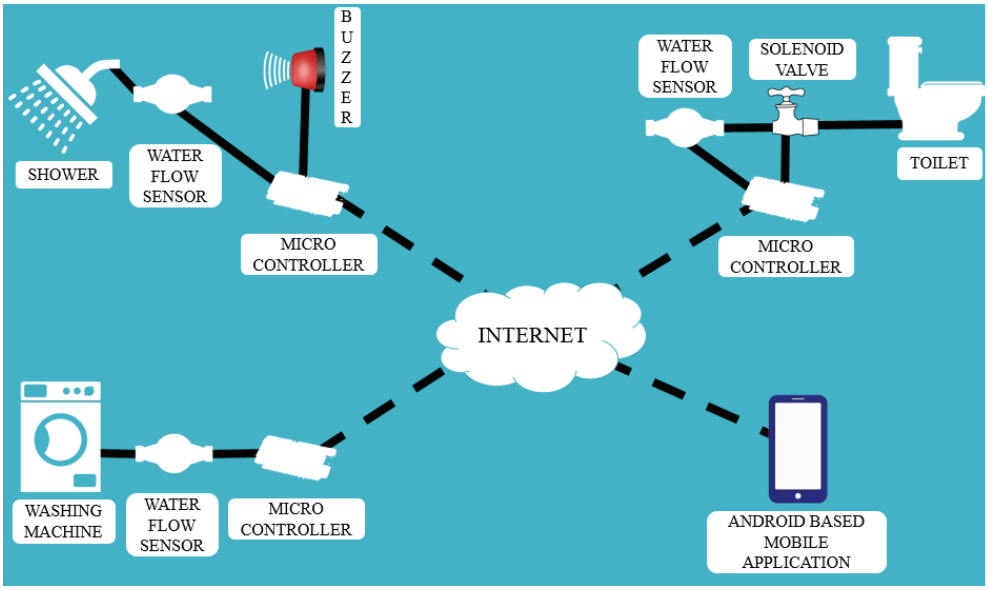

FIGURE 1. Design framework of IoT-based clean water reduction

er, and toilet's pipelines. A microcontroller that connects to each water flow sensor was utilized to send the data of water usage to the cloud server through Internet. In the case of shower, besides installing water flow sensor like in washing machine, a buzzer was installed to alarm the user before the consumption of water reached the maximum limit. User can input the maximum limit of supplying water volume for shower according to their real requirement. For the toilet, after flushing the user should press a "Refill" button on their smart phone as a signal order to open the solenoid valve to automatically fill the toilet's water tank for 6 l of clean water. The data of water consumption from these three household appliances will be sent to a cloud server and the user could access the data through an Android application.

Results and discussion

Hardware

The components used in this project of water reduction strategy are NodeMCU microcontroller, water flow sensor, solenoid valve and buzzer, which could be obtained easily from the market. The open source Arduino software (IDE) was utilized to program the NodeMCU microcontroller to read the water volume consumption, as it measures the volume of water, which flow through the water flow sensor and causing the rotor inside to spin simultaneously. At the time when the rotor spins, a voltage/pulse will be induced (Rajurkar, Prabaharan & Muthulakshmi, 2017). The use of NodeMCU module is to send water volume data read from water flow sensor to a cloud server. Water flow sensor and micro controller will be occupied along with the household appliances (washing machine, shower, and toilet) pipelines. The schematic diagram of all hardwares and its connection used in each household appliance in the present IoT-based water reduction system can be seen in Figure 2. Figure 2a exhibits the use of smart water meter in general, water flow sensor was connected to microcontroller to read water volume that flowed through washing machine's pipeline. In Figure 2b, a buzzer was connected to the microcontroller that used for the shower's pipeline. The buzzer's function is to alarm the user with different sounds that represents the usage of water to the consumption limit in percentage (75, 85 and 95%).

The user can lock the maximum limitation for shower water consumption, for example at 25 l. So, the sound of alarm will alert the shower's user when the water usage has exceeded 18.75, 21.25 and 23.75 l before it stops when the water consumption in shower reaches 25 l. Schematic for toilet's pipeline is depicted in Figure 2c. Additional components used are solenoid valve, 12 V power supply, 2.2 K resistor, TIP120 transistor, and diode. The 12 V power supply was used to power the solenoid valve which has the function to stop and control the water flow, while other components were used to support the control of solenoid valve. Solenoid valve has a magnetic rod which could block the water flow to the pipe when the rod is closed or to let the water flows when the rod is open (Gopalakrishnan, Abhishek, Ranjith, Venkatesh & Jai Suriya, 2017).

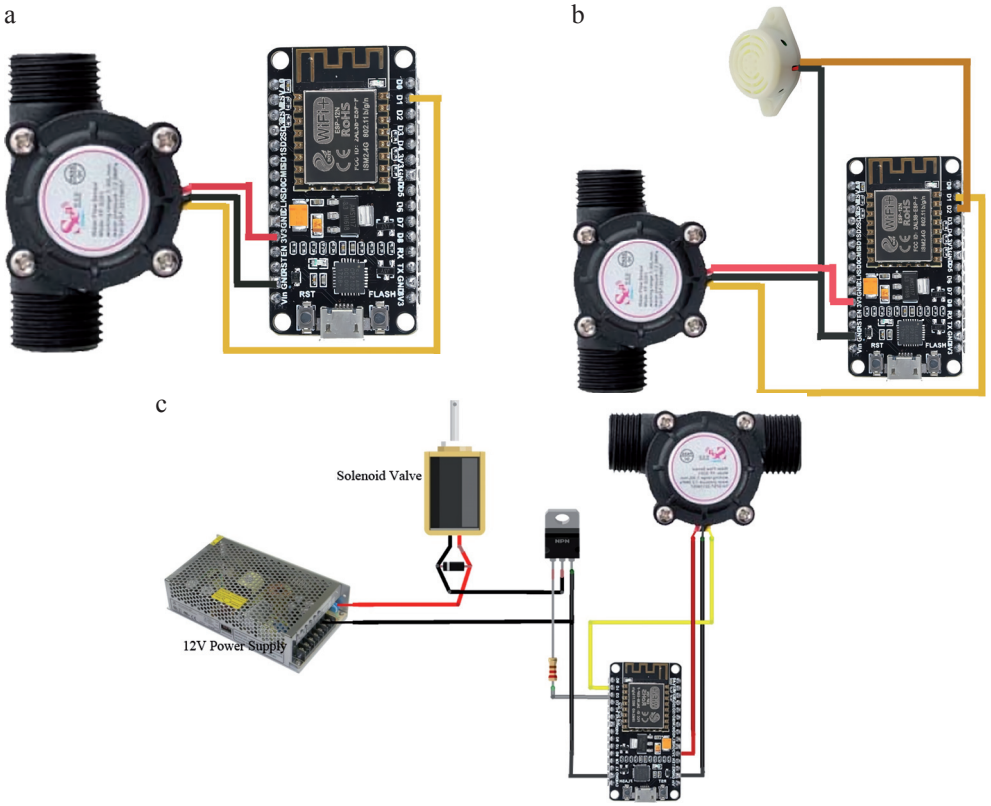

FIGURE 2. Schematic connection for hardware: a – used in washing machine's pipeline; b – used in shower's pipeline; c – used in toilet's pipeline

Application design

In this digital era, smart phones have changed the way we live our lives. Things could be easily done through the help of a smart phone. By developing such application (app), users could access information regarding their water usage anytime and anywhere in real-time. In this study the Android-based application has been developed using the assistance of Android development program of Android Studio to visualize the water volume that has been consumed through the water flow sensor and to control the solenoid valve to refill toilet's water tank. The use of Android application as the user interface will make it easier for user to interact with the developed system. Protocol based on IoT is used to guarantee delivery of messages throughout the system. The microcontrollers will send the data of the water volume usage to the cloud server every time when the water flow passes through. In additional to that, whenever the application is accessed by the user, it connects automatically to the cloud server that provides the information of the water usage. The information of water usage of the three household appliances will be presented, and the sum

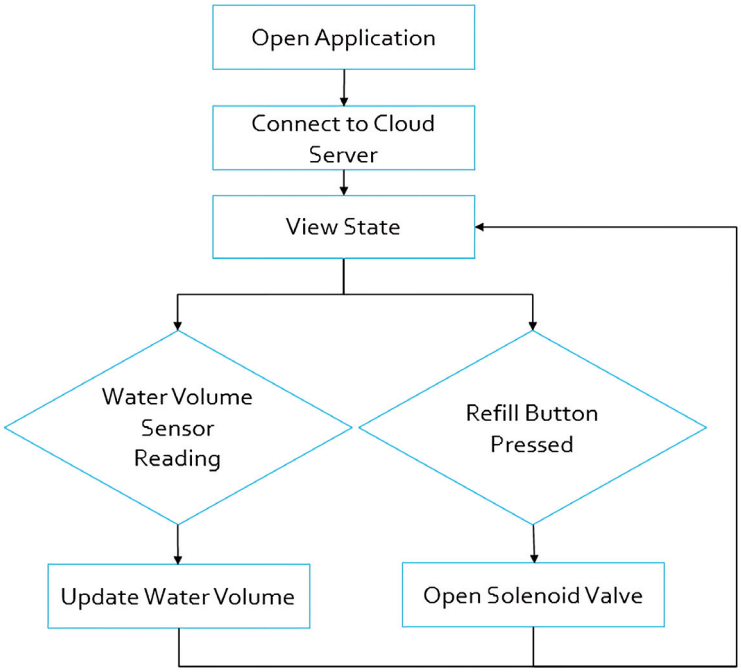

FIGURE 3. Flow of Android application process

of water usage will also be shown to the user. An addition of a "Refill" button was made to power up the solenoid valve in the toilet's pipeline and fills the toilet's water tank.

The flow diagram of Android application process can be seen at Figure 3. The associated visual display for Android-based mobile application in user's smart phone to monitor the water consumption is depicted in Figure 4.

Experimental result of the components

One of the components that we use in this project is water flow sensor, and this component must be firstly calibrated to measure the water volume passed through the pipe shows the accurate measuring number. Experiments were carried out to compare the water volume measured by the water flow sensor in particular time (sensor read) and the water volume that manually measured by a cylinder glass (real volume). The calibration of water flow sensor was made by adjusting the Arduino IDE program so that the volume of water passing through the sensor was set not to exceed 7% of the actual volume. The measurement result of the quantity of water that being passed through the water flow sensor in predetermined time, the actual volume water and the percentage error as the comparison of those two is exhibited in the table. As shown in there, the comparison of the water volume that read by sensor and that are manually measured by cylinder glass shows no significant difference. This means that the sensor used in this

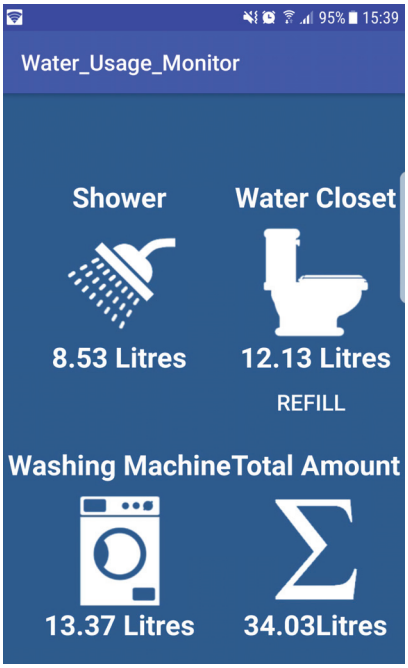

FIGURE 4. Android-based mobile application GUI

experiment was capable enough to measure the actual water consumption. The same procedures have been performed to other devices and the result shows the similar result of percentage errors, which lower than 5%. With the percentage error lower than 5%, this result shows that the device prototype work properly and its function performance in measuring water volume is in accordance with the project's objective.

Potential water reduction of the developed system

The potential of clean water which might be saved by practical implementing of our system can be explained from the following feasibility study. Suppose a person uses 31.4 l of clean water for shower (Jordán-Cuebas et al., 2018), and 13 l of water for each flush (Gormley et al., 2017) for toilet use in a day. By using this system, a user can possibly reduce their water consumption on shower to 25 l which saves 6.4 l of clean water per day. As for the consumption used in conventional toilet can be reduced through solenoid valve in our system to 6 l per flush of water use, refers to USDoE policy (USDoE, 2013), thus it can save 7 l of water for once use of flushing toilet. For the reduction of clean water in washing machine usage, it will depend on the user by their own consideration in consuming the water. Through the water consumption data displayed on the system, the user is expected to have awareness and to realize the importance of regulating water reduction for subsequent use in washing machine usage. Suppose that the contribution of water reduction will come from the use of shower and toilet, the user can possibly save as much as 13.4 l of clean water per day. Within a month, each user could potentially save around 402 l of clean water or even more.

With the many advantages that can be obtained through the application of IoT-based smart water meters compared to the conventional one, such as: reducing the labour costs and direct control to the real water consumption, it will become appropriate if this system can be adopted and widespread implemented in residential customers to save million litres of clean water. In addition of being able to be used as one of the approaches to integrated water resource management, this system may also be one of the answers to key issues of water scarcity and water quality which are emerged in several parts of the world.

Conclusions

We have successfully designed and implement the IoT-based water reduction system as a one way to realize the clean water reduction strategy or water conservation. This system which may potentially be implemented in such a small house or apartment, can monitor and provide real-time information on how much water consumed by the user daily. In this project, we used NodeMCU microcontroller, water flow sensor, solenoid valve, and buzzer to monitor water volume consumption at three household appliances (washing machine, shower, and toilet). Experimental testing of the smart meters in measuring the quantity of water supplied shows that these tools provide performance accuracy more than 95% from the actual water volume, which is good enough to be used for estimating the real water consumption of the user. The reliability of the remote access data through Android-based mobile application demonstrates the good result to keep updates the water consumption records. Based on the feasibility study, each user may potentially save clean water up to 402 l monthly. Through this research, the IoT-based water management system program using smart water meters must be promoted as a substitution of the use of traditional water meter because it has several advantages, especially in motivating users to contribute to water conservation for more sustainable and desirable future.

TABLE. Testing data result for the water flow sensor read after calibration

No	Sensor read [ml]	Real volume [ml]	Percentage error [%]
1	640	650	1.54
2	997	945	4.95
3	905	863	4.86
4	844	815	3.56
5	848	835	1.53
6	891	880	1.23
7	813	830	2.05
8	975	940	3.72
9	945	915	3.28
10	612	625	2.08
Average percentage error			2.88

References

Gopalakrishnan, P., Abhishek, S., Ranjith, R., Venkatesh, R. & Jai Suriya, V. (2017). Smart Pipeline Water Leakage Detection System. *International Journal of Applied Engineering Research*, *12*(16), 5559-5564.

Gormley, M., Aspray, T.J., Kelly, D.A. & Rodriguez-Gil, C. (2017). Pathogen cross-transmission via building sanitary plumbing systems in a full scale pilot test-rig. *PLoS ONE*, *12*(2), e0171556. https://doi.org/10.1371/journal.pone.0171556

Jordán-Cuebas, F, Krogmann, U., Andrews, C.J., Senick, J.A., Hewitt, E.L., Wener, R.E., Sorensen Allaci, M.A. & Plotnik, D. (2018). Understanding apartment end-use water consumption in two green residential multistory buildings. *ASCE's Journal of Water Resources Planning and Management*, *144*(4), 04018009. https://doi.org/10.1061/(ASCE)WR.1943-5452.0000911

Kanakoudis, V., Papadopoulou, A., Tsitsifli, S., Curk, B.C., Karleusa, B., Matic, B., Altran, E. & Banovec, P. (2017). Policy recommendation for drinking water supply cross-border networking in the Adriatic region. *Journal of Water Supply: Research and Technology – AQUA*, *66*(7), 409-508.

Liu, J., Yang, H., Gosling, S.N., Kummu, M., Flörke, M., Pfister, S., Hanasaki, N., Wada, Y., Zhang, X., Zheng, C, Almaco, J. & Oki, T. (2017). Water scarcity assessments in the

past, present, and future. *Earth's Future*, *5*(6), 545-559.

Queensland Government (2009). *Water smart buildings: water use reduction in government built assets*. Queensland: Queensland Department of Public Works. Retrieved from: http://www.hpw.qld.gov.au/SiteCollectionDocuments/WaterMgtPracNote.pdf

Rajurkar, C., Prabaharan, S.R.S., & Muthulakshmi, S. (2017). IoT based water management. In *International Conference on Nextgen Electronic Technologies*: *Gaza City 23-24 October 2019* (pp. 255-259). Piscataway Township, New Jersey: IEEE.

Sønderlund, A.L., Smith, J.R., Hutton, C. & Kapelan, Z. (2014). Using smart meters for household water consumption feedback: knowns and unknowns. *Proceedia Engineering*, *89*, 990-997.

United States Department of Energy [USDoE] (2013). *Energy and water conservation standards: Title 10. Energy, Section 430, Subpart C.* Washington: USDoE. Retrieved from: http://www.gpo.gov/fdsys/pkg/CFR-2011-title10-vol3/pdf/CFR-2011-title10-vol3-sec430-2.pdf

Summary

Development of IoT-based water reduction system for improving clean water conservation. Water is one of the basic necessities of life; however, due to the increased growth of population and without any changes of people's current water consumption rate the world would face water scarcity in the near future. Developing tools and techniques that aim to combat the loss of water quantity becomes a priority action due to it can provide actionable information to the community in its contribution to clean water conservation. In this study, the IoT-based water reduction system has been developed to measure water volume at three household appliances (washing machine, shower, and toilet) by installing flow sensors to those of each pipeline. Each sensor was connected to a microcontroller that sends water volume data and it will be stored in the cloud server. This technology could help users in reducing clean water consumption by: alarming user whenever water volume reaches 75, 85 and 95% of the limit volume for each showering session by installing a buzzer to the shower's pipeline; limiting the water used for the toilet flushing by installing a solenoid valve for the toilets' pipelines; and allowing users to access the information of all water consumption through Android-based mobile application. Through this study, IoT technology has great potential to support clean water reduction strategy due to it could save clean water up to 402 l monthly. Application of IoT technology can be started to be installed in such a small house or apartment in which the user can directly monitor their water consumption.

Authors' address:
Hwi-Chie Ho, Kevin Steven Puika
Bina Nusantara University
Faculty of Engineering
Industrial Engineering Department
Jakarta, Indonesia 11480
e-mail: hhchie@binus.edu
kevin_stvn@yahoo.com

Tota Pirdo Kasih (corresponding author)
(https://orcid.org/0000-0001-8001-7969)
Bina Nusantara University
Faculty of Engineering
Professional Engineer Program Department
Jl. K.H. Syahdan 9 Palmerah, Kemanggisan
Jakarta, Indonesia 11480
e-mail: tkasih@binus.edu

Scientific Review – Engineering and Environmental Sciences (2020), 29 (1), 62–71
Sci. Rev. Eng. Env. Sci. (2020), 29 (1)
Przegląd Naukowy – Inżynieria i Kształtowanie Środowiska (2020), 29 (1), 62–71
Prz. Nauk. Inż. Kszt. Środ. (2020), 29 (1)
http://iks.pn.sggw.pl
DOI 10.22630/PNIKS.2020.29.1.6

Ryszard WASIELEWSKI, Krzysztof GŁÓD

Institute for Chemical Processing of Coal

Emission results of combustion process of fatty acids distillation residue in an oil boiler – comparison to heavy fuel oil

Key words: distillation residue of the fatty acids, combustion, oil boiler, emission of pollutants into the atmosphere

Introduction

During many production processes there are created accessory substances, which could be used at the site of the plant in auxiliary installations to e.g. manufacture technological media. Running these type of operations usually brings about an economic gain, but before they are undertaken, an environment impact analysis should also be conducted.

Paying more attention to environmental issues inclines to searching the alternative fuels, which could supersede fossil fuels. In many research activities conducted in technical scale, pilot and industrial scales there is suggested to replace diesel oil or heating oil from petroleum by liquid fuels like: bioethanol, biodiesel, butanol, water-oil emulsions and others (Marmentini Vivas & Zanoelo, 2011; Nigam & Singh, 2011; Chelemuge, Yoshikawa, Takeshita & Fujiwara, 2012; Ghorbani & Bazooyar, 2012; May-Carle et al., 2012; Sáez, Flores-Maradiaga & Toledo, 2012; Keramiotis, Zannis, Skevis & Founti, 2013; Lazaroiu et al., 2018; Plante et al., 2019). The main objective of the research is to achieve a stability of combustion process and a high heat capacity at the lowest possible pollution emission into the atmosphere.

In Poland, many research activities on energy utilization of liquid fuels of biogenic origin apply to animal and vegetable fats (Orszulik & Lenkiewicz, 2007; Szulc & Golimowski, 2010; Karcz, 2014; Krajewska, Śląska-Grzywna & Andrejko, 2015). An advantage of using heating oils, made from new and used vegetable fats and animal fats is that these fuels are biodegradable, nontoxic and also they come from renewable energy sources.

In one of the national industrial installations to process animal fats, the

fat coming from meat industry is being processed. That material belongs to the category 3 of products unfit for consumption according to the Regulation (EC) No 1069/2009.

In the technological process fat is preliminarily cleaned by filtration with the use of the bleaching earth, and afterwards is broken (in reaction of hydrolysis at the elevated temperature, ca. 250°C and at the elevated pressure ca. 5.5 MPa). In this process there occurs a physical splitting of the material to water solution of glycerin and to fat acids. The fatty acids after separation from water solution of glycerin are distilled in order to isolate each fractions of fat acids. As a result of this process, also the residue after distilling fatty acids is obtained (so-called FADR) – which is a heavy fraction containing the heaviest hydrocarbons (> C18) in the amount of 5–8%, which requires further management. Fatty acids distillation residues make up a material of biogenic origin, formed only as a result of physical processing of animal fats without using additional chemicals.

At the Institute of Chemical Processing of Coal the research was undertaken to manage/use the FADR as a liquid fuel in the boiler house of the plant, exploiting oil boilers fired with heavy heating oil (HFO). The purpose of this research was to determine the impact of the FADR on the process of combustion and change of emission of the pollution to the atmosphere in comparison to combustion of HFO.

Materials and methods

Samples of the fatty acids distillation residues (FADR) and of the heavy fuel oil (HFO) currently burned in boiler room of the plant were subjected to examination of the essential parameters in terms of potential energy usage as a liquid fuel. To complete each separate determination (of the parameters) the same research methodology has been applied.

Density was determined by the aerometric analysis at the temperature of 60°C. Ignition temperature was determined by the Marcusson method. The sample was placed in an open crucible and heated with constant rate of ($3°C \cdot min^{-1}$). To the sample of a liquid fuel the flame of the blowtorch was brought closer, after achieving gain of the temperature by 1°C, till ignition of the volatile products released from the fuel. The ash content was determined in accordance with the technical procedure of Institute for Chemical Processing of Coal at the temperature of 815°C. Measurement of dynamic viscosity was made by means of the Engler viscometer. Selection of temperatures at which to measure the dynamic viscosity was dependent on the texture/consistence of the products and technological conditions during the test of combustion. Measurements of viscosity have been conducted at the shearing velocity of 500 $1 \cdot s^{-1}$. To conduct an ultimate analysis the analyser of company named Elementar model Vario Cub was used. Distillation has been conducted in a typical setup of laboratory distillation used in research of coke tar and oils derived from its processing, in accordance with prerequisites specified in a standard PN-C-97055:2001. The higher heating value and lower heating value were determined in a calorimeter with application of the typical methodology to test the heating oils.

Afterwards there have been conducted tests of combustion of both materials in industrial conditions with usage of fire and water tube steam boiler of the type of FH4000 made by LOOS.

This boiler is used to make steam for technological or heating purposes. Boiler installation does not have a system of the flue gas cleaning, which are fed directly into the stack. At the boiler the burner of a C.I.B. Unigas S.p.A. model PBY510 is mounted. This is a monoblock type burner with axial air flow to the burners, which ensures an even distribution of air essential for high efficiency of heating oil combustion in wide range of capacity. Hot flue gases from the burner flow through the fire tubes and outside water tubes. Table 1 lists basic operating parameters of the PBY510 burner. Figure 1 presents a diagram of boiler installation at which the research was conducted.

TABLE 1. Parameters of the oil boiler burner – heavy fuel oil (own studies)

Parameter	Unit	Value
Fuel flowrate	$kg \cdot h^{-1}$	130–400
Minimum capacity	kW	1 500
Rated capacity	kW	4 500

Comparative tests of combustion of HFO and FADR were conducted at the nominal and reduced capacities of the boiler. The boiler during combusting of each of the evaluated substance was operating at the conditions of the present burner capacity. Boiler capacity was controlled by means of changing the steam flow rate at the maintained constant thermal parameters of the boiler that are presented in Table 2.

Both tests were conducted according to the same testing procedure. A reference fuel (HFO) was pumped into the boiler burner from existing fuel supply installation equipped with a main tank and also with a small intermediate tank heated up to 120°C. On the other hand, FADR was supplied into the burner from a special plastic container through a heated small intermediate tank.

During each test there were conducted emission measurements in range

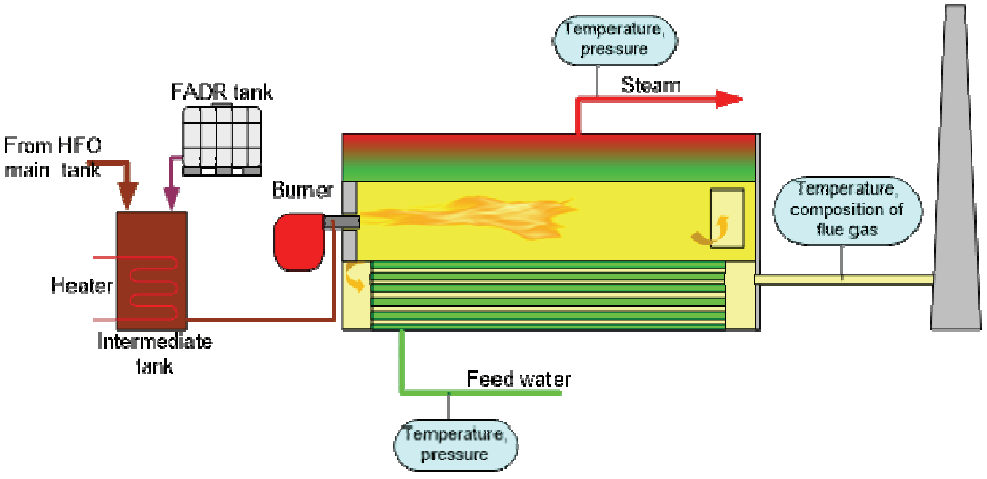

FIGURE 1. Diagram of oil boiler installation at which the research was conducted (own elaboration)

TABLE 2. Oil boiler operating parameters (own studies)

Parameter	Unit	Value
Steam temperature	°C	170–175
Pressure in boiler	bar	8.4–8.6
Feedwater temperature	°C	106

of: dust, CO and CO_2, NO_X, SO_2 and also polycyclic aromatic hydrocarbons (PAHs). Flue gas samples were taken in a measurement point localized in flue directly upstream of the stack.

To measure composition of the flue gas there was used an analyser GASMET DX4000 + analyser of oxygen. Analyser GASMET DX4000 is equipped with a heated sampling channel and it operates based on a method of analysis of absorption of the infra-red radiation of gases (FTIR). This system makes it possible to measure gas constituents concentrations in ranges of: CO_2: 0–100% and 0–45%, CO: 0–6,000 ppm and 0–50%, NO_2: 0–200 ppm, NO: 0–1,000 ppm, N_2O: 0–200 ppm, SO_2: 0–6,000 ppm, SO_3: 0–6,000 ppm, COS: 0–100 ppm, CS_2: 0–100 ppm, H_2O: 0–30%.

Flue gas samples to determine concentration of PAHs were retrieved through setup that consists of an aspiration probe, heated ash separator, moisture separator, tubes filled with sorption material (resin XAD-2 and activated carbon) and also of a gas aspirator.

Concentration of each PAH was determined by means of a gas chromatograph (Trace-GC) equipped with ZB-5MS column and flame ionization detector.

Results and discussion

In Table 3 there are presented physico-chemical properties of both burned materials. FADR is a viscous, fatty substance that has dark colour and also a distinctive and characteristic odour. Texture/consistence of the substance changes into liquid in temperature above 30°C. From research represented in Table 1 it results that HFO as well as FADR have similar physico-chemical properties. Nonetheless FADR is characterized by lower ash and sulphur content, which is beneficial due to

TABLE 3. Physico-chemical properties of the distillation residues and reference fuel (heavy heating oil) used in the test (own studies)

Parameter	HFO	FADR
Density at 60°C [kg·m^{-3}]	864	882
$T_{flashpoint}$ [°C]	250	227
Ash [%]	0.36	0.28
Dynamic viscosity [Pa·s^{-1}]		
in 60°C	0.0570	0.0255
in 80°C	0.0244	0.0142
C [%]	85.0	76.6
H [%]	13.51	12.45
N [%]	0.56	0.85
S [%]	0.62	0.16
Cl [%]	< 0.050	< 0.005
Distillation beginning [°C]	168	98
to 235°C [%]	2.0	1.9
235–270°C [%]	1.8	1.0
270–300°C [%]	2.4	3.0
300–330°C [%]	5.5	52.5
330–360°C [%]	35.9	–
Distillation residue [%]	47.5	31.9
Distillation losses [%]	4.9	9.7
HHV [MJ·kg^{-1}]	45.222	39.914
LHV [MJ·kg^{-1}]	42.251	36.619

potential pollution emission during combustion. Both materials practically do not contain chlorine, which prevents formation of polychlorinated dioxins and furans in a combustion process. FADR has a lighter character than HFO. Distillation of FADR starts and ends in lower temperature. Main ingredient of distillation of a tested sample of FADR is boiling fraction in the range of 300–330°C (52.5%). In contrast for HFO – boiling fraction is in the range of 330–360°C (35.9%). Lower heating value of both tested products is on a similar level, although it is slightly higher for heating oil. The results of research shows that usefulness of the tested material (FADR) as a substitute or a component of heating oil.

During operation of the boiler with the maximum of the burner capacity, combustion process proceeded stably, without explicit differences related to type of the fuel burnt. The obtained temperature of the flue gas at the maximum capacity of the boiler for both fuels was fluctuating in the range of 295–325°C. Combustion of the additional fuel can occur as well as simultaneously as separately to the combustion of heavy heating oil. During the research it was not ascertained technological contraindications in area of mixing FADR with HFO. Both substances do not exhibit symptoms of mutual chemical interaction. For both fuels as well as their mixtures there could be used existing storage layout and handling fuel to oil boilers.

Changes of concentrations of basic ingredients of actual flue gases during tests are presented in Figures 2 and 3. Averaged values of concentrations of each ingredients of the flue gases meas-

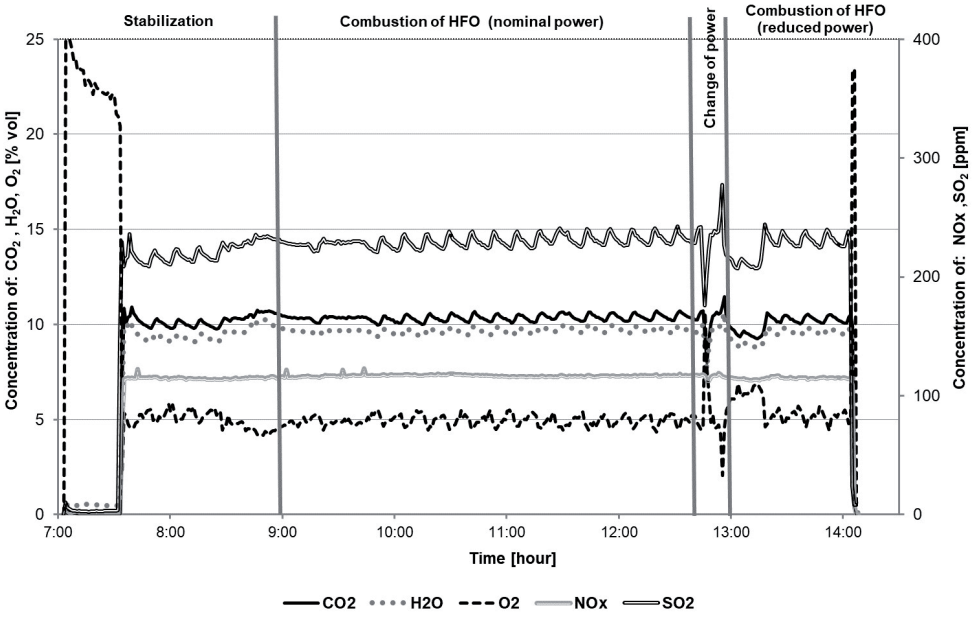

FIGURE 2. Concentration of main ingredients of the flue gases during combustion of heavy heating oil (real flue gases) (own studies)

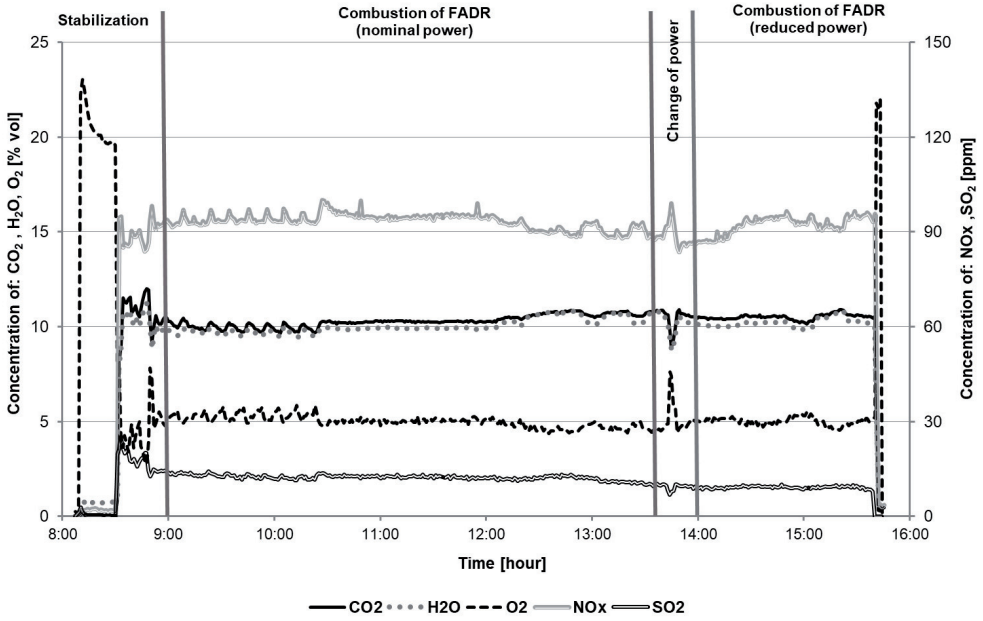

FIGURE 3. Concentration of main ingredients of the flue gases during combustion of the distillation residue (real flue gases) (own studies)

ured during stable work of the boiler are shown in Table 4.

In calculations of average values were neglected the temporary states of instability of the combustion process, which have taken place during combustion of the distillation residue of the fatty acids at the reduced capacity of the boiler.

TABLE 4. Main composition of the flue gases (real flue gases) during combustion of the reference fuel (heavy heating oil) and the fat acid distillation residue (own studies)

Compound	Unit	Mean value/Population standard deviation							
		HFO				FADR			
		nominal power		reduced power		nominal power		reduced power	
CO_2	%	11.57	0.12	11.69	0.65	11.60	0.17	11.84	0.09
CO	ppm	5.70	1.11	2.13	1.10	3.76	1.66	1.88	0.74
NO_2	ppm	0.08	0.25	0.10	0.30	0.00	0	0.00	0
NO	ppm	132.02	2.26	132.26	10.40	104.91	4.12	103.92	3.22
NH_3	ppm	0.001	0.01	0.00	0.00	0.380	0.38	0.050	0.05
SO_2	ppm	256.87	2.69	261.33	14.31	13.82	1.05	10.37	0.34
SO_3	ppm	0.00	0.0	0.00	0.0	0.34	0.13	0.47	0.05
COS	ppm	0.0071	0.01	0.0217	0.01	0.0002	0.0	0.0000	0.0
H_2O	%	10.80	0.11	10.93	0.64	11.29	0.24	11.49	0.16

The combustion process of both substances was stable during the tests. However, concentration of NO and SO_2 in flue gas presented insignificant fluctuations. It was observed that those fluctuations for HFO were more evident for reduced burner efficiency then for nominal. The data shown clearly indicates a lower emission of SO_2 during combustion of FADR, which derives mainly from the very low content of sulphur in this material. Also emission of nitric oxides in case of combustion of FADR was lower in comparison to heavy heating oil in spite of a bit higher content of this element (i.e. nitrogen) in FADR. It was found that the burner of the tested boiler works clearly more effectively at the level of higher capacity. This is reflected in comparison of emission of the same pollutants during combustion of each of the tested materials for two levels of boiler capacity (see Table 1). The only exception is emission of ammonia NH_3, which is higher during combustion of FADR. Concentrations of NH_3 calculated for the only one emitter of this compound do not exceed, however a 10% hourly reference value and do not exceed mandatory standards of air quality in Poland, which is evidence of its slight influence on air. The largest concentration fluctuations in

TABLE 5. Emissions of polycyclic aromatic hydrocarbons [$\mu g \cdot m^{-3}_n$] (own studies)

Compound	Emission (recalculated into 3% oxygen content in dry flue gas)			
	HFO		FADR	
	nominal power	reduced power	nominal power	reduced power
Naphtalene	1.5	4.9	2.7	0.9
Acenaphtylene	18.1	17.1	9.9	12.2
Acenaphtene	2.7	3.4	5.5	4.7
Fluorene	1.0	4.6	2.9	1.5
Phenanthrene	5.8	18.4	30.2	12.6
Anthracene	96.4	99.5	55.1	102.0
Fluoranthene	2.4	8.0	6.2	5.2
Pyrene	17.6	18.6	11.9	18.1
Benzo(a)anthracene	0.9	0.9	4.1	3.8
Chrysene	2.5	0.9	4.9	3.2
Benzo(b+k)fluoranthene	27.7	33.9	23.4	33.0
Benzo(e)pyrene	0.9	0.9	5.1	1.8
Benzo(a)pyrene	2.0	7.3	1.8	4.8
Perylene	111.5	7.2	5.7	4.9
Dibenzo(a,h)anthracene+indeno(1,2,3)pyrene	0.9	0.9	6.4	4.6
Benzo(g,h,i)perylene	0.9	0.9	9.1	4.1
Total PAHs	289.4	222.8	184.8	214.7

flue gas were observed for NO and SO_2 (with HFO much higher at reduced efficiency). In Table 5 there are arranged concentrations of each 16 PAHs in flue gases during combustion of HFO and FADR in a tested oil boiler (referred to the 3% O_2 content basis).

Although emission of PAH is not, in a tested case, limited by the emission standards however it is worth to notice that, despite differences for each hydrocarbons their combined concentrations in the flue gases are lower for combustion of FADR in comparison to HFO in both tested capacity levels of the boiler.

Measured emissions of the selected flue gas ingredients were compared with legal mandatory standards of emission. Values of acceptable emissions of NO_x, SO_2 and dust regarding combustion of liquid fuels were taken from the Resolution of Environment Minister from 1 March 2018 (appendix 4) and were compared to values obtained during phase of stable combustion of heavy heating oil and also of the distillation residue. This comparison is featured in Table 6.

Featured data indicates the fulfillment of the emission standards of SO_2, NO_x and ash regarding tested installation with combustion of both liquid fuels, but for FADR it has been observed twenty-fold lower emission of SO_2. Emissions of NO_x during combustion of FADR are 30% lower in comparison to combustion of HFO. Measurements of concentrations of particulates in the flue gases demonstrated that, both combusted materials have in this range a very similar characteristics. The level of ash/particulates emission for both fuels is noticeable, especially at the minimum capacity of the boiler. Admittedly still FADR is characterized by lower ash content in comparison to the tested HFO.

Conclusions

Physico-chemical properties of FADR point to possibility of using this material in a combustion process as a substitute of HFO or as a component of liquid fuel. During industrial tests it was stated that combustion of FADR in a tested oil boiler does not cause any difficulty and does not require intervention in existing technological layout of the boiler room. No threats were demonstrated related to the increase of pollu-

TABLE 6. Comparison of pollution emissions* during combustion of HFO and a FADR with the emission standards valid for the oil boiler installation (own studies)

Emitted substance	Unit	Permitted emission	Measured emission			
			HFO		FADR	
			nominal power	reduced power	nominal power	reduced power
SO_2	$mg \cdot m^{-3}_u$	850	813	827	44	33
NO_x	$mg \cdot m^{-3}_u$	400	300	300	239	237
Dust	$mg \cdot m^{-3}_u$	50	47.0	47.0	43.2	46.0

*Substance concentration in flue gas in stipulated conditions recalculated into 3% oxygen content in flue gas.

tion emission in to the atmosphere. Boiler installation meets emission standards required for combustion of liquid fuels. Combustion of FADR contributes to the reduction of the previous emission of pollutants from burning of the HFO, significantly in scope of SO_2. Energy usage of FADR can bring also additional ecological and economical effects, because this material is considered as zero emission biomass in relation to CO_2 (i.e. it is CO_2 neutral).

Acknowledgements

The results presented in this paper were obtained during the research project entitled "Alternative fuels market in Poland – production and use for energy purposes" (IChPW 11.19.005.001.001) financed by the Ministry of Science and Higher Education.

References

Chelemuge, N.T., Yoshikawa, K., Takeshita, M. & Fujiwara, K. (2012). Commercial-scale demonstration of pollutant emission reduction and energy saving for industrial boilers by employing water/oil emulsified fuel. *Applied Energy*, *93*, 517-522.

Ghorbani, A. & Bazooyar, B. (2012). Optimization of the combustion of SOME (soybean oil methyl ester), B5, B10, B20 and petrodiesel in a semi industrial boiler. *Energy*, *44*(1), 217-227.

Karcz, H. (2014). Możliwości wykorzystania biopaliw roślinnych i zwierzęcych, a w szczególności gliceryny technicznej w kotłach energetycznych [The usability of animal fat and plant-based biofuels, technical grade glycerin in particular, in power plant boilers]. *Piece Przemysłowe & Kotły*, *3-4*, 8-27.

Keramiotis, C., Zannis, G., Skevis, G. & Founti, M.A. (2013). Performance investigation of Fischer–Tropsch kerosene blends in a laboratory-scale premixed flame burner. *Experimental Thermal and Fluid Science*, *44*, 868-874.

Krajewska, M., Śląska-Grzywna, B. & Andrejko, D. (2015). Tłuszcz jako cenny surowiec energetyczny [Fat as a valuable source of energy]. *Logistyka*, *5*, 227-232.

Lazaroiu, G., Mihaescu, L., Negreanu, G., Pana, C., Pisa, I., Cernat, A. & Ciupageanu, D. (2018). Experimental investigations of innovative biomass energy harnessing solutions. *Energies, 11*(12), 3469. https://doi.org/10.3390/en11123469

Marmentini Vivas, B.M. & Zanoelo, É.F. (2011). An experimental investigation of flammability limits and autoignition temperatures of petrofuels and biofuels in a tubular burner. *Combustion Science and Technology*, *183*(12), 1433-1444.

May-Carle, J.B., Pidol, L., Nicolle, A., Anderlohr, J.M., Togbé, C. & Dagaut, P. (2012). Experimental and Numerical Study of F-T/Biodiesel/Bioethanol Surrogate Fuel Oxidation in Jet-Stirred Reactor. *Combustion Science and Technology*, *184*(7-8), 901-915.

Nigam, P.S. & Singh, A. (2011). Production of liquid biofuels from renewable resources. *Progress in Energy and Combustion Science*, *37*(1), 52-68.

Orszulik, E. & Lenkiewicz, D. (2007). Zastosowanie tłuszczów utylizacyjnych jako paliwa do spalania w kotłach grzewczych [The use of rendering fats as a fuel for combustion in boilers]. *Energetyka*, *642*(12), 891-895.

Plante, L., Sheehan, N., Bier, P., Murray, K., Quell, K., Ouellette, Ch. & Martinez, E. (2019). Bioenergy from biofuel residues and waste. *Water Environment Research*, *91*(10), 1199-1204.

PN-C-97055:2001. Produkty węglopochodne. Destylacja normalna [Carbon-based products. Normal distillation].

Regulation (EC) No 1069/2009 of the European Parliament and of the Council of 21 October 2009 laying down health rules as regards animal by-products and derived products not intended for human consumption and repealing Regulation (EC) No 1774/2002. OJ L 300 of 14.11.2009.

Rozporządzenie Ministra Środowiska z dnia 1 marca 2018 r. w sprawie standardów

emisyjnych dla niektórych rodzajów instalacji, źródeł spalania paliw oraz urządzeń spalania lub współspalania odpadów. Dz.U. 2018, poz. 680 [Resolution of the Minister of the Environment of 1 March 2018 on emission standards for certain types of installations, fuel combustion sources and incineration or co-incineration devices for waste. Journal of Laws 2018, item 680].

Sáez, A., Flores-Maradiaga, A. & Toledo, M. (2012). Liquid butane as an alternative fuel for diesel oil burners. *Applied Thermal Engineering*, *45-46*, 1-8.

Szulc, R. & Golimowski, W. (2010). Strategia i możliwości produkcji biopaliw z tłuszczów zwierzęcych w Polsce [Strategy and possibilities of biofuels production from animal fat in Poland]. *Journal of Research and Applications in Agricultural Engineering*, *55*(2), 88-91.

Summary

Emission results of combustion process of fatty acids distillation residue in an oil boiler – comparison to heavy fuel oil. The results of the research on energy usage of the fatty acids distillation residue are presented. Distillation residue constitutes a material of biogenic origin, which is created only as a result of physical processing of animal fats without using additional chemicals. This material exhibits similar physicochemical properties as the heavy heating oil and may be its substitute. Industrial comparative tests of combusting of distillation residue and also of the heavy heating oil in an oil boiler were conducted. The research was conducted at the rated and minimum capacities of the boiler. It has been stated that combusting of the distillation residue of the fatty acids in a tested oil boiler does not bring about any technological difficulties. No threat of the elevated emission of pollutants into the atmosphere was exhibited. Installation of the boiler fulfill all emission standards required for combustion of the liquid fuels. Combustion of fatty acids distillation residue contributes to the reduction of the previous emission of pollutants from burning of the heavy fuel oil, significantly in scope of SO_2.

Authors' address:
Ryszard Wasielewski
(https://orcid.org/0000-0001-6955-2215)
Krzysztof Głód
(https://orcid.org/0000-0003-3863-1863)
Instytut Chemicznej Przeróbki Węgla
ul. Zamkowa 1, 41-803 Zabrze
Poland
e-mail: rwasielewski@ichpw.pl
kglod@ichpw.pl

Scientific Review – Engineering and Environmental Sciences (2020), 29 (1), 72–80
Sci. Rev. Eng. Env. Sci. (2020), 29 (1)
Przegląd Naukowy – Inżynieria i Kształtowanie Środowiska (2020), 29 (1), 72–80
Prz. Nauk. Inż. Kszt. Środ. (2020), 29 (1)
http://iks.pn.sggw.pl
DOI 10.22630/PNIKS.2020.29.1.7

Grzegorz WRZESIŃSKI

Institute of Civil Engineering, Warsaw University of Life Sciences – SGGW

Permeability coefficient tests in non-cohesive soils

Key words: permeability coefficient, non-cohesive soil, pumping test, consolidation test, groundwater

Introduction

Permeability coefficient (k) is the basic parameter that characterizes the soil properties from the point of view of construction works (Matusiewicz & Wrzesiński, 2018; Wrzesiński, Kowalski & Miszkowska, 2018). This parameter characterizes the filtration ability of water in laminar movement through the soil and is a measure of the soil's hydraulic permeability. Filtration takes place through a network of channels formed from soil pores. The permeability coefficient depends on the soil properties, i.e.: soil type, porosity, grain size, soil structure, water viscosity (Todd, 1980). Approximate typical ranges of the permeability coefficient for cohesive and non-cohesive soils are presented in Table 1.

TABLE 1. Approximate typical ranges of the permeability coefficient for cohesive and non-cohesive soils (Wiłun, 2013)

Soil	Permeability coefficient (k) [m·s^{-1}]
Fine gravel	10^{-2}–10^{-3}
Coarse and medium sand	10^{-3}–10^{-4}
Fine sand	10^{-4}–10^{-5}
Silty sand	10^{-5}–10^{-6}
Silt	10^{-6}–10^{-8}
Clay with I_p = 10–20%	10^{-8}–10^{-10}
Clay with I_p = 20–30%	10^{-9}–10^{-11}
Clay with I_p > 30%	10^{-10}–10^{-12}

There are many methods for determining the permeability coefficient, ranging from uncomplicated calculations to complex field and laboratory methods (Wdowska & Lipiński, 2016). Each of the methods gives more or less similar value of the permeability coefficient to the real value. The choice of a method for determining the permeability coef-

ficient depends largely on the soil type. Eurocode 7 distinguishes four methods of testing the permeability coefficient: empirical correlations, field tests, laboratory tests and estimation based on the oedometer test. In non-cohesive soils, the permeability coefficient is often determined based on empirical formulas. On the basis of empirical formulas, the value of the permeability coefficient is determined with regard to the grain size of the soil (most often the effective diameter of grain d_{10}), porosity and specific surface area (Twardowski & Drożdżak, 2006; Szymkiewicz & Kryczałło, 2011). On the other hand, empirical formulas do not take into account the influence of soil structure, anisotropy of permeability and the shape of soil grain. Research indicates that the permeability coefficient of the same material calculated on the basis of different empirical relationships may vary significantly (Parylak, Zięba, Bułdys & Witek, 2013). As a result, the approximate value of the permeability coefficient is often obtained on the basis of empirical formulas. Field tests that reflect the heterogeneity of the geological structure of the subsoil and anisotropy of hydraulic permeability are the most accurate way to determine the permeability coefficient. The most commonly used method of field tests is pumping test, which involves pumping water out of a well to obtain a hydrodynamic reaction of the subsoil (MacDonald, Barker & Davies, 2008; Polak, Kaznowska-Opala, Pawlecka & Klich, 2014). This reaction allows identification of permeability parameters of the subsoil, well performance parameters and inflow conditions. Pumping test can only be used to determine the permeability coefficient in well-permeable soils. In low-permeable soils, the BAT probe test is most often used. The BAT probe test involves combining a piezometer with a probe measuring part which has a glass water container. The test entails registration of the pressure changes inside the container. The permeability coefficient is calculated based on pressure changes as a function of time. In the laboratory constant or variable gradient methods are used to measure the permeability coefficient. Constant gradient methods are applied to measure the permeability coefficient in well-permeable soils. The most common constant-gradient tests are the ones in the Rowe chamber, ZW-K2 apparatus or Trautwein system (Head & Epps, 2011). Variable-gradient methods are only used to determine the permeable parameters of low-permeable soils. The most common are tests in a modified oedometer supplemented with a burette, test using a Kamieński tube and flow-pump method. Of the above mentioned variable-gradient methods in laboratory conditions, the most common is the flow-pump method. This method involves setting a constant speed of water flow through the sample and measuring the pressure difference at the bottom and top of the soil sample. The test continues until the pressure difference between the bottom and the top of the sample stabilizes.

Laboratory tests for determining the permeability coefficient are less accurate compared to field tests, especially for non-cohesive soils. In laboratory tests, the value of permeable parameter is mainly affected by the change in geological structure in relation to field conditions.

The purpose of the research presented in the paper is to determine and compare the values of the permeability coefficient in non-cohesive soils determined in selected laboratory and field tests.

Materials and methods

Permeability coefficient tests were carried out by the pumping method and in a consolidometer. Pumping tests were started by selecting sites in the field where the subsoil has homogeneous permeable soils and it is possible to carry out the tests. A total of 18 sites were selected for testing. Pumping tests were performed according to the standard method (Driscoll, 1986; Krusemann & de Ridder, 1994; Dąbrowski & Przybyłek, 2005; ICRC, 2011). In each test site one well and two piezometers were installed. Field tests began with the installation of a well with a diameter of 400 mm at designated test sites. Depending on the borehole, the wells were installed to a depth of 1.20––1.80 m. Piezometers with a diameter of 140 mm were installed near each well. One at a distance of 2.0 m from the edge of the well, while the other at a distance of 5.0 m. Installation was carried out excluding the causes and effects of adverse events (Rybka, Bondar-Nowakowska & Połoński 2016). Wells and piezometers were made of ready-made PVC materials. The wells and piezometers used in the research are shown in Figures 1 and 2. A typical schematic of the test pumping system is shown in Figure 3.

Before pumping test, a dynamic light probe SL tests were performed near the well to determine the density index of the tested soils. Simultaneously, soil

FIGURE 1. Well with a diameter of 400 mm made of PVC material used in pumping tests

FIGURE 2. Piezometer with a diameter of 140 mm made of PVC material used in pumping tests

samples for laboratory tests were taken from the subsoil. Pumping tests consisted of pumping water out of the well and measuring the changes of the water table in piezometer. In each well the tests were performed several times to verify

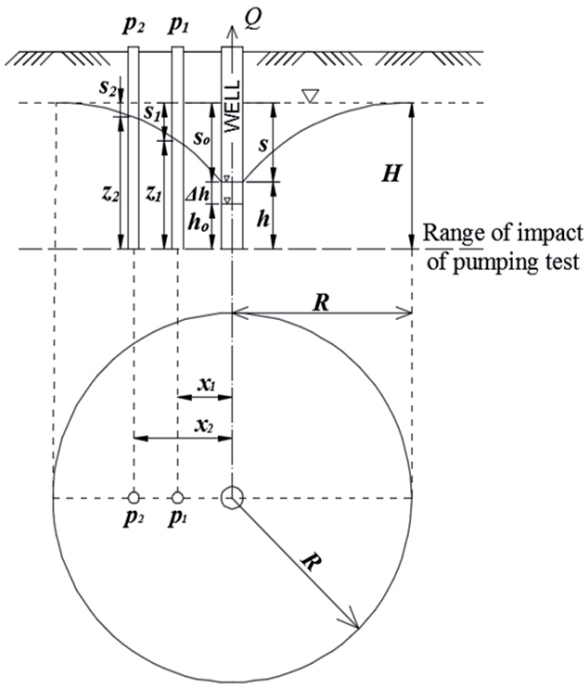

FIGURE 3. Typical schematic of the pumping test system: p_1 – piezometer 1, p_2 – piezometer 2, h – water table outside the well, h_0 – water table inside the well, Δh – difference in water table inside and outside the well, s – lowering the water table at the well, s_0 – lowering the water table inside the well, s_1 – lowering the water table in the piezometer 1, s_2 – lowering the water table in the piezometer 2, z_1 – water table in the piezometer 1, z_2 – water table in the piezometer 2, R – distance of lowering the water table around the well

the obtained results. The differences between the values of permeability coefficients obtained at the same test site did not exceed 5%. Measurements in the piezometers were also carried out for 30 days after the finish of the pumping tests. The permeability coefficient (k) was determined according to the equation:

$$k = \frac{\dfrac{Q}{\Pi\left(z_2^2 - z_1^2\right)}\ln x_2}{x_1}$$

where:
Q – flow of pumped water,
z_1 – water table in piezometer 1,
z_2 – water table in piezometer 2,
x_1 – distance between piezometer 1 and well,
x_2 – distance between piezometer 2 and well.

The following tests were carried out in the laboratory: tests on soil grain size, tests on a scanning electron microscope and tests on a permeability coefficient. Tests on soil grain size were performed to determine soil type according to EN ISO 14688-1:2002 and EN ISO 14688--2:2004. Photos in a scanning electron microscope (XL series, QUANTA 200) were taken to determine the shape of

particles of the tested soil. Some photos for the same soil type and similar density index from two different test sites are shown in Figure 4. Permeability coefficient tests were carried out in a laboratory using consolidometer (Fig. 5). Testing of the permeability coefficient in the consolidometer began with the compaction of soil samples in the Proctor apparatus to the density index determined in the field tests with a light dynamic probe SL (Head, 1980; Tymosiak & Sulewska, 2016).

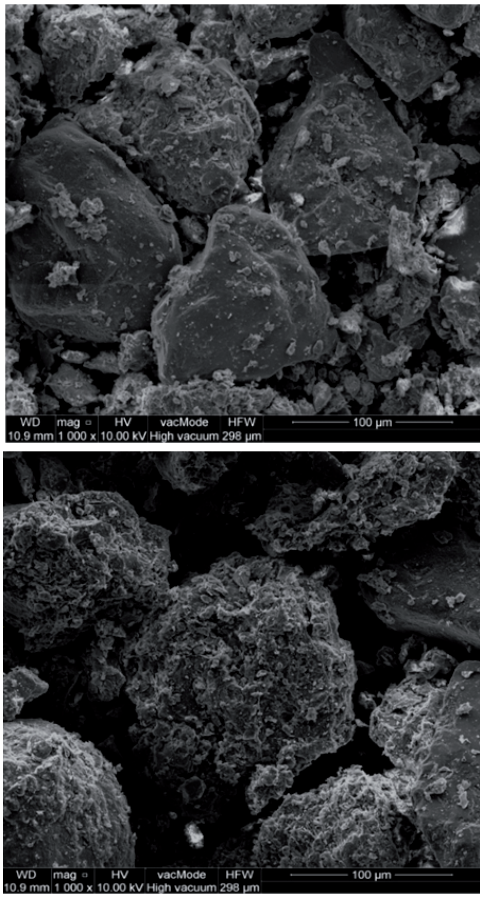

FIGURE 4. Photos of fine sand (FSa) with similar density index (I_D) from two different test sites (wells 1 and 6)

FIGURE 5. Consolidometer used in tests

After compaction, the sample with a diameter of 150 mm and a height of 60 mm, was placed in a consolidometer. The tests were carried out with a continuous inflow of water from below with constant gradients of 0.50. The differences between the values of filtration permeability obtained with the same gradients did not exceed 5% for each soil. Summary of grain size distribution and density indexes of analysed soils are presented in Table 2.

Results and discussion

The performed tests allowed to determine the permeability coefficient of selected non-cohesive soils by two methods: pumping test and consolidometer test. The values of obtained permeability coefficients for the tested soils are presented in Table 3.

TABLE 2. Grain size distribution and density indexes of analysed soils

Well	Soil	Fraction* [%]				Density index (I_D) [-]
		Gr	Sa	Si	Cl	0.55
1	FSa	0	91	9	0	0.49
2	FSa	1	90	9	0	0.67
3	FSa	0	92	8	0	0.61
4	FSa	1	92	7	0	0.64
5	FSa	2	90	8	0	0.41
6	FSa	0	94	6	0	0.54
7	FSa	1	93	6	0	0.51
8	FSa	0	97	3	0	0.56
9	FSa	0	95	3	2	0.39
10	FSa	0	95	5	0	0.50
11	MSa	0	99	1	0	0.48
12	MSa	0	98	1	1	0.41
13	MSa	1	96	3	0	0.58
14	MSa	2	97	3	0	0.52
15	MSa	0	98	2	0	0.61
16	CSa	8	92	0	0	0.71
17	CSa	12	87	1	0	0.68
18	CSa	19	81	0	0	0.59

*According to EN ISO 14688-1:2002 and EN ISO 14688-2:2004.

The performed research indicates that lower permeability coefficients were obtained in laboratory tests compared to field tests. The impact of the density index on the obtained permeability coefficients are important in the tested non-cohesive soils. Generally, lower permeability coefficients were obtained in soils that were characterized by a higher density index.

It should be noted that the value of the permeability coefficient is influenced by the shape of soil particles and their mutual arrangement. Irregularly shaped sand grains hold more water bound in the micro-cavities compared to more regular ones which was confirmed in the performed tests. In the cases of the same soil type and similar density index, the differences in the values of the permeability coefficient are significant. For instance, in the case of fine sand (FSa) from wells 1 and 6, the difference in the values of the permeability coefficient is two times. The influence of grain shape and density index on the value of the permeability coefficient is greatest in fine sands (FSa).

Differences in the values of tested parameter obtained in field and laboratory tests indicate that only field tests reflect actual field conditions. The value of permeability coefficient in non-cohesive

TABLE 3. Values of permeability coefficient from pumping test and consolidometer test

Well	Soil	Permeability coefficient (k) [m·s^{-1}]	
		pumping test	consolidometer test
1	FSa	$2.31 \cdot 10^{-5}$	$2.19 \cdot 10^{-5}$
2	FSa	$3.70 \cdot 10^{-5}$	$3.41 \cdot 10^{-5}$
3	FSa	$2.08 \cdot 10^{-5}$	$1.99 \cdot 10^{-5}$
4	FSa	$1.25 \cdot 10^{-5}$	$1.34 \cdot 10^{-5}$
5	FSa	$5.76 \cdot 10^{-5}$	$5.65 \cdot 10^{-5}$
6	FSa	$4.67 \cdot 10^{-5}$	$4.44 \cdot 10^{-5}$
7	FSa	$3.78 \cdot 10^{-5}$	$3.65 \cdot 10^{-5}$
8	FSa	$4.39 \cdot 10^{-5}$	$3.98 \cdot 10^{-5}$
9	FSa	$4.79 \cdot 10^{-5}$	$4.65 \cdot 10^{-5}$
10	FSa	$5.60 \cdot 10^{-5}$	$5.28 \cdot 10^{-5}$
11	MSa	$1.68 \cdot 10^{-4}$	$1.57 \cdot 10^{-4}$
12	MSa	$2.98 \cdot 10^{-4}$	$2.93 \cdot 10^{-4}$
13	MSa	$2.27 \cdot 10^{-4}$	$2.12 \cdot 10^{-4}$
14	MSa	$1.50 \cdot 10^{-4}$	$1.45 \cdot 10^{-4}$
15	MSa	$1.31 \cdot 10^{-4}$	$1.32 \cdot 10^{-4}$
16	CSa	$3.72 \cdot 10^{-4}$	$3.68 \cdot 10^{-4}$
17	CSa	$4.12 \cdot 10^{-4}$	$3.84 \cdot 10^{-4}$
18	CSa	$4.86 \cdot 10^{-4}$	$4.78 \cdot 10^{-4}$

soils is largely influenced by the heterogeneity of the subsoil and the geological structure, which is very difficult to reflect in laboratory tests.

Conclusions

The paper aims to comparison the permeability coefficient in non-cohesive soils by the method of pumping test and based on tests in a consolidometer. The performed research indicates that lower permeability coefficients were obtained in laboratory tests compared to field tests. The impact of the density index and the shape of soil grains on the obtained permeability coefficients are significant in the tested non-cohesive soils. For the same soils but with different density indexes, the permeability coefficient differs even several times. Studies have shown that also large differences in the values of the permeability coefficient are in the case of the same soils with a similar density index but with different grain shapes. Permeability coefficient tests are often carried out only for large construction projects, while in smaller investments the values of permeability coefficients are calculated with empirical formulas. Using empirical formulas to determine permeability coefficients results in approximate values often several times smaller or larger than the real ones in the field. Field tests are costly, which is why permeability coefficient

are often determined based on laboratory tests or empirical formulas. In laboratory tests, the value of permeability parameter is often affected by the changed geological structure in relation to field conditions. Empirical formulas give only approximate values of the permeability coefficient, because they do not embrace real field conditions. In the case of non-cohesive soils, it is difficult to reproduce the appropriate compaction and mutual arrangement of soil particles, which can immensely affect test results. Field tests allow to determine reliable results since they reflect the real heterogeneity of the geological structure of the subsoil and anisotropy of hydraulic permeability. This is due to the representation of a larger soil surface in field studies compared to laboratory tests and occurrence of natural conditions in the subsoil.

It is hard to carry out the pumping test in densely built-up areas due to their impact on neighbouring buildings and if the change of the water table goes beyond the plot area, the additional water and legal permits are required. Therefore, laboratory tests, both the test methodology and apparatus, should be improved to best reflect the real conditions that occur in the field.

References

Dąbrowski, S. & Przybyłek, J. (2005). *Metodyka próbnych pompowań w dokumentowaniu zasobów wód podziemnych. Poradnik metodyczny* [Methods of test pumping in documenting groundwater resources. A methodological guide]. Poznań: Bogucki Wydawnictwo Naukowe.

Driscoll, F. (1986). *Groundwater and Wells*. St Paul, MN: Johnson Filtration Systems.

EN ISO 14688-1:2002. Geotechnical Investigation and Testing. Identification and Classification of Soil. Part 1: Identification and Description.

EN ISO 14688-2:2004. Geotechnical Investigation and Testing. Identification and Classification of Soil. Part 2: Principles for a Classification.

Head, K. & Epps, R. (2011). *Manual of soil laboratory testing.* Vol. 2. *Permeability, shear strength and compressibility test*. Dunbeath Mill: Whittles Publishing.

Head, K. (1980). *Manual of soil laboratory testing.* Vol. 1. *Soil classification and compaction test*. London: Pentech Press.

International Committee of the Red Cross [ICRC] (2011). *Technical review. Practical guidelines for test pumping in water wells.* Geneva.

Kruseman, G.P. & Ridder, N.A. de (1994). *Analysis and Evaluation of Pumping Test Data*. Wageningen: International Institute for Land Reclamation and Improvement.

MacDonald, A., Barker, J. & Davies, J. (2008). The bailer test: A simple effective pumping test for assessing borehole success. *Hydrogeology Journal*, *16*(6), 1065-1075.

Matusiewicz, W. & Wrzesiński, G. (2018). Odwodnienie stref bezodpływowych małej zlewni miejskiej [Drainage of the depression area in a small urban catchment]. *Acta Scientiarum Polonorum Architectura*, *17*(3), 131-144. https://doi.org/10.22630/ASPA.2018.17.3.35

Parylak, K., Zięba, Z., Bułdys, A. & Witek, K. (2013). Weryfikacja wyznaczania współczynnika filtracji gruntów niespoistych za pomocą wzorów empirycznych w ujęciu ich mikrostruktury [The verification of determining a permeability coefficient of noncohesive soil based on empirical formulas including its microstructure]. *Acta Scientiarum Polonorum Architectura*, *12*(2), 43-51.

Polak, K., Kaznowska-Opala, K., Pawlecka, K. & Klich, J. (2014). Analiza przebiegu próbnych pompowań na przykładzie studni badawczej AGH-1 [Interpretation of pumping tests results on the basis of examination of AGH-1 well]. *Przegląd Górniczy*, *10*, 106-111.

Rybka, I., Bondar-Nowakowska, E. & Połoński, M. (2016). Causes and effects of adverse events during water supply and sewerage system constructions. *Archives of Civil Engineering*, *62*(1), 173-184.

Szymkiewicz, A. & Kryczałło, A. (2011). Obliczanie współczynnika filtracji piasków i żwirów na podstawie krzywej uziarnienia: przegląd wzorów empirycznych [Calculation of permeability coefficient of sands and gravel based on grain size distribution curve: review of empirical relations]. *Inżynieria Morska i Geotechnika*, *2*, 110-121.

Todd, D. (1980). *Groundwater Hydrology*. Chichester: John Wiley & Sons.

Twardowski, K. & Drożdżak, R. (2006). Pośrednie metody oceny właściwości filtracyjnych gruntów [Indirect methods for assessing soil filtration properties]. *Wiertnictwo, Nafta, Gaz*, *23*(1), 477-486.

Tymosiak, D. & Sulewska, M.J. (2016). Badania parametrów zagęszczalności gruntów niespoistych metodą Proctora [The study of compactibility parameters in non-cohesive soils by Proctor compaction test]. *Acta Scientiarum Polonorum Architectura*, *15*(3), 43-54.

Wdowska, M.K. & Lipiński, M.J. (2016). Ocena efektywności wyznaczania współczynnika filtracji metodami pośrednimi w różnych gruntach drobnoziarnistych [Effectivness of indirect approach of determination of coefficient of permeability in fine grained soils]. *Acta Scientiarum Polonorum Architectura*, *15*(4), 79-89.

Wiłun, Z. (2013). *Zarys geotechniki*. Warszawa: Wydawnictwa Komunikacji i Łączności.

Wrzesiński, G., Kowalski, J. & Miszkowska, A. (2018). Numerical analysis of dewatering process of deep excavation. *International Multidisciplinary Scientific GeoConference SGEM*, *18*(1.2), 497-504. https://www.doi.org/10.5593/sgem2018/1.2/S02.063

Summary

Permeability coefficient tests in non-cohesive soils. The paper aims to comparison the permeability coefficient in non-cohesive soils by the method of test pumping and based on tests in a consolidometer. The tests were carried out on 18 types of non-cohesive soils with different fraction. Pumping tests were carried out according to the standard method i.e. by making one well with a diameter of 400 mm and installing two piezometers at different distances from the well. The water table change was measured in piezometers during water pumping from the well. Tests in the consolidometer were carried out on soil samples that were first compacted to the same density index as in the test site. The tests were carried out with a continuous inflow of water from below with constant gradients of 0.50. The tests presented in the paper allow to verify and compare the values of the permeability coefficient in non-cohesive soils determined in the field and laboratory tests.

Author's address:
Grzegorz Wrzesiński
(https://orcid.org/0000-0001-7715-3927)
Szkoła Główna Gospodarstwa Wiejskiego
w Warszawie
Instytut Inżynierii Lądowej
ul. Nowoursynowska 159, 02-776 Warszawa
Poland
e-mail: grzegorz_wrzesinski@sggw.pl

Scientific Review – Engineering and Environmental Sciences (2020), 29 (1), 81–92
Sci. Rev. Eng. Env. Sci. (2020), 29 (1)
Przegląd Naukowy – Inżynieria i Kształtowanie Środowiska (2020), 29 (1), 81–92
Prz. Nauk. Inż. Kszt. Środ. (2020), 29 (1)
http://iks.pn.sggw.pl
DOI 10.22630/PNIKS.2020.29.1.8

Ewa FIGIEL, Dorota LECIEJ-PIRCZEWSKA

Faculty of Civil and Architecture, West Pomeranian University of Technology

The way to limit emission – energy efficient buildings. The example of the largest facility in Poland in nearly zero-energy building standard

Key words: carbon dioxide impact, nearly zero-energy building, energy consumption, renewable energy

Introduction

The concentration of gases responsible for the development of global warming has been steadily rising for decades. Global energy-related CO_2 emissions grew by 1.7% in 2018 to reach a historic high of 33.1 Gt CO_2 (IEA, 2019). It turns out, that it's biggest contribution can be accredited to urban areas. Although they occupy only 3% of the area of our globe, they are responsible for over 70% of emissions. According to American estimations, the on-going trend of population migration from rural areas to cities will still transpire in the decades ahead. While today 55% of the world's population lives in cities, it is estimated that in 2050 it will be 68% (UN DESA, 2018). In the EU 70% of the population already are city inhabitants. The progressing urbanization and population growth may cause main metropolises to contribute to the further increase of greenhouse gases emissions in the world, if one does not take any remedial steps. The major sources of urban emissions at present are residential houses, office buildings and other buildings, which generate over half of all greenhouse gases emitted by these agglomerations. On the EU scale the entire municipal-household sector produces approx. 36% of CO_2 emissions, and it's development is connected to the further increase in demand for energy (Report COM(2013) 483 final/2). According to the Ecofys report (Wong, Jager & van Breevoort, 2016), buildings in Poland consume as much as 40% of all energy used in the country, 70% of which is accounted for heating. Right at first sight one can recognize, that it is

this sector where considerable savings can be sought.

Emissions from buildings are contributing not only to the issue of global warming. The external air quality is important for the natural environment and human health. It is known, that the air pollution in urban agglomerations, which generate smog, comes mainly from individual heating devices used in the municipal-household sector. In order to reduce the emissions, apart from implementing technologies utilizing renewable energy sources, the EU promotes and puts into action energy efficiency and smart buildings. The last one is the reaction to the recent development of the computer systems: building management system (BMS) and building and energy management system (BEMS).

In 2010 together with the revision of the Directive 2002/91/EC energy performance in buildings directive (Directive 2002/91/EC; Directive 2010/31/EU), the EU introduced as a goal "Nearly zero-energy buildings" and requires implementing this standard for a building in newly erected facilities from January 2021 onwards in all member countries. As an important building type to diminish energy use and greenhouse gas emissions in the construction industry, NZEB has attracted much attention since 2006 already (Christian, Richards, Atchley, Childs & Moon, 2006). An overview of definitions and energy-efficient measures of NZEB is presented in detail in Deng, Wang and Dai (2014). The low amount of energy that NZEB require comes mostly from renewable energy sources. Beginning on 1 January 2021 in Poland a building which is to be considered nearly zero energy needs to fulfil the requirements of heat protection of buildings included in the 2017 technical conditions (Regulation of the Minister of Infrastructure and Construction of 12 April 2002). For public buildings, it means that the value of the non-renewable primary energy indicator *EP* for heating, preparing hot water, cooling and integrated lighting or the one ensured by the auxiliary equipment in these systems cannot exceed 95 $kWh \cdot m^{-2} \cdot year^{-1}$ for buildings without a cooling system and 120 $kWh \cdot m^{-2} \cdot year^{-1}$ for buildings with a cooling system.

The above-mentioned EU directives have recently been changed as part of the "Clean energy for all Europeans package". Also, after this EU amendment in 2018 (Directive (EU) 2018/844), the planning of buildings in accordance to the NZEB standard, which integrate renewable energy sources, becomes mandatory.

The enumerated EU directives are a very significant instrument for enforcing actions, that will help in achieving highly efficient and decarbonised building resources by 2050.

Due to the above mentioned requirements many new and modernized buildings are currently being built in Europe in NZEB standard (Attia, Polyvios, Xeni & Morlot, 2017; Brambilla, Salvalai, Imperadori & Sesana, 2018). One of them is the Posejdon complex in Szczecin, Poland.

Analysed object

The Posejdon service complex (Fig. 1) is the largest facility in Poland with low energy consumption (NZEB). It is situated in the very centre of Szczecin

FIGURE 1. Visualisation – A partial view on the historic facade of the Posejdon building (author: Federacyjne Biuro Architektoniczne)

and consolidates the existing building of the former department store with a completely new part which together will constitute one functional unit. The existing building was erected on 28 November 1928 and was opened to the public the following year as the department store DeFaKa (Deutches Familien-Kaufhaus). After the war, the preserved part of the building was restored – but in a different shape from the original and in a less embellished form. Already in 1951 the building was opened again to the public as the universal department store and had been in business until 2009. Since 2015 the owner of the city block, in which the store had been located, has been the Szczecin Porto company, which received a building permit in October 2016 and the investment is planned to be completed at the end of 2019.

The complex will include an office building with an area of nearly 20,000 m^2, a conference centre for approx. 1,000 people and two hotels belonging to the Marriott chain – courtyard by Marriott and Moxy – which together will offer 255 hotel rooms. The compound will encompass a publicly available patio on the first floor of the office part where a vertical wall of green, several meters high, will be created (Fig. 2). This living green external wall acts as extra insulation with a layer of air between the plants and the wall. It also reduces noise levels by reflecting, refracting as well as absorbing acoustic energy. Like all plants, green wall plants remove carbon dioxide from the air and release oxygen. This air filtering process of the most significant greenhouse gases is certainly a remarkable improvement to air quality. Achieving BREEAM Excellent status was one of the primary objectives for this project and one contributory factor to realising this was the specification of a green wall solution.

The Posejdon complex in Szczecin will self-sufficiently generate most of the necessary heat and cooling. It will be

FIGURE 2. Visualisation – the vertical wall of green of the Posejdon patio (author: Federacyjne Biuro Architektonicze)

equipped with, among others, a modern HVAC installation based on RES technology, powered by photovoltaic cells situated on the roof of the building and a rainwater system for toilets, and devices characterised by very high energy efficiency.

Installations in the Posejdon NZEB

A huge ground heat exchanger was constructed under the building and therefore it will be possible to derive energy from the ground. The exchanger consists of 46 vertical boreholes, each 300-meter deep, situated under a foundation slab in the area of the underground garage (Figs. 3–4). The installation is filled with 28% ethylene glycol. It's design temperatures will amount to 12/8°C in winter and 26/30°C in summer. The medium from ground exchangers is directed to two exchangers – water/glycol (power of

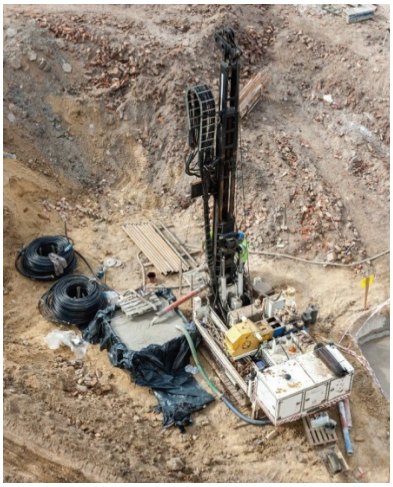

FIGURE 3. Drilling for the ground heat exchanger (source: www.posejdoncenter.pl)

2 × 400 kW) working for the water loop heat pumps (WLHP) system. In case the temperature at the outlet from the heat pump loop reaches its minimal value (6°C), the system starts operating with water/glycol exchangers supported by a reserve heat pump. In the summertime, the cooling system is to be backed up by

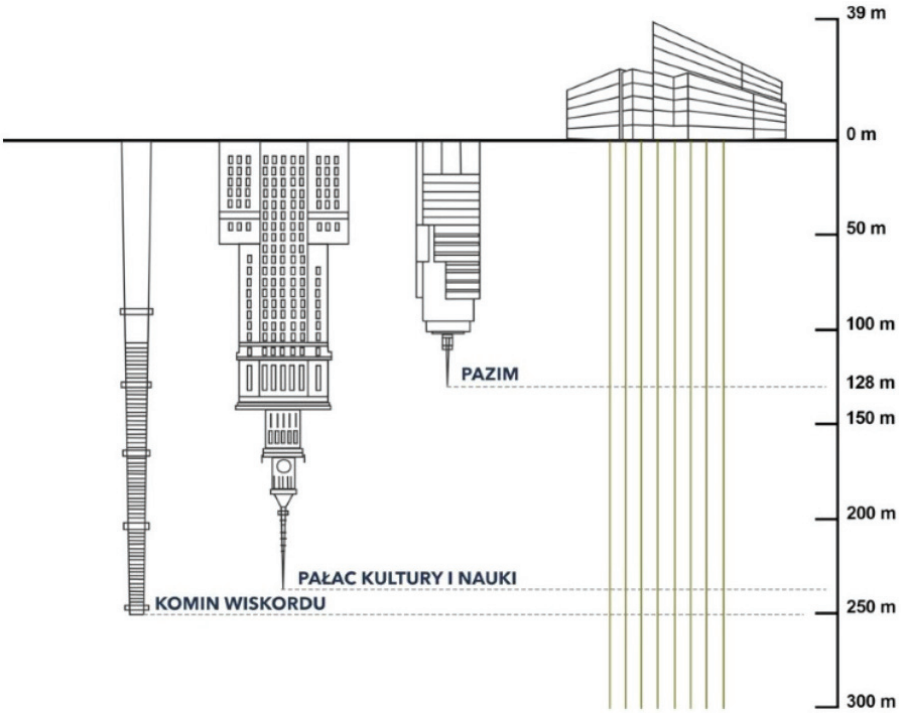

FIGURE 4. The comparison of the depth of the ground heat exchanger with the highest buildings in Szczecin and the Palace of Culture and Science in Warsaw (source: www.posejdoncenter.pl)

two evaporator-cooling towers built on the roof of the building.

Energy extracted from the ground will be used to heat the facility by means of high-efficiency local heat pumps (WLHP) in the office and service areas and also for the needs of producing domestic hot water for the hotel. On the other hand, in summer, cooling derived from the ground will be used for air-conditioning of the office and service areas also thanks to the local heat pumps (WLHP). For this purpose, the office and service part of the complex was equipped with 910 inverter heat pumps units (WLHP) placed under the ceiling, which will be responsible for maintaining the required temperatures in the rooms. The energy efficiency class of the applied units in ventilation and air-conditioning systems is A+ both for heating and cooling.

The primary heat source for the system of producing domestic hot water will be the district heating substation with hot water storage tanks. Additionally, hot water will be preheated using energy from ground heat exchangers. It was estimated that 50% of the demand for domestic hot water will be generated from the district heating substation, whereas the remaining 50% from the RES system. Cooling achieved in this way by use of the heat pump will decrease the water temperature in the water loop.

Electric energy necessary to supply auxiliary energy in HVAC installations, circulation pumps in the RES system and pumps in the district heating substation,

DHW electric heaters (intended for the office part) and internal lighting will be taken from the PV panel system with a total power of approx. 102.6 kWp (kWp is the peak power of a PV system). The installation will be constructed on the roof of the building and will consist of 342 photovoltaic monocrystalline modules. The planned annual production of electric energy from the PV roof panels system amounts to approx. 81,880 kWh.

Artificial lighting in rooms where users are in temporarily (bathrooms, staircases, an underground car park) will be controlled by motion sensors. The application of motion sensors allows to obtain relevant savings resulting from rational electric energy consumption.

The building will be equipped with LED lamps. Due to low energy needs, they contribute to the decrease of energy production which directly affects the reduction of carbon dioxide emission harmful for the environment.

In the building many solutions to limit water use have been envisaged. Treated rainwater (a grey water system) is supposed to be used for toilet flushing, watering green roofs and a green wall. Consequently, a separate installation of treated water run to bathrooms of the office part and to water the greenery on a publicly available patio situated over the ground floor has been designed.

Heating and cooling of the office--service part

In the office-service part mainly air heating and cooling systems have been provided. On the roof of the building and in technical rooms there are air handling units equipped with a high efficiency heat recovery system based on rotary or crossflow heat exchangers. The units for the office part are additionally equipped with coolers running on an ethylene glycol solution. The air handling units supply air, which will be humidified to a humidity of 40%. The air distribution system will be equipped with CAV controllers. The ventilation system has been designed with consideration for the variable flow rate depending on the internal air quality and controlled by the automation and BMS systems. The ventilation flow rate will be decreased to a minimum, when users are not present in the building. The introduced solutions should substantially reduce the energy consumption of the ventilation and air--conditioning systems.

The heating and cooling of the office and service area will be carried out by means of the water–air heat pumps, so--called water loop heat pumps (WLHP), which are also denoted in literature as water system heat pump (WSHP) systems and are the alternative to conventional air conditioning with heating systems. In the Posejdon office-service complex part there are 910 such pumps. The main feature of the system is generating heating and cooling energy directly in the location where it is used (thus, the system is decentralised), which has a positive impact on energy efficiency. However, the system needs a central heat and cooling source. In the case of Posejdon, the ground is the main heat source. When the demand for heat is maximal, glycol/ /water exchangers can be supported by a reserve heat pump. The cooling source is also the ground exchanger backed up by cooling towers (Fig. 5).

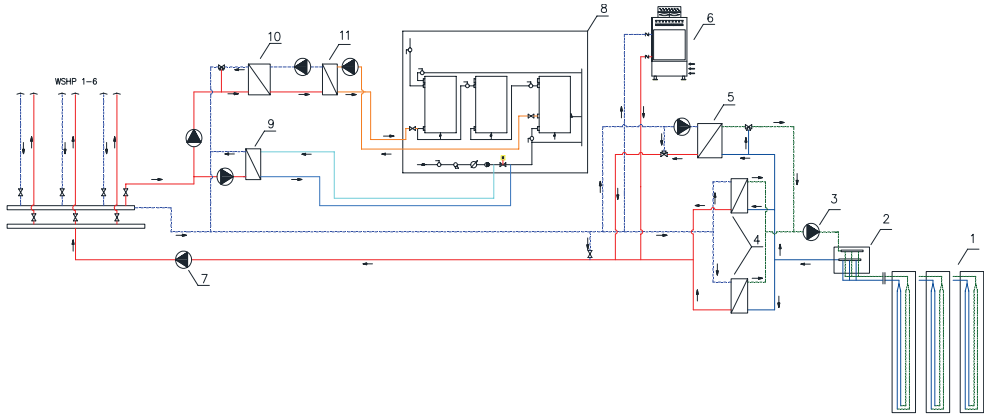

FIGURE 5. The diagram of the heat source: 1 – the ground heat exchanger (48 vertical boreholes with double-*U* geothermal probes); 2 – manifold wells; 3 – the pump set (three pumps adapted for operation in 2 + 1 system); 4 – water/glycol exchangers (with power of 2 × 400 kW); 5 – the reserve heat pump; 6 – two evaporator-cooling towers built on the roof of the building; 7 – the set of circulation pumps (three pumps adapted for operation in 2 + 1 system); 8 – the two-step district heating substation in a serial-parallel connection with hot water storage tanks for the hotel part; 9 – the water/water exchanger for preheating tap water; 10 – the water/water heat pump for heating warm water; 11 – the flow heat exchanger for heating water in load circulation of hot water storage tanks, WSHP 1-6 – 910 local heat pumps creating six two-pipe loops diagram of the heat source (author: Dorota Leciej-Pirczewska)

Single heat pumps have the certificate of high energy efficiency class (A+) with ratings: $COP > 4.1$, $EER > 5.9$, $LW_{max} < 37.5$ dB_A. They are responsible for maintaining the required temperature in the office and commercial-service rooms. Each of the 910 heat pumps will be connected to the installation by a piping system with a control valve, a sieve filter and shutoff valves (Fig. 6). Due to the variable needs for cooling and heating by the rooms being operated by the water loop, it is essential to apply a very accurate flow regulation. Because

FIGURE 6. The heat pump (WLHP) connected to the water installation by the pipe system with the control valve, the sieve filter and shut off valves (author: Dorota Leciej-Pirczewska)

of that, modern balancing ABQM valves with the newest NovoCon® digital drive of the Danfoss company have been chosen as control valves.

In order to constitute a coherent and well-functioning unity with all building energy systems, the building will operate the building management system (BMS) – an advanced system of automatic regulation and control complemented by the functionalities allowing to manage energy consumption.

The standard of the HVAC and electricity systems in Posejdon goes far beyond currently existing norms. Additionally, applied technologies allowed to obtain the prestigious BREEAM ecological certificate in the latest version New Construction 2016 on the level "Excellent".

Environmental impact: CO_2 emissions savings in analysed object

In accordance with the previously mentioned EU directives, reference is made to the importance of the reduction of CO_2 emissions in the generation of energy associated with buildings. Consequently, the most important objective of this paper is to characterize the CO_2 building emissions and savings in CO_2 emissions achieved thanks to the operation of all technologies installed in the renovated office-service part of the Posejdon building.

Methodology of research

The amount of CO_2 emission generated by the grid for heating, obtaining hot water, air conditioning, ventilation and room lighting is directly affected by the energy performance of the building. The emissions are obtained after calculation of energy use in accordance with Polish and European regulations using climatic conditions taken from a Polish meteorological database for the region Szczecin-Dąbie. The heat consumption was verified according to the regulation on the methodology of determining the energy performance of a building (Regulation of the Minister of Infrastructure and Construction of 20 December 2016) valid in Poland. The general calculations of the energy demand for heating, cooling and ventilation are based on methods from CEN standards (EN ISO 13790:2008). Emission factors for electricity are taken from the report of National Centre for Emission Management (KOBiZE, 2018). Emission rate for the district heat, a value in accordance to the regulation on the methodology of determining the energy performance of a building (Regulation of the Minister of Infrastructure and Construction of 27 February 2015), was assumed, because of a lack of data from the supplier. On that basis, CO_2 emissions were calculated. The energy consumption necessary to fulfil the building's energy demands were compared for a WLHP system together with the described below combination of auxiliary heat sources and a conventional district heating substation, which was used for the energy supply of the building before modernisation.

Results

The calculated index of annual demand for final energy for heating and ventilation of the analysed office-ser-

vice building before renovation is EK_H = = 201.71 kWh·m^{-2}·year^{-1}. The improvement of the energy performance due to the renovation results in a reduction of approx. 85% of building energy demand referring to final energy for heating in the modernised building. This means the value of EK_H decreases to EK_H = 29.28 kWh·m^{-2}·year^{-1}. As Figure 7 shows, heating, ventilation, and air-conditioning (HVAC) consume most of this energy, followed by lighting. This building presents little demand for domestic hot water (DHW). Indoor heating accounts for approx. 36% of the energy demand, whereas 12% of the total energy consumption is to meet cooling requirements.

In the case of electrical energy that is taken from the grid a reduction of 81,880 kWh·year^{-1} results from the application of photovoltaic panels, which will cover approx. 36% of the required electrical energy that concerns the energy performance of the building in question (Regulation of the Minister of Infrastructure and Construction of 20 December 2016). According to this regulation it applies to indoor lighting, auxiliary energy, running devices of the HVAC system and heating domestic hot water.

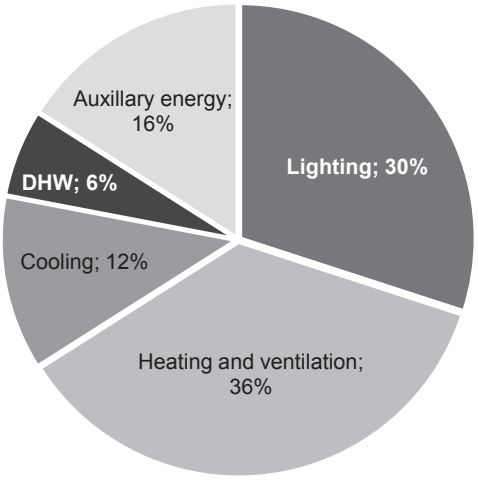

FIGURE 7. Percentages of the consumed final energy in the analysed office building after renovation

It was calculated by (KOBiZE, 2018), that the average CO_2 emissions for electricity in Poland are approx. 778 g CO_2·kWh^{-1}. Using this specific CO_2-factor for electricity in the Posejdon building, savings from the photovoltaic installation amount to 64.7 t of CO_2·year^{-1}.

Figure 8 shows the improvement of the thermal characteristic of the building envelope after the renovations. The results show that the implementation of these strategies as well as using renewable energy sources and ensuring a high energy efficiency of the installed systems, instead of conventional solutions before building renovation, could reduce CO_2 emissions up to 752.7 t·year^{-1} (Fig. 9), thus minimising the environmental impact. This constitutes a reduction of CO_2 emission on the level of 90%.

As a result, in this modernised building it was possible to achieve a very low CO_2 emission factor related to the usable area of the building. It is on the level of approx. 5.35 kg CO_2·m^{-2}·year^{-1}. In both cases, before and after renovation, there is no emission directly from the building, but released indirectly through the district heating and power plants.

It was calculated in Communication COM/2011/0112 that in order to reach the EU's 2050 target CO_2 reductions of 80%, a reduction of emission of approx. 90% in the building stock would be sufficient. The presented building meets these requirements.

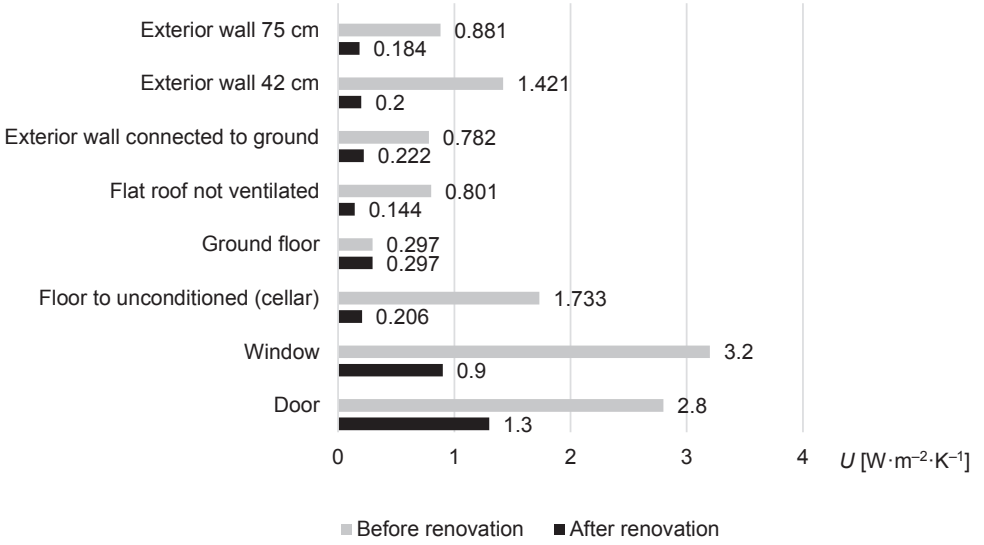

FIGURE 8. Thermal transmittance (U) of the building envelope before and after renovation

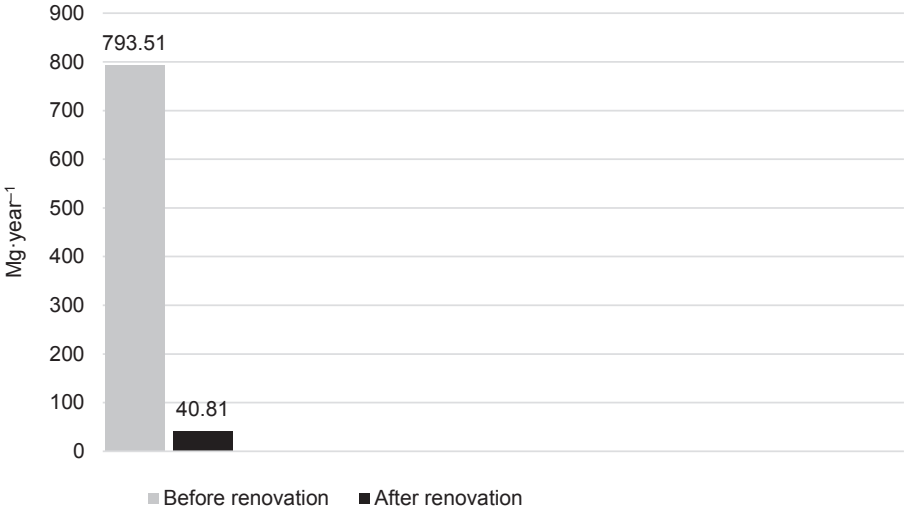

FIGURE 9. Carbon dioxide emission savings in office-service part of the Posejdon building

Conclusions

From the example of the modernised building Posejdon it can be concluded, that the energy performance, CO_2 emission and other gases responsible for global warming can be significantly improved by upgrading the building's envelope, using a more energy efficient HVAC system and by generating energy from renewable energy sources as well as applying occupancy-dependent smart

controls. In this aspect the Posejdon building is an example of best practices in the area of energy efficient renovation of non-residential buildings for the full decarbonisation of the European building stock by 2050. The list of elements being included in the renovation strategy, as set out in this article, provides an example that can be used as a guideline to fulfil this target.

References

Attia, S., Polyvios, E., Xeni, F. & Morlot R. (2017). Overview and future challenges of nearly Zero Energy Buildings (nZEB) design in Southern Europe. *Energy and Buildings*, *155*, 439-458.

Brambilla, A., Salvalai, G., Imperadori, M. & Sesana, M.M. (2018). Nearly zero energy building renovation: From energy efficiency to environmental efficiency, a pilot case study. *Energy and Buildings*, *166*, 271-283.

Christian, J.E., Richards, L., Childs, P., Atchley, J. & Moon, H. (2006). Energy Efficiency, SIPS, Geothermal, and Solar PV Used in Near Zero-Energy House. *ASHRAE Transactions*, *112*, *Part 2*, QC-06-026, 275-284.

Communication from the commission to the European Parliament, the Council, the European Economic and Social Committee and the Committee of the regions. A Roadmap for moving to a competitive low carbon economy in 2050. COM/2011/0112 final of 08.03.2011.

Deng, S., Wang, R.Z. & Dai, Y.J. (2014). How to evaluate performance of net zero energy building – a literature research. *Energy*, *71*, 1-16.

Directive (EU) 2018/844 of the European Parliament and of the council of 30 May 2018 amending Directive 2010/31/EU on the energy performance of buildings and Directive 2012/27/EU on energy efficiency. OJ L 156/75 of 19.06.2018.

Directive 2002/91/EC of the European Parliament and of the Council of 16 December 2002 on the energy performance of buildings. OJ L 1/65 of 04.01.2003.

Directive 2010/31/EU of the European Parliament and the Council of 19 May 2010 on the energy performance of buildings (recast). OJ L 153 of 18.06.2010.

EN ISO 13790:2008. Energy performance of buildings. Calculation of energy use for space heating and cooling.

International Energy Agency [IEA] (2019). *Global Energy & CO_2 Status Report 2018. The latest trends in energy and emissions in 2018*. International Energy Agency. Retrieved from: https://www.eenews.net/assets/2019/03/26/document_cw_01.pdf

Krajowy Ośrodek Bilansowania i Zarządzania Emisjami [KOBiZE] (2018). *Wskaźniki emisyjności CO_2, SO_2, NO_x, CO i pyłu całkowitego dla energii elektrycznej na podstawie informacji zawartych w Krajowej bazie o emisjach gazów cieplarnianych i innych substancji za 2017 rok* [*Emission factors of CO_2, SO_2, NO_x, CO and TSP for electricity on the basis of information contained in the National Base on Emissions greenhouse gases and other substances for 2017*]. Warszawa: KOBiZE.

Population Division of the United Nations Department of Economic and Social Affairs [UN DESA]. (2018). *World Urbanization Prospects. The 2018 Revision. Methodology*. New York: United Nations. Retrieved from: https://population.un.org/wup/Publications/Files/WUP2018-Methodology.pdf

Report from the Commission to the European Parliament and the Council. Progress by Member States towards Nearly Zero-Energy Buildings. COM(2013) 483 final/2 of 07.10.2013.

Rozporządzenie Ministra Infrastruktury i Budownictwa z dnia 20 grudnia 2016 r. zmieniające Rozporządzenie w sprawie metodologii wyznaczania charakterystyki energetycznej budynku lub części budynku oraz świadectw charakterystyki energetycznej. Dz.U. 2017, poz. 22 [Regulation of the Minister of Infrastructure and Construction of 20 December 2016 on the methodology of determining the energy performance of a building or part of a building and energy performance certificates. Journal of Laws 2017, item 22].

Rozporządzenie Ministra Infrastruktury i Rozwoju z dnia 27 lutego 2015 r. w sprawie metodologii wyznaczania charakterystyki energetycznej budynku lub części budynku oraz świadectw charakterystyki energetycznej. Dz.U. 2015, poz. 376 [Regulation of the Minister of Infrastructure and Construction of 27 February 2015 amending the regulation on the methodology of determining the energy performance of a building or part of a building and energy performance certificates. Journal of Laws 2015, item 376].

Rozporządzenie Ministra Infrastruktury z dnia 12 kwietnia 2002 r. w sprawie warunków technicznych, jakim powinny odpowiadać budynki i ich usytuowanie. Warunki techniczne 2017. Dz.U. 2002 nr 75, poz. 690 [Regulation of the Minister of Infrastructure and Construction of 12 April 2002 on the technical conditions to be met by buildings and their location. Technical conditions 2017. Journal of Laws 2002 No 75, item 690].

Wong, L., Jager, D. de & Breevoort, P. van (2016). *The incompatibility of high-efficient coal technology with 2°C scenarios*. Utrecht: Ecofys. Retrieved from: http://www.ecofys.com/files/files/ecofys-2016-incompatibility-of-hele-coal-w-2c-scenarios.pdf

Summary

The way to limit emission – energy efficient buildings. The example of the largest facility in Poland in nearly zero-energy building standard. In Szczecin a mixed-use complex Posejdon is being constructed. It will be the first nearly zero-energy building (NZEB) in Poland that meets the strict ecological standards that all buildings will have to meet after January 2021. The project was presented at the COP24 United Nations Climate Change Conference in Katowice. The calculated building CO_2 emission is very low. Based on the example of the Posejdon complex's office-service section before and after renovation modern technical solutions for meeting the buildings energy demand and the resulting reduction of CO_2 emission have been presented. The emissions were obtained after the calculation of energy use in accordance with Polish and European regulations concerning the energy performance of buildings using climatic conditions taken from a Polish meteorological database. The described renewable energy technologies implemented in the Posejdon building, serve as a reference to export management and design strategies to other NZEB with similar characteristics in the same region.

Authors' address:
Ewa Figiel
(https://orcid.org/0000-0001-7034-371X)
Dorota Leciej-Pirczewska
(https://orcid.org/0000-0003-1676-1683)
Zachodniopomorski Uniwersytet Technologiczny w Szczecinie
Wydział Budownictwa i Architektury
al. Piastów 50, 70-311 Szczecin
Polska
e-mail: figiel@zut.edu.pl
dlp@zut.edu.pl

Scientific Review – Engineering and Environmental Sciences (2020), 29 (1), 93–107
Sci. Rev. Eng. Env. Sci. (2020), 29 (1)
Przegląd Naukowy – Inżynieria i Kształtowanie Środowiska (2020), 29 (1), 93–107
Prz. Nauk. Inż. Kszt. Środ. (2020), 29 (1)
http://iks.pn.sggw.pl
DOI 10.22630/PNIKS.2020.29.1.9

Sugiono SUGIONO[1], Siti NURLAELA[2], Andyka KUSUMA[3], Achmad WICAKSONO[1], Rio P. LUKODONO[1]

[1] Faculty of Engineering, Brawijaya University
[2] Faculty of Civil, Planning, and Geo Engineering, Institut Teknologi Sepuluh Nopember
[3] Faculty of Engineering, Universitas Indonesia

Impact of elevated outdoor MRT station towards passenger thermal comfort: A case study in Jakarta MRT

Key words: elevated MRT station, thermal comfort, computational fluid dynamic (CFD), predicted mean vote (*PMV*), predicted percentage of dissatisfied (*PPD*)

Introduction

Human comfort is affected by both physical and psychological factors. Human requires an optimum environmental condition to work effectively and efficiently. Bridger (2003) in his book mentioned several things that cause human comfort, for instance: temperature, light emitting, humidity, air circulation, odor, dust, sound and lighting. The microclimatic parameters around the MRT depend on its layout, material, size, air/wind flow through the surrounding buildings and quality of the air carried by a moving train. The British standard BS EN ISO 7730:2005 defines heat comfort as conditions and situations of the human mind that express his/her satisfaction towards the heat level of the surrounding environment. Heat comfort describes psychological conditions that indicate feeling cold or hot. Heat comfort is subjective and as the result, it is difficult to define what "comfortable" is. According to the standard ASHRAE 55-2004, thermal comfort is the level of human perception related in expressing their satisfaction towards the thermal environment and this perception depends upon subjective views. Ponni and Baskar (2015) explained that thermal performance of a building is a description of the process of modeling energy transfer between a building and its environment.

The Health and Safety Executive noted that the most suitable indicator of heat comfort is number of individuals

working in a workspace who are satisfied with the temperature of the workspace. Therefore, HSE believe that a minimum of 80% of workers occupying a building should find the temperature reasonable (HSE, 2017). Höppe (2002) stated three types of thermal comfort approaches: thermophysiological, heat balance and psychological. Researchers have investigated thermal comfort for trains, both thermal comfort on the train and at the station. Jenkins, Gilbey, Hall, Glenis and Kilsby (2014) investigated the impact of thermal discomfort due to clime change in underground railways. Temperature changes due to urban development will have an impact on human thermal comfort of MRT passengers. As an addition, Li et al. (2009) used computational fluid dynamics (CFD) simulations to evaluate the level of thermal comfort through three air conditioning installation schemes. This research mainly investigated the influence of wind speed, temperature, altitude and angle from the improvement of air circulation through air conditioners. The strong majority of the research studies concerning on MRT thermal comfort inside the MRT train and inside the underground MRT station. That is no specific research which discussed thermal comfort in outdoor elevated MRT station more than 20 m above ground level. Assimakopoulos and Katavoutas (2017) discussed the thermal comfort affected by the occupation of the railroad platform, namely the depth of the railroad canal to the train station surface. Furthermore, they were investigated thermal comfort conditions at the 0 m platforms of the outdoor Athens Metro. Tropical and subtropical climates will also make a difference in the character of thermal comfort.

Geographically, Jakarta has tropical climate and therefore, the highest average temperature takes place in October (36.2°C for north-south and 37.7°C for the east-west), while the lowest occurs in November and February (approximately 32.5°C) (Maru, Ahmad, Malaysia & Malaysia, 2014). Rural Chemical Industries (Aust) Pty Ltd (n.d.) in their article mentioned that the highest relative humidity in Jakarta takes place in February (85%) and the lowest one is in August (68%). Another factor contributing to this is that the fact that Indonesia is situated between two oceans and two continents. Indonesian standard SNI 6390:2011 described the national guidelines of thermal comfort. It explains that temperature comfort of working space is 25.5°C (±1.5°C) and relative humidity (*RH*) is 60% (±5%). For semi-outdoor space such as lobby, and open-space MRT station, temperature for thermal comfort is 28.5°C (±1.5°C) with relative humidity of 60% (±10%). In general, human starts to produce sweat at the temperature of 26°C. Human productivity is degrading when the temperature is higher than 24°C (Lan, Wargocki & Lian, 2011). Working performance decreases by 2% when the temperature increases by 1°C above 25°C (Seppänen, Fisk & Faulkner, 2005). It is difficult for human to work at the temperature between 33.5 and 35.5°C. Human being cannot perform well at the temperature of over 36°C (Sugiono, Swara, Wijanarko & Sulistyarini, 2017).

Comfort thermal evaluation using predicted mean vote (*PMV*) is suitable for semi-outdoor building, for example elevated MRT station. Predicted mean vote will measure comfort by calculating the combination between ambient tempera-

ture and relative humidity. AREN 3050 (2005) used *PMV* scale translated from the ASHRAE thermal sensation scale guideline. Kurazumi et al. (2012) emphasized on the use of *PMV* to analyze climate change and stress level of urban community. Predicted percentage of dissatisfied (*PPD*) represents satisfaction level of residents towards thermal comfort. Based on standard ASHRAE 55-2004, the acceptable and recommended *PPD* for thermal comfort is lower than 10% of dissatisfied residents (Stanton, Hedge, Brookhuis, Salas & Hendrick, 2004). Many scholars used *PPD* to analyze thermal level, for instance Pourshaghaghy and Omidvari (2012) investigating thermal comfort in hospital building. Simion, Socaciu and Unguresan (2016) used *PPD*/*PMV* to analyze thermal comfort in vehicles. Computational fluid dynamic simulation was developed to describe airflow pattern that hit human. Studies involving CFD to predict thermal comfort were conducted by several researchers, for example Mochida, Yoshino, Takeda, Kakegawa and Miyauchi (2005), Stavrakakis, Zervas, Sarimveis and Markatos (2010), Alajmi, Baddar and Bourisli (2015).

Research theory

Thermal comfort

Höppe (2002) mentioned three approaches of thermal comfort, thermophysiological, heat balance, and psychology. Karyono (2001) defined thermal comfort as hot or cold sensation as response from our skin towards the surrounding temperature. Parsons (2014) argued that it is the thermal state of the human body that determines the thermal sensation. Standard BS EN ISO 7730:2005 stated that condition of mind expresses satisfaction with the thermal environment (Epstein & Moran, 2006) and is assessed by subjective evaluation (ASHRAE 55-2004; Bean, 2012). According to standard ISO 7730:2005 thermal (heat) balance is obtained when the internal heat production in the body is equal to the loss of heat to the environment. Boutet (1987) noted that psychological factor is an aspect to consider in thermal comfort as each individual has different perception on comfort (Purnomo & Rizal, 2000).

Heat is the main factor affecting human activities and performance. To perform well, human requires a comfortable and constant temperature. Lippsmeier (1997) stated that the suitable temperature for people living in the equator is between 19 and 26°C. The classification is as follows:

- at the temperature of 26°C, human in general starts to produce sweat;
- between 26 and 30°C, resistance and performance start to decline;
- between 33.5 and 35.5°C, human can barely adapt to the condition of the environment;
- between 35 and 36°C, human can no longer adapt to the condition of the environment.

Human body produces heat as the result of metabolism and controls it while maintaining body heat balance. Increase or decrease of internal temperature (higher or lower than the normal range) will disturb both mental and physical activities, and in an extreme temperature difference, serious physiological or health issues may take place. Human or animals increase their temperature so that their

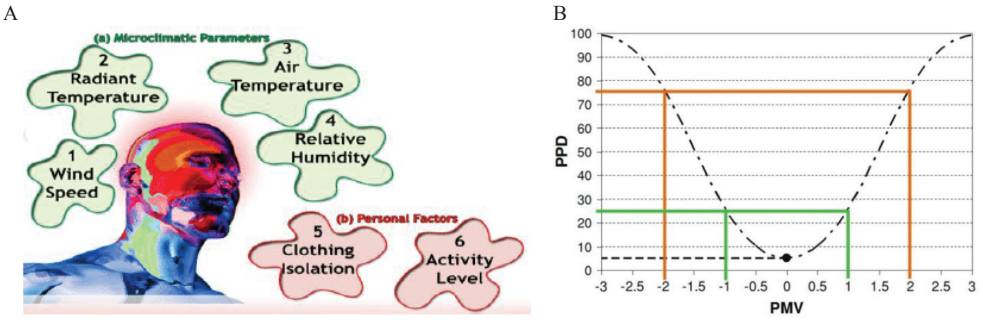

FIGURE 1. Predicted mean vote and predicted percentage of dissatisfied: A – six parameters of the *PMV* in human thermal comfort (Sugiono et al., 2017); B – *PPD* calculation based on *PMV* (ASHRAE 55-2004)

immune system can work effectively to kill bacteria or viruses.

Predicted mean vote refers to index used to predict an overall thermal sensation that individuals in a large group experience (Stanton et al., 2004). Model of *PMV* shows that thermal sensation can be described as function of thermal load in effector mechanism of the human thermoregulatory system. In normal situation, the thermoregulatory system will automatically modify skin temperature and sweat secretion to maintain body heat balance. Predicted mean vote determines range of temperature sensation human experiences towards his or her surrounding. Predicted mean vote scale is between –3 (extremely cold) and +3 (extremely hot). Figure 1a explains six factors of *PMV* to define the human thermal comfort. According to the figure, it can be divided into two categories: microclimatic parameters (radiant temperature, air temperature, wind speed, and relative humidity) and personal factors (clothing isolation and activity level). Predicted mean vote equation can be used when activity (metabolism pace) and clothing (thermal resistance) are estimated, and some parameters of the environment, such as: temperature, mean radiant temperature, relative air velocity, and relative humidity, are measured directly (Simion et al., 2016).

Predicted mean vote can be estimated based on Equation 1 combining four microclimatic parameters and two personal factors mentioned previously (Stanton et al., 2004).

$$PMV = (0.303e^{-0.036M} + 0.028)\{(M - W) - 3.05 \cdot 10^{-3}[5733 - 6.99(M - W) - p_a] - 0.42[(M - W) - 58.15] - 1.7 \cdot 10^{-5} M(5867 - p_a) - 0.0014M(34 - t_a) - 3.96 \cdot 10^{-8} f_{cl}[(t_{cl} + 273)^4 - (MRT + 273)^4] - f_{cl} h_c (t_{cl} - t_a)\} \quad (1)$$

In which:

$$t_{cl} = 3.57 - 0.028(M - W) - I_{cl}\{3.96 \cdot 10^{-8} f_{cl}[(t_{cl} + 273)^4 - (\overline{t_r} + 273)^4] + f_{cl} \cdot h_c \cdot (t_{cl} - t_a)\} h_c =$$

$$= 2.38(t_{cl} - t_a)^{0.25}$$

$$\text{for } 2.38(t_{cl} - t_a)^{0.25} > 12.1\sqrt{v_{ar}}$$

$$h_c = 12.1\sqrt{v_{ar}} \text{ for } 2.38(t_{cl} - t_a)^{0.25} < 12.1\sqrt{v_{ar}}$$

$f_{cl} = 1.00 + 1.290\ I_{cl}$
for $I_{cl} \leq 0.078\ m^2 \cdot °C^{-1} \cdot W^{-1}$

$f_{cl} = 1.05 + 0.645\ I_{cl}$

for $I_{cl} > 0.078\ m^2 \cdot °C^{-1} \cdot W^{-1}$

Predicted percentage of dissatisfied (*PPD*) is derivation of *PMV* predicting percentage of dissatisfied individuals from a large group towards the temperature (thermal comfort) (Stanton et al., 2004). Once *PMV* has been obtained, *PPD* can be measured based on Equation 2:

$$PPD = 100 - 95 \cdot \cdot e^{-(0.03353 \cdot PMV^4 + 0.2179 \cdot PMV^2)} \quad (2)$$

To measure *PPD* for room with direct sun radiation, we should make some adjustment towards the equations first. Equation 3 (Chaiyapinunt, Mangkornsaksit & Phueakphongsuriya, 2004) is the result of the adjustment. Figure 1b shows the relationship of *PMV* and *PPD* values for human thermal comfort. Environmental conditions that are too hot (+*PMV*) and too cold (–*PMV*) give a high *PPD* value (discomfort perception). According to the graph, the lowest percentage of *PPD* is 5%, it means that even in neutral condition 5% individuals will be dissatisfied

$$PPD = PPD_{\text{no solar}} + PPD_{\text{solar radiation}} \quad (3)$$

Human heat stress

Heat stress can be defined as combination of environmental and non-environmental factors that cause heat radiation to enter the body or prevent heat dissipation by the body (Bridger, 1995). Heat stress can occur when the body absorbs or produces more heat than that can be discharged through the thermoregulatory process, and illness and death can occur as a result of rising core temperatures (Stanton et al., 2004). Outdoor conditions can indicate the risk of heat stress that people who live in hot climates can experience. Heat stress can occur in unique situations, such as fire fighting. Indoor, heat stress occurs in many workplaces, such as iron and steel smelting, glass making factories, bread making factories, commercial kitchens, laundry, and power plants. Individual behavioral factors, such as wearing protective clothing can also increase risk of heat stress. Heat stress varies between individuals depending on physiological risk factors that an individual has.

Heat stress may result in several heat disorders and severe heat disorders may cause death. According to EU-OSHA (2012), some examples of heat disorders induced by heat stress are: heat stroke, heat exhaustion, heat syncope, heat cramps, heat rash, and transient heat fatigue among others. Heat stroke has several symptoms, namely hot, red, freckled or bluish dry skin, perspiration, confusion, loss of consciousness, seizure, fast pulse, and rectal temperature higher than 40°C. The cause of heat stroke is partial or overall failure of sweat mechanism and as the result, the body is unable to get rid of excess heat. Treatments for heat stroke are contacting medical professionals and reducing victim's temperature immediately. Heat stroke can be prevented by acclimation, close monitoring on the symptoms of heat stroke, medical screening, and plenty of water. Transient heat fatigue has several symptoms, such as decreasing working perform-

ance, particulary in skilled physical labor, mental labor and type of work where concentration is required. The causes of transient heat fatigue are discomfort and exposure to heat. Transient heat fatigue can be prevented by acclimation and training. Thermal comfort on trains occurs in many locations which are divided into three locations: inside the train, inside the station and locations outside to the station. Based on the initial survey, the high temperature outside the station (> 30°C) and setting the temperature inside the train at temperatures of 20–22°C is a problem that must be investigated. Furthermore, passengers were feel hot and cold in some location of Jakarta MRT.

Research methodology

As mentioned before, the main objective of this paper is to measure the existing thermal comfort of passengers in the elevated MRT station and then to give some recommendations to gain more comfort. There are seven elevated stations (outdoor) in the city so far, namely Lebak Bulus, Fatmawati, Cipete Raya, Haji Nawi, Blok A, Blok M, and Sisingamangaraja. Based on the review of related literatures, the approaches used to evaluate thermal comfort of passsengers in MRT station were *PMV* and *PPD* that involved six factors, including clothing isolation, pace of metabolism, relative wind speed, temperature, relative humidity, and a series of average temperature.

To understand design of the existing MRT stations from thermal comfort point of view is a vital aspect in this study. To achieve the goal, the study used descriptive approach. Descriptive study comprises of exploration, clarification, and interpretation of phenomena on thermal comfort. The primary data, condition of the MRT stations, were obtained from field observation, while data on the parameters thermal comfort and a 3D model of the MRT stations were obtained from direct measurement, observation and interviews. Observation was conducted to identify passenger's activities, the reference for the pace of metabolism (contact), and passenger's clothes, the reference to determine cloth insolation score (clo). Airvelometer (Alnor AVM440-A) is used to measure velocity, temperature, humidity and calculates flow and actual/standard velocity. The secondary data were readily available data or ones prepared by the MRT officials. The secondary data were the dimensions of the elevated MRT stations and its interior design.

Figure 2a shows the research procedures which are starting from data collection, *PMV* and *PPD* calculation and probing ideas on solutions of the passengers' heat stress. The first step was to collect data on *PMV* factors from several MRT locations. Predicted mean vote was used to predict *PPD* using Equation 2. The following steps were to develop a 3D model of the MRT using the CAD and test it using the CFD simulation to describe the real situation from the distribution of air velocity, temperature and relative humidity contour. Computational fluid dynamics (CFD) is a computational method used to identify dimension, area and volume of fluid media; it shows calculation for each denominator. The advantages of CFD software are it is time and cost-efficient. The CFD can

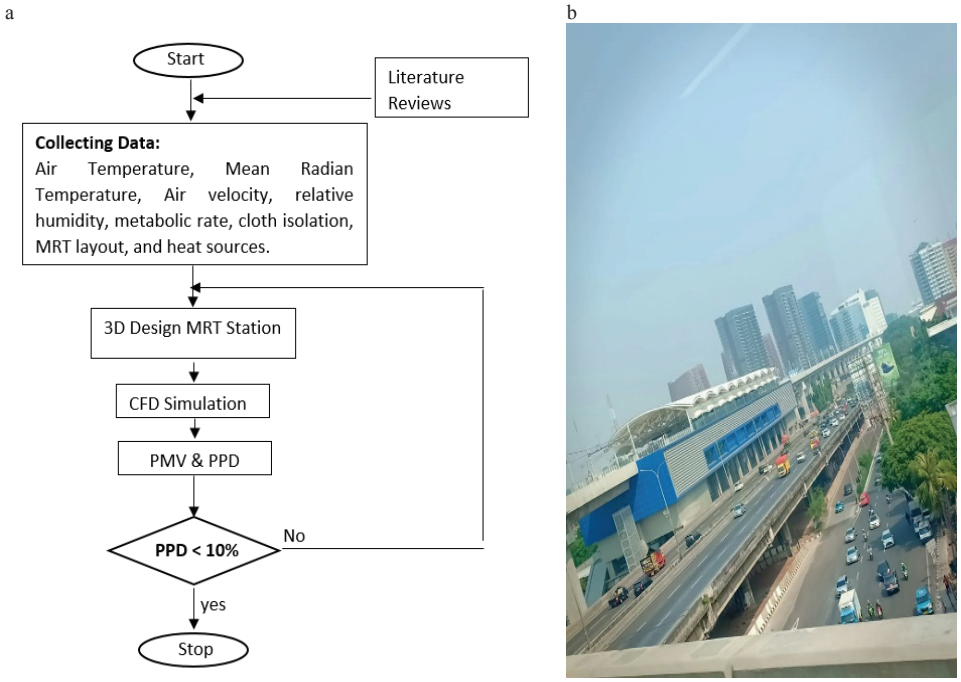

FIGURE 2. Research methodology and object: a – steps for identifying the best MRT station design in terms of thermal comfort; b – Fatmawati station

also be used to measure the parameters of airflow such as velocity, relative humidity, temperature, and average radiant temperature. The CFD can reduce design engineering process. These are the importance of CFD simulation to understanding characteristics of flow of fluid in studies on heat. This simulation provides graphic, vector, contours and animated videos. Validation was conducted by making comparison between *PMV* score from the primary data and one from CFD simulation. When average *PPD* is higher than 10%, changes should be made on the condition of the MRT station. In this case, CAD model and CFD simulation were the key factors to improve heat comfort of the warehouse workers.

The object of the study was Fatmawati MRT station, the highest elevated MRT station in Jakarta. Other considerations to select the MRT station as the object were its building complexity and the flyovers nearby (Fig. 2b). The length of Fatmawati MRT station is 175 m, width is 22.3 m, and height reached 34.3 m (from the surface of the road to the roof of the station) and 25.6 m (from the surface of the road to the passenger platform). The station roof adopted natural ventilation system allowing air circulation freely. Measurement of the environment (temperature, air velocity, and relative humidity) was conducted on the ground, the first and the second floor (platform). The researchers selected several locations in which a lot of passengers passed

by or conduct their activities. There are four locations for collecting the environmental data: ticket purchase queue, MRT station entrance, passenger waiting room and cafe. Data collection was conducted between 7:00 a.m. to 8:00 p.m. based on the ASHRAE. The highest temperature occurred between 11:00 a.m. to 3:00 p.m on the dry season (June, July and August). Passenger's metabolism was evaluated based on how much they sit down and walk, while clothing isolation data were obtained based on casual or working attires the passengers wore.

Results and discussions

Investigation of parameters thermal comfort in elevated MRT station worked in three conditions: train arriving, train departing, train arriving and departing.

Comparison of six factors (relative wind velocity that hit the passengers, metabolism rate, relative humidity, mean radiant temperature, air temperature and cloth insolation), represented in *PMV* score, at four seats in the station (right/ /left of the train) are the basis for identifying and improving the elevated MRT station design. Figure 3 shows a 3D model of the highest elevated MRT station – Fatmawati station. Unlike the other stations, this MRT station has an intermediate area located under the concourse area. For easy access from the road to the intermediate area, passengers can choose one among the three staircases, two escalator, and one elevator. The MRT officials will add another escalator later. To get to the concourse area from the intermediate area, passengers can select one of the two staircases, two escalators, and one elevator. The best roof for the three stations it is working on is the U-650. This roof mounting system does not require any bolt and therefore, causes no damage to the roof and reduces the risk of leakage in the overlap. The advantage of this system is its seaming technology on the overlap between the sheets. Wave height of 100 mm makes the U-650 roof very effective for buildings with a small degree of slope, up to 2°. Roofs with high waves can drain rainwater more effectively. U-650 roof can be installed for buildings with very wide spans. U-650 is a product that has been obtained FM APPROVED certification under FM APPROVAL Standard Class 4471 with a mixture of zinc and aluminum.

First step investigation is to compare the *PMV* scale between real condition and CFD simulation results. The input parameters of the *PMV* calculation that need to be considered in comparison are microclimate parameters in the form of ambient temperature, relative humidity and wind speed. Based on the comparison, it can be concluded that a 3D model is valid with level of error of 0.95%. Both *PMV* and *PPD* were employed to describe thermal comfort or discomfort of passenger at Fatmawati MRT station. The data shows that the highest temperature was 34.8°C with the relative humidity of 63.28% and the wind velocity of 0.32 $m \cdot s^{-1}$. The analysis was conducted at the height of 100 cm from the floor level (passenger chest area when sitting position) (Piasecki, Fedorczak-Cisak, Furtak & Biskupski, 2019). Types of clothing MRT passengers are divided into two: casual wear (t-shirt, shorts and sandals) and formal wear (suits/shirts and shoes). Based on the cloth insola-

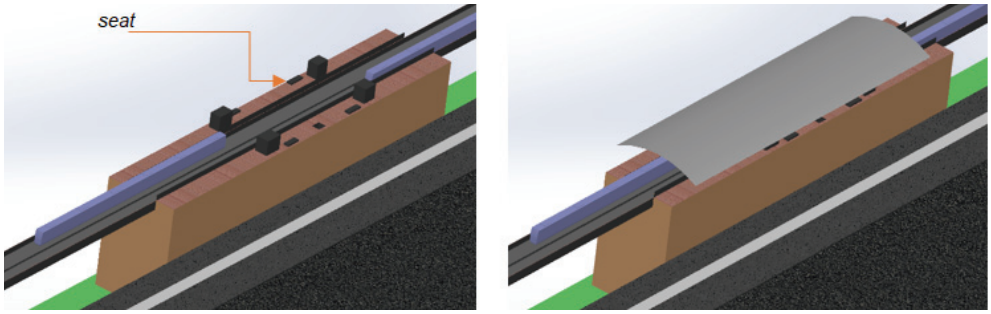

FIGURE 3. Elevated MRT station (Fatmawati station) in a 3D CAD model

tion table ASHRAE 2004:16, insolation of each condition is 0.3 and 1.1 clo. Furthermore, the metabolism of the MRT passengers while they are sitting on the platform is low (1 met) (Stanton et al., 2004). Predicted mean vote can be measured using Equation 1, *PMV* scores of the four sitting positions were 3.65, 3.66, 3.64 and 3.65 (extremely hot) with the *PPD* of 100% (everyone felt discomfort). Predicted mean vote of the arrival of one or two trains does not have significant influence towards the overall *PMV*; change occurred only when the wind hit the passengers.

Figure 4 shows the impact of wind speed due to train arrival. When there are no trains coming or leaving the station, the wind speed only comes from outside the station (Fig. 4a). The wind speed that arises and hits the seated passenger is around 0.258 $m \cdot s^{-1}$ and will produce *PMV* equal 3.67. When the MRT train enters the station at low speed, the train carries a gust of wind that hits passengers sitting in the platform waiting room (Fig. 4b). Gusts of wind from the coming train have changed the distribution of wind speed. The results of the simulation show that the average velocity of the wind (v) around the seat is 0.271 $m \cdot s^{-1}$ and produces *PMV* of 3.63, slightly lower than without a train. The third condition (Fig. 4c) is the arrival of trains and trains leaving the MRT station, which also changes the contour of the airspace that hits passengers sitting in the waiting room. From the CFD simulation, v of 0.271 $m \cdot s^{-1}$ and *PMV* of 3.62 are produced. Changes in wind speed due to trains do not significantly reduce *PMV* values.

Based on the simulation as described on Figure 4, arrival and departure of the train at the elevated MRT station did not have significant influence towards wind velocity that hit the passengers. Furthermore, change of wind velocity was unable to maintain passengers' thermal comfort by decreasing *PMV* and *PPD* at extremely hot category. Using the first and second formulation, sensitivity factor that develops *PMV* and *PPD*, which can reduce heat stress level rapidly, was to decrease temperature. To improve thermal comfort, the relationship between temperature, *PMV* and *PPD* must be known. This relationship was tested in the temperature range of 25–36°C, as shown in Figure 5. From these graphs it can be explained that at temperatures less than 27°C will give a negative *PMV* value (increasingly felt cold) and vice versa at temperatures greater than 27°C will give

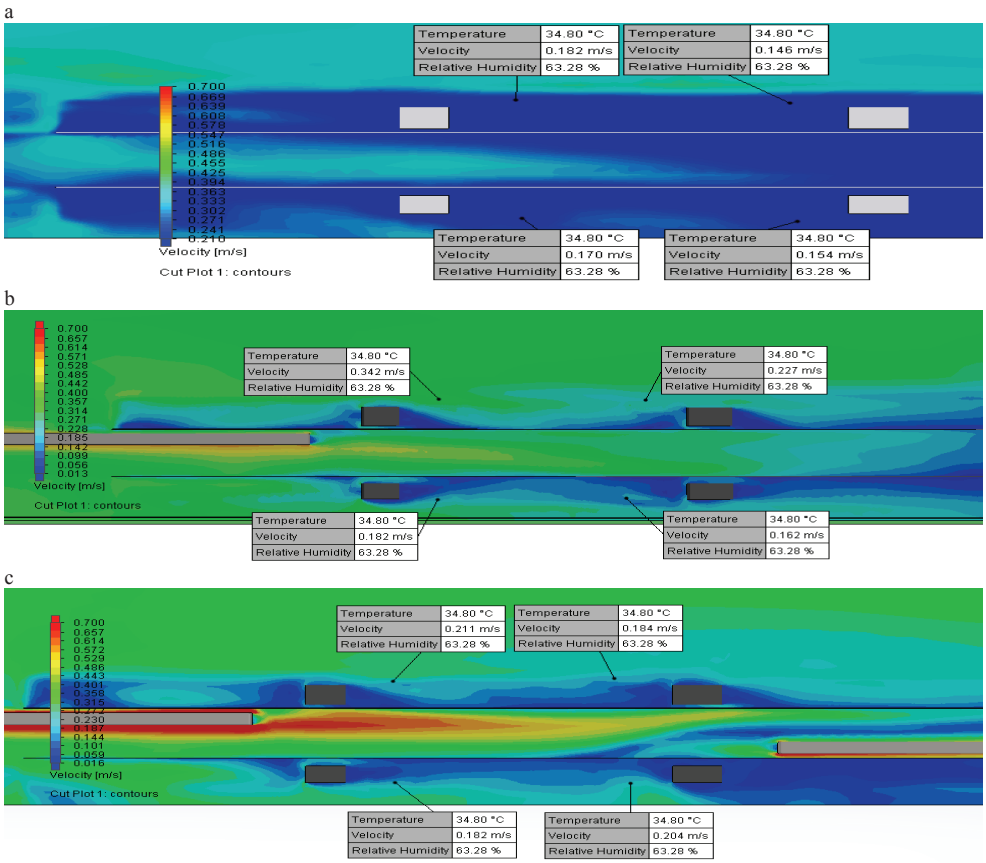

FIGURE 4. Impact of wind hitting chest of a sitting person (1 m above the floor level) on the passenger platform due to train arrival, when: a – there is no train; b – a train is arriving; c – different train is arriving and departing at the same time

a positive *PMV* value (the more heat is felt). This situation is used as a basis for determining the target temperature balance that occurs in the passenger lounge for elevated MRT stations. Simulations will be conducted at two temperature values: at 26°C which produces *PMV* of –0.74 with *PPD* of 16.7% and at 29°C which produces *PMV* of 0.71 with *PPD* of 15.8%. Standard ASHRAE 55-1992R which states that the maximum allowable *PPD* value of 10% will be used as a reference to find the right temperature value in the passenger's waiting room.

There are several alternatives to reduce the temperature around the waiting room of the elevated MRT station of which height is higher than 25 m from the ground surface. The alternatives are to install air conditioning, add certain types of plant in the waiting room, and reduce heat exposure by modifying the material used for the station roof. Previous studies (Sugiono et al., 2017) have investi-

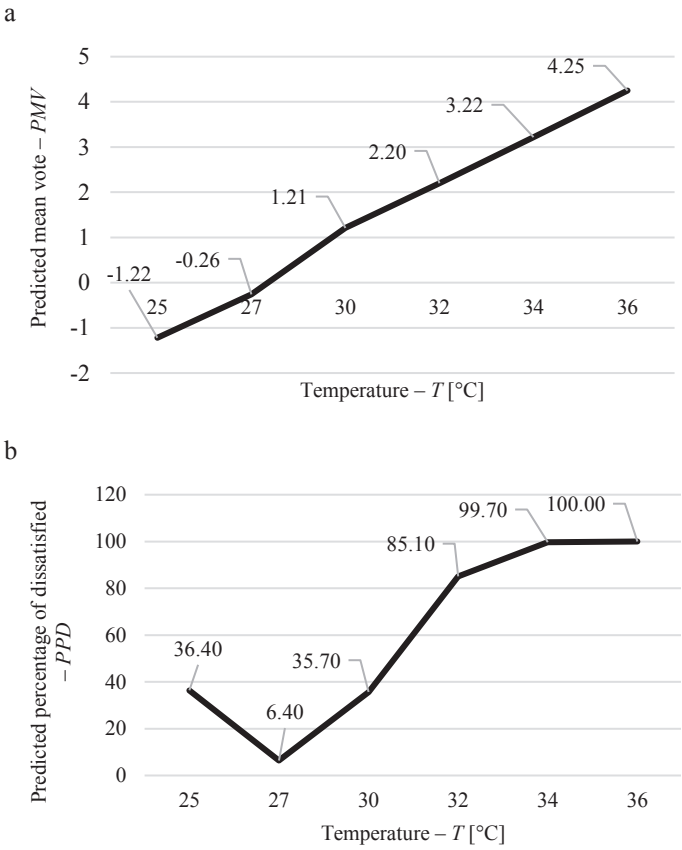

FIGURE 5. Sensitivity of the change of *PPD* and *PMV* scores towards the change of temperature at range of 25–36°C: a – relationship between value changes of *T* and *PMV*; relationship between value changes of *T* and *PPD*

gated the effectiveness of plants (English Ivy, peace lily, Boston fern and *Rhoeo spathacea*) to improve thermal comfort. Plants are able to maintain slower heart rate compared to people in a room without any plants. Predicted percentage of dissatisfied for room without plants was 59.1% and white lily reduced *PPD* drastically to 11.1% and Boston fern reduced the index to 14.3%. In conclusion, plants can reduce heat stress among human and work like air conditioning. Heat transfer through conduction, convection, and radiation from a building mostly takes place through wall, windows and ceilings (Humphreys & Fergus Nicol, 2002). Roof with high solar reflective index (*SRI*) and high emission play pivotal role in cooling down a building and increasing thermal comfort (Latha, Darshana & Venugopal, 2015). The roof of Jakarta MRT station is made of zinc–aluminium, has low absorptivity (short wave) and emissivity (long wave) from sun radiation. Uemoto Sato and John (2010) explained that lime silica brick (0.45 absorptivity, 55% brightness)

and pine wood (0.4 absorptivity, 50% brightness) are suitable material for roof.

Another alternative to reduce the temperature is changing the design of the elevated MRT station from semi-outdoor to indoor station and then, to add air conditioning (AC). Installation of six units of AC is adjusted to the velocity contour plot from the existing model that hit the train station, so that airflow from the AC decreases the temperature of the waiting room more effectively. Figure 6a shows the installation site for six air conditioners (2pk) located on the station wall. Several experiments with CFD simulations were carried out to get the right AC setting temperature, which is at 23°C for $AC_{1,2,3,4,5}$ and 24°C for AC_6. Based on the simulation, AC installation reduced *PMV* in a significant manner to the targeted thermal comfort. Referring to Figure 6b, the *PMV* for Seat 1 (T = 26.64°C, RH = 48.16%, v = 0.116 m·s^{-1}) is –0.03 with *PPD* of 5%, for Seat 2 (T = 25.85°C, RH = 44.68%, v = 0.147 m·s^{-1}) is –0.04 with *PPD* of 8.3%, for Seat 3 (T = 26.70°C, RH = 48.42%, v = 0.118 m·s^{-1}) is –0.03 with *PPD* of 5%), and for Seat 4 (T = =25.73°C, RH = 44.22%, v = 0.181 m·s^{-1}) is –0.58 with *PPD* of 12.1%. In conclusion, installation of six units of AC can effectively change the passengers' perception of a room from discomfort/extremely hot (*PMV* = ±3.6) to neutral/comfortable (*PMV* = ±0.04).

a

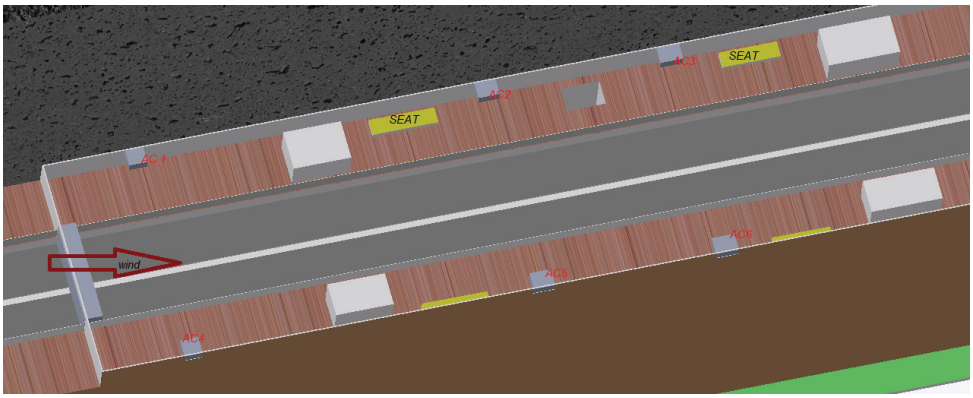

b

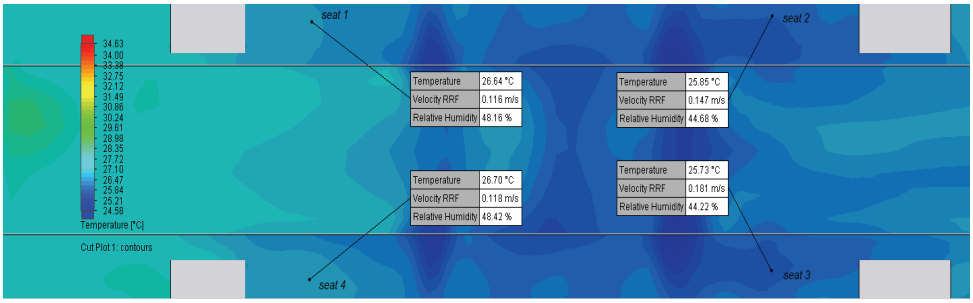

FIGURE 6. Semi-outdoor elevated MRT station with additional AC installations: a – axonometric overview; b – contour plot, result of the CFD simulation

Conclusions

The paper shows how to employee thermal comfort knowledge to optimise the design of elevated MRT stations at Jakarta. The investigation worked to find the best set up of air conditioning which will consume less energy. Thermal comfort method of predicted mean vote (*PMV*) and predicted percentage of dissatisfied (*PPD*) involved six main parameters: air temperature, mean radian temperature, wind velocity, relative humidity, cloth insolation and metabolic rate. Based on the analysis, the thermal comfort of existing station model produced *PMV* of 3.6 and *PPD* of 100% (all passengers in the waiting room feel discomfort due to heat).

Based on the CFD simulation, variety of *PMV* parameters for relative humidity, wind speed, metabolism, and clothing insolation did not reduce *PMV* value significantly as the higher of air temperature. As consequence, to increase the human thermal comfort needed to control (reduce) air temperature by using air conditioning (AC) in indoor elevated MRT station. Installing six units of AC (2pk, 23°C for $AC_{1,2,3,4,5}$, 24°C for AC_6) successfully reduced *PMV* scale into –0.04 (comfort zone) with *PPD* less than 10%. Putting some trees/flowers can also improve air quality and air fresh (more oxygen) that indirectly maintain thermal comfort.

Acknowledgements

Our acknowledgement goes to the Ministry of National Education of the Republic of Indonesia for supporting this study. The researchers would also like to express their gratitude to the research partners: Universitas Brawijaya (UB), ITS and Universitas Indonesia (UI), for their extraordinary courage.

References

AREN 3050 (2005). Environmental Systems for Buildings I.

ASHRAE 55-1992R. Thermal environmental conditions for human occupancy.

ASHRAE 55-2004. Thermal environmental conditions for human occupancy.

Alajmi, A.F., Baddar, F.A. & Bourisli, R.I. (2015). Thermal comfort assessment of an office building served by under-floor air distribution (UFAD) system – a case study. *Building and Environment*, *85*, 153-159. https://doi.org/10.1016/j.buildenv.2014.11.027

Assimakopoulos, M.N. & Katavoutas, G. (2017). Thermal comfort conditions at the platforms of the Athens Metro. *Procedia Engineering*, *180*, 925-931. https://doi.org/10.1016/j.proeng.2017.04.252

Bean, R. (2012). *Thermal comfort and indoor air quality* [Online slides]. Retieved from www.healthyheating.com/Thermal-comfort-and-indoor-air-quality/Thermal-comfort-and-indoor-air-quality.pdf

Boutet, S.T. (1987). *Controlling air movement*. New York: McGraw Hill Book Company.

Bridger, R.S. (1995). *Introduction to ergonomics*. Boca Raton: CRC Press. https://doi.org/10.4324/9780203426135

BS EN ISO 7730:2005. Ergonomics of the thermal environment. Analytical determination and interpretation of thermal comfort using calculation of the PMV and PPD indices and local thermal comfort criteria.

Chaiyapinunt, S., Mangkornsaksit, K. & Phueakphongsuriya, B. (2004). Development of cooling load temperature differential values for building envelopes in Thailand. Journal of the Chinese Institute of Engineers, 27(5), 677-688. https://doi.org/10.1080/02533839.2004.9670915

Epstein, Y. & Moran, D.S. (2006). Thermal comfort and the heat stress indices. *Industrial Health*, *44*, 388-398. https://doi.org/10.2486/indhealth.44.388

European Agency for Safety and Health at Work [EU-OSHA] (2012). *Annual Report*. Bilbao: European Agency for Safety and Health. https://doi.org/10.2802/51178

Health and Safety Executive [HSE] (2017). *Work-related stress, depression or anxiety statistics in Great Britain 2017*. Bootle: Health and Safety Executive.

Höppe, P. (2002). Different aspects of assessing indoor and outdoor thermal comfort. *Energy and Buildings*, *34*(6), 661-665. https://doi.org/10.1016/S0378-7788(02)00017-8

Humphreys, M.A. & Fergus Nicol, J. (2002). The validity of ISO-PMV for predicting comfort votes in every-day thermal environments. *Energy and Buildings*, *34*(6), 667-684. https://doi.org/10.1016/S0378-7788(02)00018-X

ISO 7730:2005. Ergonomics of the thermal environment. Analytical determination and interpretation of thermal comfort using calculation of the PMV and PPD indices and local thermal comfort criteria.

Jenkins, K., Gilbey, M., Hall, J., Glenis, V. & Kilsby, C. (2014). Implications of climate change for thermal discomfort on underground railways. *Transportation Research Part D: Transport and Environment*, *30*, 1-9. https://doi.org/10.1016/j.trd.2014.05.002

Karyono, T. (2015). Predicting comfort temperature in Indonesia, an initial step to reduce cooling energy consumption. *Buildings*, *5*(3), 802-813. https://doi.org/10.3390/buildings5030802

Kurazumi, Y., Tsuchikawa, T., Kondo, E., Ishii, J., Fukagawa, K., Yamato, Y., Ando, Y., Matsubara, S. & Horikoshi, T. (2012). Thermal comfort zone in outdoor environment. *Journal of Human and Living Environment*, *19*(2), 115--127. https://doi.org/10.24538/jhesj.19.2_115

Lan, L., Wargocki, P. & Lian, Z. (2011). Quantitative measurement of productivity loss due to thermal discomfort. *Energy and Buildings*, *43*(5), 1057-1062. https://doi.org/10.1016/j.enbuild.2010.09.001

Latha, P.K., Darshana, Y. & Venugopal, V. (2015). Role of building material in thermal comfort in tropical climates – a review. *Journal of Building Engineering*, *3*, 104-113. https://doi.org/10.1016/j.jobe.2015.06.003

Li, Q., Yoshino, H., Mochida, A., Lei, B., Meng, Q., Zhao, L. & Lun, Y. (2009). CFD study of the thermal environment in an air-conditioned train station building. *Building and Environment*, *44*(7), 1452-1465. https://doi.org/10.1016/j.buildenv.2008.08.010

Lippsmeier, I. (1997). *Bangunan Tropis* [*Tropical buildings*]. Jakarta: Penerbis Erlangga.

Mochida, A., Yoshino, H., Takeda, T., Kakegawa, T. & Miyauchi, S. (2005). Methods for controlling airflow in and around a building under cross-ventilation to improve indoor thermal comfort. *Journal of Wind Engineering and Industrial Aerodynamics*, *93*(6), 437-449. https://doi.org/10.1016/j.jweia.2005.02.003

Parsons, K. (2014). *Human thermal environments: The effects of hot, moderate, and cold environments on human health, comfort, and performance.* 3rd ed. Boca Raton: CRC Press. https://doi.org/10.1201/b16750

Piasecki, M., Fedorczak-Cisak, M., Furtak, M. & Biskupski, J. (2019). Experimental confirmation of the reliability of fanger's thermal comfort model – case study of a near-zero energy building (NZEB) office building. *Sustainability (Switzerland)*, *11*(9), 2461. https://doi.org/10.3390/su11092461

Ponni, M. & Baskar, R. (2015). Comparative study of different types of roof and indoor temperatures in tropical climate. *International Journal of Engineering and Technology*, *7*(2), 530-536.

Pourshaghaghy, A. & Omidvari, M. (2012). Examination of thermal comfort in a hospital using PMV-PPD model. *Applied Ergonomics*, *43*(6), 1089-1095. https://doi.org/10.1016/j.apergo.2012.03.010

Purnomo, H. & Rizal (2000). Pengaruh Kelembaban,Temperatur Udara dan Beban Kerja terhadap Kondisi Faal Tubuh Manusia [Effects of humidity, air temperature and workload on the physiological condition of the human body]. *Logika*, *4*(5), 35-47.

Maru, R. & Ahmad, S., Malaysia, B., Malaysia (2014). Daytime temperature trend analysis in the City of Jakarta, Indonesia. *World Applied Sciences Journal*, *32*(9), 1808-1813.

Rural Chemical Industries (Aust) Pty Ltd (n.d.). Country: indonesia temperature & relative humidity range. Retrieved form https://www.heatstress.info/Portals/38/TEMPIND(updated).pdf

Seppänen, O., Fisk, W.J. & Faulkner, D. (2005). *Control of temperature for health and productivity in offices*. Berkeley: Lawrence Berkeley National Laboratory.

Setaih, K., Hamza, N., Mohammed, M.A., Dudek, S. & Townshend, T. (2014). CFD modeling as a tool for assessing outdoor thermal comfort conditions in urban settings in hot arid climates. *Journal of Information Technology in Construction*, *19*, 248-269.

Simion, M., Socaciu, L. & Unguresan, P. (2016). Factors which influence the thermal comfort inside of vehicles. *Energy Procedia*, *85*, 472-480. https://doi.org/10.1016/j.egypro.2015.

SNI 6390:2011. Konservasi energi sistem tata udara pada bangunan gedung [Energy saving in air conditioning of buildings].

Stanton, N.A., Hedge, A., Brookhuis, K., Salas, E. & Hendrick, H.W. (Eds.) (2004). *Handbook of human factors and ergonomics methods*. Boca Raton: CRC Press. https://doi.org/10.1201/9780203489925

Stavrakakis, G.M., Zervas, P.L., Sarimveis, H. & Markatos, N.C. (2010). Development of a computational tool to quantify architectural-design effects on thermal comfort in naturally ventilated rural houses. *Building and Environment*, *45*(1), 65-80. https://doi.org/10.1016/j.buildenv.2009.05.006

Sugiono, S., Swara, S.E., Wijanarko, W. & Sulistyarini, D.H. (2017). Investigating the impact of ornamental plants correlated with indoor thermal comfort and eco-energy. *International Review of Civil Engineering*, *8*(5), 221-226. https://doi.org/10.15866/irece.v8i5.12703

Uemoto, K.L., Sato, N.M.N. & John, V.M. (2010). Estimating thermal performance of cool colored paints. *Energy and Buildings*, *42*(1), 17-22. https://doi.org/10.1016/j.enbuild.2009.07.026

Summary

Impact of elevated outdoor MRT station towards passenger thermal comfort: A case study in Jakarta MRT. Comfort of the train passengers is the main priority of modern mass rapid transit (MRT) management. Objective of this paper is to investigate the thermal comfort of the elevated MRT station in tropical climate. The first step of this study was to conduct literature review on human thermal comfort, environment ergonomics, computational fluid dynamic (CFD), computational aeroacoustics (CAA), and predicted mean vote (*PMV*). Air quality in elevated MRT station was measured based on several parameters: relative humidity, wind speed, temperature, and wind direction. A 3D model of MRT designed was used to describe existing condition prior to simulations with CFD and CAA softwares. Predicted mean vote is arranged based on the value of metabolism, wind speed, ambient temperature, mean radiant temperature, amount of insulation from clothing, and relative humidity. Whereas predicted percentage of dissatisfied (*PPD*) can be derived from *PMV* calculations. The analysis shows that the average *PMV* of existing condition for elevated outdoor MRT station is 3.6 (extremely hot) with *PPD* is 100% (all passengers felt discomfort). Some recommendations to reduce heat stress were addressed such as: adding plant, changing materials of the MRT station, and change the design of the elevated MRT station. Modifying open elevated MRT station into indoor elevated MRT station with installing six units of AC (2pk, ±23°C) can improve air quality and maintain the thermal comfort scale of *PMV* to be –0.04 (comfort) with *PPD* of < 8%. Based on the analysis, it can be concluded that the most suitable design for elevated MRT station in tropical climate (hot and humid) is indoor MRT station with pay attention to both direct and indirect heat exposure that hit the station.

Authors' address:
Sugiono Sugiono
(https://orcid.org/0000-0002-1605-5124)
Brawijaya University
Faculty of Engineering
Department of Industrial Engineering
Malang 65145
Indonesia
e-mail: sugiono_ub@ub.ac.id

PRACE NAUKOWO-PRZEGLĄDOWE
Research review papers

Scientific Review – Engineering and Environmental Sciences (2020), 29 (1), 108–119
Sci. Rev. Eng. Env. Sci. (2020), 29 (1)
Przegląd Naukowy – Inżynieria i Kształtowanie Środowiska (2020), 29 (1), 108–119
Prz. Nauk. Inż. Kszt. Środ. (2020), 29 (1)
http://iks.pn.sggw.pl
DOI 10.22630/PNIKS.2020.29.1.10

Justyna CZERWIŃSKA, Grzegorz WIELGOSIŃSKI
Faculty of Process and Environmental Engineering, Lodz University of Technology

Functioning of the flue gas treatment system in Polish municipal waste incineration plants

Key words: flue gas treatment, waste incineration plant, dioxins

Introduction

Waste has accompanied humanity from the beginning of the development of civilization. Always, at all stages of development, the manner of waste management was delayed in relation to the scale of generated waste and its accumulated amount. The use of thermal methods for the disposal of municipal waste began at the end of the 19th century. The first professional municipal waste incineration plant (named 'Destructor' – patent GB 3 125) was founded in 1874 in Nottingham (England). It had a capacity of about 24,000 Mg·year^{-1}. The mass use of thermal methods began in the 1960s and is currently one of the most important technologies applied in municipal waste management in the most industrialized countries of the world (Wielgosiński, 2016). In some countries it is even a dominant technology (e.g. Japan, Switzerland) with over 70% (Gohlke & Martin, 2007; Lombardi, Carnevale & Corti, 2015). More and more the so-called third world countries also decide to build incinerators – Brazil, Argentina, Chile, Egypt, Ethiopia, India, Pakistan, Malaysia, Vietnam, etc. Currently, there are over 2,000 waste incineration plants in the world (operating according to various technologies), with about 1,200 installations located in Japan, about 200 in the United States and over 250 in China. Currently, in many European Union countries, in terms of tonnage waste incineration constitutes about 30–50% of the methods used, however, in many countries, and especially in Poland, such plants raise a lot of fears and controversies, becoming a field of open conflict between local government authorities and groups of residents.

At the moment, there are nearly 500 waste incineration plants in Europe,

in which nearly 72 million Mg of municipal waste is thermally transformed (Table 1; Fraunhofer UMSICHT, 2010; ISWA, 2012).

Since the beginning of the 1980s, the construction and operation of waste incineration plants have encountered increasing social resistance, mainly due to the risk of air pollution. Numerous research works carried out in the 1990s made it possible to develop effective emission reduction technologies, while stringent legal regulations (identical in the entire EU) introduced at the beginning of the 21st century forced significant reduction of pollutant emissions. These regulations are much stricter than the requirements for combustion of

TABLE 1. Municipal waste incineration plants in Europe (data according to Eurostat for 2017)

No	State	Amount of municipal waste generated	Amount of municipal waste incinerated	Percentage of incinerated waste	Number of working municipal waste incineration plants
		thous. Mg·year^{-1}		%	pcs
1	Austria	5 018	1 944	38.74	11
2	Belgium	4 659	2 002	42.97	17
3	Czech Republic	3 643	634	17.40	4
4	Denmark	4 503	2 380	52.85	26
5	Estonia	514	217	42.22	1
6	Finland	2 812	1 646	58.53	9
7	France	34 393	12 220	35.53	126
8	Spain	21 530	2 780	12.91	12
9	The Netherlands	8 787	3 901	44.40	12
10	Ireland	2 763	480	17.37	2
11	Lithuania	1 286	236	18.35	1
12	Luxembourg	362	161	44.48	1
13	Germany	52 342	16 185	30.92	98
14	Norway	3 949	2 088	52.87	18
15	Poland	11 969	814	6.80	6
16	Portugal	5 012	988	19.71	4
17	Slovakia	2 058	197	9.57	2
18	Switzerland	5 992	2 846	47.50	30
19	Sweden	4 551	2 400	52.74	34
20	Hungary	3 768	358	9.5	1
21	Great Britain	30 911	11 578	37.46	40
22	Italy	29 583	5 634	19.04	39
	Total	240 405	71 697	29.82	494

fuels in power plants, combined heat and power plants and heating plants (Table 2), but for many people waste incineration plants are a synonym of thick black smoke from chimneys with unpleasant smell, containing a lot of toxic substances including heavy metals as well as dioxins and furans: polychlorinated dibenzo-p-dioxins and polychlorinated dibenzofurans – PCDD/Fs (Directive 2010/75/EU; European Commission, 2010).

TABLE 2. Applicable emission standards for waste incineration

Parameter	Unit	Currently applicable			BAT conclusions	
		daily average	30-minute		new	existing
			A (100%)	B (97%)		
Total suspended particles TSP	$mg \cdot m^{-3}_u$	10	30	10	2–5	
Sulfur dioxide SO_2		50	200	50	5–30	5–40
Nitrogen oxides NO_x as NO_2		200/400	400	200	50–120	50–150
Carbon monoxide CO		50	100[a]	150[b]	10–50	10–50
The sum of organic compounds as TOC		10	20	10	3–10	3–10
Hydrogen chloride HCl		10	60	10	2–6	2–8
Hydrogen fluoride HF		1	4	2	< 1	< 1
Ammonia NH_3		–	–	–	2–10	2–10
Mercury and its compounds as Hg		50[c]			5–20[c]	5–20[c]
		–			1–10[e]	1–10[e]
Cadmium and thallium and their compounds as Cd + Tl		0.05[c]			0.005–0.02[c]	
Antimony, arsenic, lead, chromium, cobalt, copper, manganese, nickel and vanadium and their compounds as Sb + As + Pb + Cr + Co + + Cu + Mn + Ni + V		0.5[c]			0.1–0.3[c]	
PCDD/Fs	$ng\ I\text{-}TEQ \cdot m^{-3}_u$	0.1[d]			0.01–0.04[d]	0.01–0.06[d]
		–			0.01–0.06[e]	0.01–0.08[e]
PCDD/Fs + dl-PCBs	$ng\ WHO \cdot m^{-3}_u$	–			0.01–0.06[d]	0.01–0.08[d]
					0.01–0.08[e]	0.01–0.10[e]

A – 100% of the daily average results for the year may not exceed the limit values given in column A; B – 97% of the daily average results for the year may not exceed the limit values given in column B. [a] for fluidized bed installations, the standard is 100 $mg \cdot m^{-3}$ as an hourly average; [b] 10-minute average value; [c] average value for measurement lasting for from 30 min to 8 h; [d] average value for measurement lasting for 6–8 h; [e] average value for measurement lasting at least 14–30 days.

Permissible concentrations of pollutants in flue gases from waste incineration plants in accordance with the currently applicable regulations (Directive 2010/75/EU; European Commission, 2010; Regulation of the Minister of the Environment of 1 March 2018) and the proposed so-called best available technique (BAT) conclusions that will apply starting from 2023 are given in Table 2.

In order to meet the emission standards shown in Table 2, waste incineration plants are equipped with efficient and effective flue gas treatment systems. At the turn of the 20th and 21st centuries, it was widely believed that the flue gas treatment system at a waste incineration plant must consist of an electrostatic precipitator for dust removal, a wet scrubber for acid gas removal and an SCR catalyst to reduce nitrogen oxides and decompose PCDD/Fs (Quina, Bordado & Quinta-Rerreira, 2011). This system was often supplemented with a permanent adsorber with activated coke to remove dioxins and heavy metals (Wielgosiński, 2016). Currently, thanks to the progress made in textile technology, as well as in methods for removing impurities from waste gases, a typical exhaust gas treatment system in the incineration plant consists of a dry or semi-dry scrubber for acid gas removal, a fabric filter and a system for non-catalytic reduction of nitrogen oxides – SNCR (Gottschalk, Buttmann & Johansson, 1996; Liu, Wang, Wang & Zhu, 2015; Jurczyk, Mikus & Dziedzic, 2016a, 2016b). It is often supplemented with an injection of powdered activated carbon before entering the fabric filter. This system allows for equally effective removal of impurities from waste gases as previously used systems with an electrostatic precipitator, absorber and catalyst, and is much cheaper (Wielgosiński & Zarzycki, 2018).

At present, there are eight modern municipal waste incineration plants in Poland. In addition to a small incineration plant launched in 2001 in Warsaw, in the years 2013–2018 incineration plants were built in Białystok, Bydgoszcz, Konin, Kraków, Poznań, Szczecin and Rzeszów. Table 3 presents a summary of the most important parameters of the waste incineration plants in Poland.

TABLE 3. Summary of parameters of Polish waste incineration plants

Location	Annual yield	Number of lines	One line capacity	Thermal power	Electrical power
	$Mg \cdot year^{-1}$	pcs	$Mg \cdot h^{-1}$	MW_t	MW_e
Kraków	220 000	2	14.1	35	10.7
Poznań	210 000	2	13.5	34	15
Bydgoszcz	180 000	2	11.5	27.7	9.2
Szczecin	150 000	2	10.0	32	9.4
Białystok	120 000	1	15.5	17.5	6.1
Rzeszów	100 000	1	12.5	16.5	4.6
Konin	94 000	1	12.05	15.5	4.4
Warsaw	40 000	1	5.4	9.1	1.4

The total capacity of Polish waste incineration plants currently amounts to approx. 1.1 million Mg per year, which is about 9.3% of the total amount of municipal waste generated in Poland. This is definitely not enough to complete the municipal waste management system in our country. In particular, the problem today is the need to burn about 2.5–3 million Mg of combustible (oversize) fraction separated from the municipal waste stream in mechanical-biological waste treatment installations, usually called refuse derived fuel (RDF). Part of this stream is burned in the existing municipal waste incineration plants, part in cement plants, but approx. 2 million Mg annually cannot be managed. Table 4 presents the amount of waste incinerated in Polish waste incineration plants.

TABLE 4. The amount of waste burned in Polish waste incineration plants in 2016–2018

Location	Annual yield	Amount of waste burned			Amount of refuse derived fuel	
		2016	2017	2018	2017	2018
	Mg·year^{-1}				%	
Kraków	220 000	115 583	219 994	218 351	48.2	44.0
Poznań	210 000	–	210 000	209 972	0	0
Bydgoszcz	180 000	135 873	138 875	154 464	32.0	36.5
Szczecin	150 000	–	–	113 537	–	88.8
Białystok	120 000	105 999	114 703	114 121	53.1	64.8
Rzeszów	100 000	–	–	–	–	–
Konin	94 000	93 952	93 454	89 081	40.1	31.0
Warsaw	40 000	52 339	37 147	46 021	17.8	19.6
Total	1 114 000	503 746	814 173	945 547	–	–

Flue gas treatment systems

There are many methods for flue gas treatment. Taking into account the way they are carried out, they can be divided into primary and secondary. Primary methods are based on interference in the technological process of thermal waste conversion and creating such conditions that the amount of pollutants generated is as low as possible. The primary methods include good incineration process conditions, proper temperature in the incineration process and its distribution in the installation, high flue gas flow rate (high flow turbulence) in heat recovery systems, exhaust gas recirculation, or an appropriate level of oxygenation of the incineration zone. Secondary methods are based on the use of physical, chemical or physicochemical methods. The following processes are used here: dust removal (electrostatic precipitator, fabric filter), acid gas removal (wet, semi-dry and dry methods), removal of nitrogen oxides (SCR, SNCR), removal of organic impurities and volatile heavy metals (adsorption on activated carbon) (Jannelli & Minutillo, 2007; Pozzo, Antonioni, Guglielmi, Stramigioli & Coz-

zani, 2016; Wielgosiński, 2016; Pozzo, Guglielmi, Antonioni & Tugnoli, 2017; Wielgosiński & Zarzycki, 2018). The flue gas treatment systems applied in European waste incineration plants are shown in Table 5 (European Commission, 2010; Fraunhofer UMSICHT, 2010; ISWA, 2012; Löschau, 2014).

The Warsaw waste incineration plant is equipped with a three-stage flue gas treatment system. The first stage is a non-catalytic reduction of nitrogen oxides (SNCR) with injection of ammonia vapours into flue gases. The next stage is dry scrubbing of acid gases with calcium hydroxide powder and dust removal on a bag filter. The last stage includes a WKV flow adsorber with activated coke. It is used to reduce emissions of dioxins, furans, heavy metals and aromatic organic compounds (Oleniacz, 2014). Flue gas flows through a 1.5-meter layer of granulated activated coke and is then directed to the chimney. The technology of incineration and flue gas treatment was provided by Italian Termomeccanica Ecologia.

In the waste incineration plants in Konin and Poznań semi-dry flue gas scrubbing systems are applied. The first stage of purification is the system for non-catalytic reduction of nitrogen oxides (SNCR), and then semi-dry scrubbing is used to remove acid gases. Dust is removed from the flue gas on a fabric filter and before that activated carbon is introduced into the gas. This ensures effective dust removal from flue gases, reduction of emissions of acid gases, organic substances as well as dioxins and furans. The technology of incineration and flue gas treatment was supplied to the Konin waste incineration plant by the Austrian company Integral and the German company Martin. The supplier of technology for the Poznań plant was the Swiss company Hitachi Zosen Inova, while the Belgian company Keppel Seghers was the supplier for the Białystok plant. Both installations have a similar flue gas treatment system as in the Konin incineration plant.

The Municipal Waste Thermal Conversion Plant in Kraków uses the same flue gas treatment system as the above-mentioned incineration plants in Konin, Białystok and Poznań. The first stage is selective non-catalytic reduction of nitrogen oxides carried out with the help of 25% aqueous urea solution. Acid impurities are removed by the semi-dry method with injection of limewater suspension. Dust is removed from the flue gas also by means of a fabric filter. As part of the flue gas treatment system, additional injection of activated carbon into the flue gas was used to reduce emissions of dioxins and volatile heavy metals. The project was carried out by the Korean POSCO company, and the boiler technology was supplied by German Doosan Lentjes.

The semi-dry flue gas scrubbing system, dust removal on a fabric filter and non-catalytic reduction of nitrogen oxides are also used in the incineration plant in Bydgoszcz. In addition, the exhaust gases after the heat recovery stage are cooled with an aqueous NaOH solution, which is an additional element of removing acidic impurities (wet method). The project was carried out by Italian companies Astaldi and Termomeccanica Ecologia.

In contrast to other installations, the Szczecin waste incineration plant is equipped with a wet scrubbing system

TABLE 5. Flue gas treatment systems in European municipal waste incineration plants (according to BREF-BAT and CEWEP and ISWA data)

State	Number of installations											
	acid gas removal (SO_2, SO_3, HCl and HF)						dust removal			reduction of NO_x emissions		
	dry system (DSI)	semi-dry system (SDS)	wet system (WS)	DSI and WS simultaneously	SDS and WS simultaneously	DSI and SDS simultaneously	electrostatic precipitator (ESP)	ESP and FF simultaneously	fabric filter (FF)	non-catalytic reduction (SNCR)	SNCR and SCR simultaneously	catalytic reduction (SCR)
Austria	1	1	9	0	0	0	4	1	6	0	0	11
Belgium	2	0	4	6	1	4	7	8	2	9	0	8
Czech Republic	0	1	0	1	0	2	0	2	2	4	0	0
Denmark	8	11	1	6	0	0	10	3	13	26	0	0
Finland	4	0	0	4	0	1	0	3	6	8	0	1
France	42	32	28	8	8	8	49	19	58	66	0	60
Spain	4	1	1	0	0	6	1	1	10	8	0	4
The Netherlands	1	5	2	4	0	0	1	3	8	4	0	8
Germany	22	5	39	22	0	10	35	20	43	43	2	53
Norway	0	8	4	6	0	0	4	1	13	17	0	1
Poland	1	6	1	0	0	0	1	0	7	8	0	0
Portugal	0	0	0	0	0	4	0	0	4	4	0	0
Sweden	21	0	8	5	0	0	12	0	22	15	0	19
Hungary	0	1	0	0	0	0	0	0	1	1	0	0
Great Britain	15	12	4	6	0	3	2	4	34	40	0	0
Italy	26	6	2	5	0	0	0	13	26	12	13	14
Total	147	89	103	73	9	38	126	78	255	265	15	179

for acid gas removal, as well as a system for non-catalytic reduction of nitrogen oxides and an adsorption system for organic substances, dioxins, furans, heavy metals and mercury on activated carbon. This is so far the only installation for the thermal treatment of waste equipped with a wet flue gas cleaning system (absorption in aqueous NaOH). The technology supplier was RAFAKO together with the German company Mitsubishi Hitachi Power Systems Europe.

The recently built incineration plant in Rzeszów uses non-catalytic reduction of nitrogen oxides, semi-dry method, fabric filter and injection of activated carbon. The technology supplier was the Italian company Termomeccanica Ecologia. An interesting fact is the recovery of heat from flue gases after their purification system, which increases the amount of heat produced.

Table 6 shows the amount of raw materials consumed in the flue gas cleaning process at individual waste treatment plants.

Efficiency of flue gas treatment systems

The most important task of flue gas treatment systems is to remove substances that after being emitted to the environment could have a negative impact on the environment, as well as people and animals (Wielgosiński, Namiecińska & Czerwińska, 2018, Xiao et al., 2018; Zhang, Yu, Shao & He, 2019). Table 7 presents a summary of emissions from five Polish waste incineration plants together with the limit values. None of the waste incineration plants shown exceeds the permissible values of the listed pollutants (Table 7). Moreover, since the beginning of their use, no cases of exceeding emission standards have been recorded. Table 8, on the other hand, presents a list of dioxin emissions from thermal waste treatment plants.

Based on the results of measurement presented above, it can be stated that none of the waste incineration plants exceeds the limit value for dioxin and furan

TABLE 6. Raw materials used for flue gas treatment (data for 2018)

Location	Amount of waste burned	Raw material consumption index				
		calcium reagent CaO, $Ca(OH)_2$	NaOH aqueous solution	activated carbon	NH_4OH aqueous solution	urea aqueous solution
	$Mg \cdot year^{-1}$	$kg \cdot Mg^{-1}$	$m^3 \cdot Mg^{-1}$	$kg \cdot Mg^{-1}$		
Kraków	218 351	0.0151	0.0018	0.3496	–	1.3962
Poznań	209 972	7.5790	–	0.2490	–	1.8249
Bydgoszcz	157 464	10.8296	3.7967	0.2901	3.5451	–
Szczecin	113 537	2.9163	2.3229	0.3122	1.0772	–
Białystok	114 121	11.6473	–	0.1793	–	1.4590
Rzeszów	–	–	–	–	–	–
Konin	89 081	12.9696	–	0.5336	4.8018	–
Warsaw	46 021	10.4730	–	0.9841	1.4615	–

TABLE 7. Average pollutant emissions in Polish waste incineration plants in 2018 [mg·m$^{-3}_{u}$]

Parameter	Rzeszów	Białystok	Szczecin	Poznań	Konin	Limit value
Total suspended particles TSP	2.00	2.15	0.35	4.59	3.29	10
Sulfur dioxide SO_2	11.20	7.15	5.40	19.90	19.28	50
Nitrogen oxides NO_x as NO_2	145.60	74.85	132.50	176.13	155.84	200
Carbon monoxide CO	14.70	5.20	29.00	3.31	6.12	50
Total organic compounds as TOC	1.24	0.35	1.20	0.34	0.29	10
Hydrogen chloride HCl	1.20	0.73	0.30	2.51	2.63	10
Hydrogen fluoride HF	0.44	0.00	0.11	0.16	0.02	1
Mercury and its compounds as Hg	0.001	0.002	0.005	0.001	0.001	0.05
Cadmium and thallium and their compounds as Cd + Tl	0.023	0.018	0.020	0.001	0.011	0.050
Antimony, arsenic, lead, chromium, cobalt, copper, manganese, nickel and vanadium and their compounds as Sb + As + + Pb + Cr + Co + Cu + Mn + Ni + V	0.080	0.007	0.070	0.094	0.134	0.5

TABLE 8. Dioxin emissions in Polish waste incineration plants in 2018

Incineration plant	Number of measurements	Measurements PCDD/Fs emissions			Average as percent of limit value
		minimum	maximum	average	
	TEQ·m$^{-3}_{u}$				%
Białystok	9	0.000660	0.000660	0.005682	5.68
Bydgoszcz	9	0.000190	0.021000	0.005054	5.05
Konin	9	0.002320	0.009620	0.004777	4.78
Kraków	8	0.001000	0.068000	0.015163	15.16
	8	0.000900	0.049000	0.011688	11.69
Poznań	9	0.000180	0.066000	0.015792	15.79
	9	0.000030	0.053000	0.010722	10.72
Rzeszów	4	0.007000	0.018000	0.010450	10.45
Szczecin	4	0.000864	0.006345	0.003076	3.08
	4	0.000779	0.007240	0.002834	2.83
Warsaw	7	0.002200	0.082400	0.041000	41.00

emissions, moreover, these emissions are usually around 10% of the limit values.

Conclusions

Thermal waste treatment is an important element of the municipal waste management system without which it is not possible to build the system. Waste incineration plants have been known in the world for 145 years, and for over 50 years they have been used on a massive scale, but they still give rise to fears and controversies. Despite over 2,000 installations operating successfully around the world and positive experience in the field of minimizing environmental impact, every proposal to build a new installation raises social protests. An analysis of eight municipal waste incineration plants working in Poland shows that their design and operation parameters do not differ from similar installations in other European countries, and the emission of pollutants does not exceed the permissible values. This is important because the emission of pollutants into the atmospheric air, in particular the emission of dioxins and furans, is what protesters fear the most. From the presented data it is clear that this emission is much smaller than allowed by strict regulations in this field. Taking into account that the emission standards for thermal waste treatment installations are stricter than the emission standards for energy and heating, any initiative in a heat energy company to replace an old coal boiler with a waste-burning boiler, e.g. RDF, should not cause concern, as the new source will certainly emit less pollutants (Wielgosinski et al., 2018). On the other hand, the first three years of operation in Poland of large modern municipal waste incineration plants confirm that they are safe, low-emission installations that do not cause deterioration of air quality.

Acknowledgements

The authors thank the operators of Polish waste incineration plants for providing operational data.

References

Directive 2010/75/EU of the European Parliament and of the Council of 24 November 2010 on industrial emissions (integrated pollution prevention and control). OJ L 334/17 of 17.12.2010.

European Commision (2010). Best Available Techniques (BAT). Reference Document for Waste Incineration, Industrial Emissions. Directive 2010/75/UE. Integrated Pollution Prevention and Control.

Fraunhofer UMSICHT (2010). Der Weltmarkt für Abfallverbrennungsanlagen 2010/2011 [The world market for waste incinerators 2010/2011]. Köln: Ecoprog.

Gohlke, O. & Martin, J. (2007). Drivers for innovation in waste-to-energy technology. *Waste Management Research*, *25*(3), 214-219. https://doi.org/10.1177/0734242X07079146

Gottschalk, J., Buttmann, P. & Johansson, T. (1996). Modern flue-gas clearing system for waste incineration plants. *Filtration & Separation*, *33*(5), 383-388. https://doi.org/10.1016/S0015-1882(97)84298-X

International Solid Waste Association [ISWA] (2012). Waste-to-Energy State-of-the-Art Report. Statistics. 6th edn. Copenhagen: ISWA.

Jannelli, E. & Minutillo, M. (2007). Simulation of the flue gas cleaning system of an RDF incineration power plant. *Waste Management*, *27*(5), 684-690. https://doi.org/10.1016/j.wasman.2006.03.017

Jurczyk, M., Mikus, M. & Dziedzic, K. (2016a). Flue gas cleaning in municipal waste-to--energy plants – Part 1. *Infrastructure and*

Ecology of Rural Areas, *4/1*, 1179-1193. http://dx.medra.org/10.14597/infraeco.2016.4.1.086

Jurczyk, M., Mikus, M. & Dziedzic, K. (2016b). Flue gas cleaning in municipal waste-to--energy plants – Part 2. *Infrastructure and Ecology of Rural Areas, 4/2*, 1309-1321. http://dx.medra.org/10.14597/infraeco.2016.4.2.096

Liu, X., Wang, J., Wang, X. & Zhu, T. (2015). Simultaneous removal of PCDD/Fs and NO_x from the flue gas of a municipal solid waste incinerator with a pilot plant. *Chemosphere*, *133*, 90-96. https://doi.org/10.1016/j.chemosphere.2015.04.009

Lombardi, L., Carnevale, E. & Corti, A. (2015). A review of technologies and performances of thermal treatment systems for energy recovery from waste. *Waste Management*, *37*, 26-44. https://doi.org/10.1016/j.wasman.2014.11.010

Löschau, M. (2014). *Purification of exhaust gases*. Neuruppin: TK-Verlag.

Oleniacz, R. (2014). Impact of the Municipal Solid Waste Incineration Plant in Warsaw on Air Quality. *Geomatics and Environmental Engineering*, *8*(4), 25-42. https://doi.org/10.7494/geom.2014.8.4.25

Pozzo, A.D., Antonioni, G., Guglielmi, D., Stramigioli, C. & Cozzani, V. (2016). Comparison of alternative flue gas dry treatment technologies in waste-to-energy processes. *Waste Management*, *51*, 81-90. https://doi.org/10.1016/j.wasman.2016.02.029

Pozzo, A.D., Guglielmi, D., Antonioni, G. & Tugnoli, A. (2017). Sustainability analysis of dry treatment technologies for acid gas removal in waste-to-energy plants. *Journal of Cleaner Production*, *162*, 1061-1074. https://doi.org/10.1016/j.jclepro.2017.05.203

Quina, M.J., Bordado, J.C.M. & Quinta-Rerreira, R.M. (2011). Air Pollution Control In Municipal Solid Waste Incinerators. In M. Khallaf (Ed.), *The Impact of Air Pollution on Health, Economy, Environment and Agricultural Sources* (pp. 331-358). London: IntechOpen. https://doi.org/10.5772/17650

Rozporządzenie Ministra Środowiska z dnia 1 marca 2018 r. w sprawie standardów emisyjnych dla niektórych rodzajów instalacji, źródeł spalania paliw oraz urządzeń spalania lub współspalania odpadów. Dz.U. 2018, poz. 680 [Regulation of the Minister of the Environment of 1 March 2018 on emission standards for certain types of installations, fuel combustion sources and waste incineration or co-incineration plants. Journal of Laws 2018 item 680].

Wielgosiński, G. & Zarzycki, R. (2018). *Technologie i procesy ochrony powietrza* [*Technologies and processes of air protection*]. Warszawa: Wydawnictwo Naukowe PWN.

Wielgosiński, G. (2016). Problemy eksploatacji spalarni odpadów [Thermal treatment of municipal waste – selected issues]. *Nowa Energia*, *1*, 41-48.

Wielgosiński, G., Namiecińska, O. & Czerwińska, J. (2018). Environmental impact of emissions from incineration plants in comparison to typical heating systems. *E3S Web of Conferences*, *28*, 1-8. https://doi.org/10.1051/e3sconf/20182801038

Xiao, H., Ru, Y., Peng, Z., Yan, D., Li, L., Karstensen, K.H., Wang, N. & Huang, Q. (2018). Destruction and formation of polychlorinated dibenzo-p-dioxins and dibenzofurans during pretreatment and co-processing of municipal solid waste incineration fly ash in a cement kiln. *Chemosphere*, *210*, 779-788. https://doi.org/10.1016/j.chemosphere.2018.07.058

Zhang, H., Yu, S., Shao, L. & He, P. (2019). Estimating source strengths of HCl and SO_2 in the flue gas from waste incineration. *Journal of Environmental Sciences*, *75*, 370-377. https://doi.org/10.1016/j.jes.2018.05.019

Summary

Functioning of the flue gas treatment system in Polish municipal waste incineration plants. All municipal waste incineration plants operating in Poland are discussed and their flue gas treatment systems are described in detail in the article. A comparison of performance indicators, i.e. the amount of raw materials consumed particularly in flue gas treatment systems, is presented. The article also summarizes the results of emission measurements for eight incineration plants in the years 2016–2019.

Authors' address:
Justyna Czerwińska
Grzegorz Wielgosiński
(https://orcid.org/0000-0003-3542-8528)
Politechnika Łódzka
Wydział Inżynierii Procesowej i Ochrony Środowiska
ul. Wólczańska 214, 90-924 Łódź
Poland
e-mail: justyna.czerwinska@edu.p.lodz.pl
grzegorz.wielgosinski@p.lodz.pl

Informacje dla autorów

Na łamach *Przeglądu Naukowego – Inżynieria i Kształtowanie Środowiska* zamieszczane są **oryginalne prace naukowe w języku polskim lub angielskim, niepublikowane** w innych czasopismach. Prawa autorskie tekstów przyjętych do druku udzielone są Wydawnictwu SGGW, a artykuły są udostępniane na warunkach Open Access na zasadach licencji Creative Commons CC BY-NC (patrz oświadczenie autorów na stronie http://iks.pn.sggw.pl).

Wymagania techniczne dotyczące przygotowania prac:

1. Tekst i tabele należy złożyć w formie elektronicznej, w plikach o formacie MS Office, a rysunki – wstawione do tekstu i w oddzielnych plikach graficznych, w programach pracujących w środowisku Windows (Excel, Photoshop itp.) w wersji czarno-białej. Rysunki i zdjęcia w wersji papierowej są drukowane w skali szarości, a na stronie internetowej czasopisma wygenerowane w wersji kolorowej.
2. Objętość artykułu wraz z ilustracjami nie może przekraczać 10 stron formatu A-4, interlinia – 1,5 wiersza, marginesy – 2,5 cm, czcionka TNR 12 pkt., tekst w układzie jednokolumnowym.

Układ pracy (zgodnie z szablonem: http://iks.pn.sggw.pl/do_autorow.html):

1. Imię i nazwisko autora(-ów) – u góry z lewej strony.
2. Pod nazwiskiem – miejsce pracy w polskim i angielskim języku.
3. Tytuł pracy – w polskim i angielskim języku.
4. Słowa kluczowe (*Key words*) – w polskim i angielskim języku.
5. Tekst pracy (w języku polskim lub angielskim) powinien obejmować: **wprowadzenie, materiał i metody, wyniki, podsumowanie i dyskusję, wnioski, literaturę, streszczenie w języku angielskim (Summary), streszczenie w języku polskim, adres autora(-ów).**
6. Tytuły tabel i rysunków, opisy główki pionowej i poziomej tabel oraz wszystkie napisy na ilustracjach muszą być w polskim i angielskim języku w wersji czarno-białej.
7. W tekstach w języku polskim do oznaczania pozycji dziesiętnej liczb należy używać przecinka, a w języku angielskim – kropki.
8. Przy powoływaniu się w artykułach angielskojęzycznych na publikacje w *Przeglądzie Naukowym* autorzy proszeni są o używanie jego angielskiej nazwy.
9. Wykaz piśmiennictwa i powołania należy sporządzić według międzynarodowego formatu APA i zestawić w porządku alfabetycznym. Bliższe informacje, przykłady formatowania i program do tworzenia opisów bibliograficznych w wymaganym formacie znajdują się na stronie *Przeglądu Naukowego* (http://iks.pn.sggw.pl/do_autorow.html), np.:
   Kowalski, J. i Nowak, P. (2009). *Analiza regresji stosowana.* Warszawa: Wydawnictwo Naukowe PWN.
   Kowalski, J., Nowak, P. i Bartnik, Z. (2009). Suspended sediment sources in two small lowland agricultural catchments in the UK. *Journal of Hydrology*, *252*(1-4), 1–24. doi:10.1016/s0022-1694(01)00388-2
   Procedura recenzowania. (2014). Pobrano z lokalizacji Przegląd Naukowy Inżynieria i Kształtowanie Środowiska: http://iks.pn.sggw.pl/recenzje.html.
10. Przy pierwszym powoływaniu się w tekście na innych autorów podaje się np.: „zdaniem Kowalskiego (2002)" lub „(Kowalski, 2002)". Przy większej liczbie autorów „(Kowalski, Malinowski i Witkowski, 2002)".
11. Streszczenia powinny zawierać ok. 500 znaków.
12. Author's address:
    Jan Kowalski
    Nazwa miejsca pracy w języku polskim (uczelnia, wydział, katedra)
    ulica, kod pocztowy miejscowość, Poland
    e-mail
13. Oświadczenie o oryginalności pracy (http://iks.pn.sggw.pl/oswiadczenie.doc).